Magmatic and volcanological evolution of the Desertas rift zone (Madeira Archipelago, NE Atlantic)

Dissertation

for the doctorate degree
of the Department of Geosciences
at the University of Bremen

Submitted by

Stefanie Schwarz

Bremen
2004

Tage des Kolloquiums:

24.6.2004

Gutachter:

Prof. Dr. C. W. Devey
Prof. Dr. M. Olesch

Prüfer:

Prof. Dr. B. Peckmann
Dr. A. Klügel

Erklärung

Hiermit versichere ich, dass ich

1. die Arbeit ohne unerlaubte fremde Hilfe angefertigt habe,
2. keine anderen als die von mir angegebenen Quellen und Hilfsmittel benutzt habe,
3. die benutzten Werke wörtlich zitiert oder inhaltlich entnommene Stellen als solche kenntlich gemacht habe.

Bremen, den

Danksagung

Meinen größten Dank möchte ich Dr. Andreas Klügel aussprechen, der als Projektleiter meine Arbeit auf Madeira und den Desertas-Inseln ermöglicht hat. Als mein direkter Betreuer stand er mir jederzeit mit Rat und Tat zur Seite. Seine Unterstützung und die intensive Zusammenarbeit waren stets hervorragend. Vielen Dank auch für Schokolade und Kekse, die das Nachmittagsloch bekämpft und meine Zeit als Doktorandin "versüßt" haben.

Prof. Dr. C. W. Devey sei herzlichst gedankt für seine fachliche und organisatorische Unterstützung als Arbeitsgruppenleiter und die Erstellung des ersten Gutachtens.

Ein spezielles Dankeschön geht an Prof. Dr. M. Olesch, der sich bereit erklärt hat das Zweitgutachten für meine Arbeit zu übernehmen.

Um muito obrigada aos Directores, Sr. Costa Neves e Sra. Susana Sá Fontinha, do Parque Natural da Madeira bem como aos seus vigilantes, pela sua grande ajuda durante o desenvolvimento do meu trabalho na ilha da Madeira e nas Ilhas Desertas. Em especial gostaria ainda agradecer ao Gil Perreira pelo seu grande apoio durante as minhas estadias nas Desertas e por ter sido muito paciente com o meu português.

Vielen Dank an all die Leute des IFM-GEOMAR in Kiel, die mir viel geholfen haben. An dieser Stelle möchte ich Prof. Kaj Hoernle hervorheben, der mir mit konstruktiver Kritik immer wieder neue Anregungen für meine Arbeit gegeben hat. Dr. Paul van den Bogaard danke ich für die Durchführung der $^{40}Ar/^{39}Ar$-Analysen und seine Mithilfe bei den Kapiteln zu den Altersdatierungen. Und natürlich herzlichen Dank an Stattler und Walddorf für die unvergesslichen Stunden auf Madeira. Nicht zu vergessen Jörg "Madeira-Man" Geldmacher, der mich mit Probenmaterial und viel Madeira-Charme versorgt hat. Dr. Folkmar Hauff bin ich außerordentlich dankbar für seine Nachhilfestunden in Sachen Isotopengeochemie und die Durchführung der Sr-Nd-Pb-Isotopenanalysen im TIMS-Labor. Vielen Dank auch an Silke Vetter und Dagmar Rau, die mich mit der Probenaufbereitung und Isotopen- bzw. RFA-Analytik tatkräftig unterstützt haben.

Für die moralische Unterstützung mit vielen lustigen Kaffeepausen bedanke ich mich insbesondere bei unserer kleinen, aber feinen Arbeitsgruppe. Heike Anders und Imme Martelock danke ich zudem für die große Hilfe bei der Probenaufbereitung und der ICPMS-Analytik. Hervorheben möchte ich noch meinen Kollegen Karsten Galipp, der durch sein unkompliziertes Wesen und seine tatkräftige Mithilfe zum erfolgreichen Abschluss meines zweiten Geländeaufenthalt beigetragen hat. Ein herzliches Dankeschön geht auch an Klas Lackschewitz für die Anregungen beim Durchlesen und Korrigieren meiner Manuskripte.

Herzlichen Dank insbesondere an Rainer Schmidt, der mich all die Jahre mit seinem offenen Ohr und seiner seelischen Unterstützung in allen Lebenslagen begleitet hat.

Die Arbeit wurde finanziert von der Deutschen Forschungsgemeinschaft (DFG-Projekt KL1313/2-1).

Table of contents

Abstract

Most ocean island volcanoes have pronounced rift zones along which the islands preferably grow by intrusion and extrusion. They have a strong control on volcano growth and evolution making a knowledge of their internal structure essential. The main aim of this thesis is to provide insight into the formation and evolution of North Atlantic rift zones based on an exemplary study of Madeira Archipelago (NE Atlantic).

Madeira and the three adjacent Desertas Islands show two well-developed fossil rift zones which intersect near the São Lourenço peninsula (the eastern tip of Madeira). In order to examine a possible genetic relationship during their evolution, volcanological structures, rock ages and rock compositions were determined and investigated at the Desertas and São Lourenço which may have acted as a possible connector between the Madeira and Desertas rifts. Barometric data derived from fluid inclusion analyses and clinopyroxene-melt thermobarometry allow inferences on levels of magma stagnation beneath the two rifts indicating a multi-stage magma ascent: main fractionation occurs at multiple levels within the mantle (São Lourenço: 15-35 km depth; Desertas Islands: 17-28 km) and is followed by temporary stagnation within the crust prior to eruption (São Lourenço: 8-10 km; Desertas Islands: 2-3 km). Depths of crustal magma stagnation beneath São Lourenço and the Desertas differ significantly, and there is no evidence for a common shallow magma reservoir feeding both rift arms. These results suggest that Madeira and the Desertas represent two volcanic centres with separate magma supply systems. Detailed volcanological mapping at the Desertas Islands showed that a major volcanic centre was located at their southern end and/or near their central part.

$^{40}Ar/^{39}Ar$ age determinations revealed that subaerial Desertas volcanism lasted much longer than previously thought (>5.1-1.9 Ma) and overlaps in age with the shield-building phases of Madeira (>4.6-0.7 Ma; Geldmacher et al., 2000). Moreover, new rock ages from São Lourenço indicate that rift volcanism lasted from >5.3 to 0.9 Ma, i.e. during the entire subaerial shield stage of Madeira. A period of eruptive quiescence between 4 and 2.5 Ma at São Lourenço coincides with the period of main subaerial volcanic activity on the Desertas, suggesting some kind of coupling of the two magmatic systems. A common magma source is indicated by major element, trace element and Sr-Nd-Pb isotope compositions of volcanic rocks from São Lourenço and the Desertas, all considerably overlapping with those from central Madeira. In accordance with previously published data from Madeira, São Lourenço samples show a characteristic geochemical evolution with decreasing age: FeO_{tot}, SiO_2, Mg# and Pb and Sr isotope ratios decrease, whereas Nd isotope ratios increase. São Lourenço shield stage samples include the most depleted Sr-Nd-Pb isotope ratios, whereas rocks of similar age from the Desertas rift show the most enriched Pb and Sr isotope ratios. These extreme isotope compositions imply that São Lourenço magmas are not

compatible with either mixing of Desertas and Madeira melts at crustal or mantle depths or with lateral magma transport from the Madeira rift to the Desertas along São Lourenço.

The observations and conclusions derived from all different methods clearly indicate that Madeira and the Desertas represent two separate volcanic systems that root in particular sectors of the melting region within the Madeira source. The initiation of Desertas volcanism may have resulted from flexural stresses within the lithosphere due to the loads of Madeira and Porto Santo islands, combined with a weak pulsating mantle plume and irregular motion of the African plate. The inferred shift of volcanic activity between the neighbouring Madeira and Desertas systems is proposed to reflect an irregularly shaped plume causing lateral variations in melt production. The formation of the elongated Desertas rift is suggested to result from a local extensive stress field in-between the progressively overlapping Madeira and Desertas edifices. The evolution of the Desertas rift hence differs from that of caldera-centred, two-armed rift systems typical for Hawaiian volcanoes such as Kilauea showing that models for rift zones in Hawaii cannot necessarily be transferred to hotspot-related volcanoes associated with weak plumes and/or irregular plate motion as is the case in the eastern North Atlantic.

Zusammenfassung

Die meisten Ozeaninsel-Vulkane verfügen über ausgeprägte Riftzonen, entlang derer die Inseln durch Intrusionen sowie Extrusionen vorzugsweise wachsen. Solche Riftzonen haben einen großen Einfluss auf Wachstum und Entwicklung eines Vulkans. Ziel dieser Studie ist deshalb ein besseres Verständnis der Entstehung und Entwicklung vulkanischer Riftzonen im Nordatlantik auf der Basis einer exemplarischen Studie des Madeira-Archipels (NE-Atlantik).

Madeira und die benachbarten Desertas-Inseln besitzen zwei Riftzonen, die sich nahe der Ostspitze Madeiras, der São Lourenço-Halbinsel, schneiden. Um einen möglichen Zusammenhang der beiden Riftsysteme zu untersuchen, wurden vulkanische Strukturen, Gesteinsalter sowie Gesteinszusammensetzungen der Desertas-Inseln und der São Lourenço-Halbinsel - das mögliche Bindeglied zwischen den Madeira- und Desertas-Riftzonen - untersucht. Barometrische Ergebnisse, abgeleitet von Fluideinschlussdaten und Daten des Klinopyroxen-Schmelze-Thermobarometers, lassen Rückschlüsse auf Tiefen von Magmenreservoiren und temporären Stagnationsniveaus zu und weisen auf einen mehrstufiger Magmenaufstieg hin: Hauptfraktionierung tritt in Magmenreservoiren innerhalb des Mantels auf (São Lourenço: 15-35 km Tiefe; Desertas Islands: 17-28 km) und aufsteigende Magmen stagnieren temporär innerhalb der Kruste (São Lourenço: 8-10 km; Desertas Islands: 2-3 km). Magmenstagnationsniveaus innerhalb der Kruste unter São Lourenço unterscheiden sich deutlich von denen unterhalb der Desertas-Riftzone, und es wurden keine Hinweise auf ein gemeinsames flaches Magmenreservoir gefunden, das beide Riftarme speist. Dies deutet darauf hin, dass Madeira und die Desertas-Inseln zwei Vulkanzentren mit getrennten Magmenfördersystemen darstellen. Ergebnisse einer detaillierten vulkanologischen Kartierung auf den Desertas-Inseln deuten auf die frühere Anwesenheit eines vulkanischen Zentrums am südlichen Ende und/oder im zentralen Bereich des Desertas-Rückens hin.

$^{40}Ar/^{39}Ar$ Gesteinsalter zeigen, dass der subaerische Vulkanismus auf den Desertas-Inseln länger dauerte als zuvor angenommen (>5,1-1,9 Ma) und somit deutlich mit dem Vulkanismus der Madeira-Schildphase (>4,6-0,7 Ma; Geldmacher et al., 2000) überlappt. Zudem zeigen neue Gesteinsalter, dass der Riftzonen-Vulkanismus bei São Lourenço von >5,3 bis 0,9 Ma andauerte, d.h. während der gesamten subaerischen Madeira-Schildphase. Eine eruptive Ruhephase zwischen 4 und 2,5 Ma auf São Lourenço fällt mit der Hauptphase des subaerischen Desertas-Vulkanismus zusammen, was auf eine Kopplung beider magmatischer Systeme schließen lässt. Hauptelement-, Spurenelement- sowie Sr-Nd-Pb-Isotopen-Zusammensetzungenen von Proben der Desertas als auch von São Lourenço gleichen denen vom Zentralteil Madeiras, was auf eine gemeinsame Magmenquelle hindeutet. In Übereinstimmung mit Daten von Zentral-Madeira, zeigen die São Lourenço-Laven eine charakteristische Entwicklung mit abnehmendem Alter: FeO_{tot}, SiO_2, Mg# und Sr- und Pb-Isotopenverhältnisse nehmen ab, während Nd-Isotopenverhältnisse zunehmen. Einige der Schildphasen-Proben von São Lourenço zeigen die am stärksten verarmten Sr-Nd-Pb-

Isotopenverhältnisse, während Desertas-Proben gleichen Alters die am stärksten angereicherten Pb- und Nd-Isotopenverhältnisse zeigen. Diese extremen Isotopen-Zusammensetzungen der São Lourenço-Proben können weder auf Mischung von Desertas- und Madeira-Schmelzen innerhalb der Kruste oder des Mantels noch auf lateralen Magmentransport von der Madeira-Riftzone zu den Desertas entlang São Lourenço zurückgeführt werden.

Die Beobachtungen und Rückschlüsse basierend auf den unterschiedlichen Methoden zeigen deutlich, dass Madeira und die Desertas-Inseln zwei getrennte Vulkansysteme darstellen, die in separaten Bereichen der Magmenquelle des Madeira-Plumes wurzeln. Das Aufkommen des Desertas-Vulkanismus wurde möglicherweise durch folgende Faktoren begünstigt: eine Lithosphärenflexur infolge der Last der Vulkangebäude von Madeira und Porto Santo, ein schwacher pulsierender Mantelplume und die irreguläre Bewegung der Afrikanischen Platte. Ein Wechsel der vulkanischen Aktivität zwischen den benachbarten Madeira- und Desertas-Riftzonen wird auf einen unregelmäßig geformten Plume mit lateraler Variation der Schmelzproduktion zurückgeführt. Die Bildung des stark elongierten Desertas-Riftsystems wird vermutlich durch ein lokales extensives Stressfeld zwischen den beiden überlappenden Madeira- und Desertas-Vulkanen verursacht. Die Entwicklung der Desertas-Riftzone unterscheidet sich somit wesentlich von zweiarmigen Riftsystemen mit einer zentralen Caldera wie sie typisch für hawaiianische Vulkane wie Kilauea sind. Dies spricht gegen eine direkte Übertragbarkeit hawaiianischer Riftzonen-Modelle auf Nordatlantische Hotspot-Vulkane, die mit einem schwachen Plume und irregulärer Plattenbewegung assoziiert sind.

I Introduction

Volcanic rift zones are primary structures of oceanic island volcanoes and have been investigated at many localities such as Hawaii, Iceland, the Azores and the Canary Islands (Fiske and Jackson, 1972; Carracedo, 1994; Walker, 1999; Gudmundsson, 2000). These features are sublinear, narrow zones along which the islands preferably grow by intrusion and extrusion. Once developed, rift zones play an important role in island structure and evolution because the volcanoes accrete largely by surface eruptions along the rift axes and by dykes intruding parallel to the rift at depth (Fiske and Jackson, 1972; Dieterich, 1988). Over time, these constructive processes result in the formation of conspiceously elongated volcano piles.

Destructive processes including huge landslides and flank collapses are also found to be associated with rift zones and make them a crucial factor for the stability of volcano flanks (Duffield, 1981; Holcomb and Searle, 1991; Carracedo, 1994; Moore et al., 1994; Gee et al., 2001). The relationship between rift zone and flank stability is illustrated by the occurrence of normal faults parallel to the rift axes and repeated flank collapses as described for Hawaii (e.g. Swanson et al., 1976) or the Canary Islands (e.g. Carracedo, 1994, 1999). Rift zones may hence promote sector collapses and localise volcanic hazards in terms of landslides and associated tsunamis. Knowledge of the internal structure and evolution of volcanic rifts is thus important for assessing flank stabilities, related volcanic hazards and civil protection.

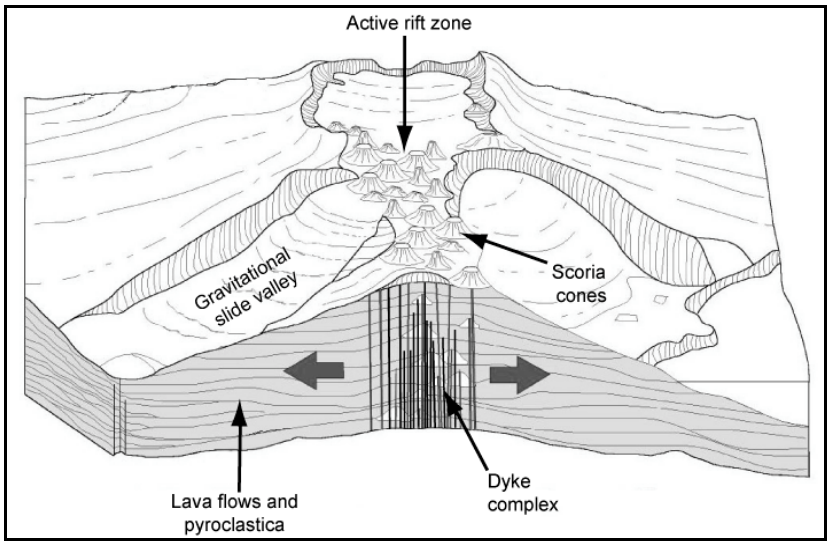

Fig. 1 Section of a rift zone modified after Carracedo (1994). Near surface, the rift zone is characterised by scoria cones and lava flows extending from the rift. A complex of coherent, steeply dipping dykes form the core of the rift. The density of the dyke complex increases with depth and towards the axis of the rift zone.

Near surface, rift zones are characterised by: (1) linear alignment of scoria and cinder cones stacked one onto another, (2) collinear dyke swarms, (3) lava flows extending from near the rift axis, and (4) rift-parallel normal faults and graben structures; (Fig. 1). The few examples where the interior of a rift zone is well exposed are restricted to deeply eroded volcanoes such as Koolau (Oahu, Hawaii; Fig. 2) which offer an insight into these systems at surface. Detailed studies of the

Koolau complex as a prototype of Hawaiian rift zones showed that they are underlain by a complex of coherent, steeply dipping dykes with increasingly dense packing with depth and towards the rift axis (Fig. 1; Walker, 1987, 1992). Since dykes develop as extensional fractures perpendicular to the direction of least compressive stress (Anderson, 1951; Fiske and Jackson, 1972; Nakamura, 1980; Gautneb and Gudmundsson, 1992), the orientation of a coherent dyke complex reflects the stress field within the volcanic edifice.

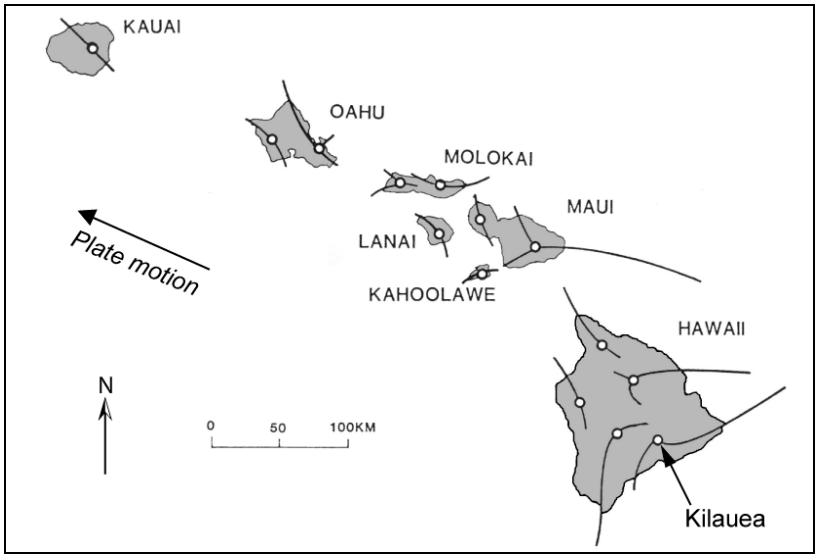

Fig. 2 Volcanic rift zones of the south-eastern Hawaiian islands (modified after Fiske and Jackson, 1972). The volcanoes are characterised by two- or three-armed rift systems. Each volcanic edifice comprises a central volcano (white circles) underlain by summit magma reservoir from which the rift arms (black lines) extend.

A deeper insight into the internal structure and the dynamics of a volcanic rift zone was provided by interdisciplinary studies at Kilauea (Hawaii; see review by Tilling and Dvorak, 1993). At this volcano, a central conduit feeds a summit reservoir at 2-4 km depth below a collapse caldera from which two rift arms emanate (Fig. 2). During a rifting event, magma migrates laterally from the summit reservoir into the adjacent rift where it can either erupt or be stored resulting in the formation of crystal mush or isolated pockets where melts differentiate and then solidify (Wright and Fiske, 1971; Garcia et al., 1989; Delaney et a.l., 1990). The composition of erupted lavas can be influenced by mixing of fresh and older magmas within the deep rift (Garcia et al., 1989, 1996) and/or by crustal assimilation during magma transport through the rift (Garcia et al., 1998). Therefore, volcanic rift systems can have a strong control on magma transport and evolution during ascent through the crust.

Why this study?

As outlined above, most of the present knowledge about rift zones is based on detailed studies at Hawaiian volcanoes such as Kilauea (e.g. Walker 1987, Dieterich 1988, Ryan 1988, Hill and Zucca 1987), and Iceland which is, however, characterised by a particular tectonic situation at the mid-

Atlantic ridge (Gudmundsson, 2000 and references therein). Hawaiian rift systems are typically characterised by a central volcano with a collapse caldera which is underlain by a summit reservoir feeding two or three rift arms (Fig. 2). Other ocean island volcanoes, however, can differ from such rift constitution. For example, studies at the Cumbre Vieja rift on La Palma (Canary Islands) show substantial differences to the rift system at Kilauea volcano (Hawaii). In particular, the Cumbre Vieja lacks a summit caldera and a shallow magma reservoir feeding the rift (Carracedo, 94; Klügel et al. 2000) which is probably related to eruption rates being lower on La Palma (0.15-0.37 km³/1000a; Ancochea et al., 1994) than at Kilauea (10-100 km³/1000a; Tilling and Dvorak, 1993). The question arises, then, if and how models for Hawaiian rift zones can be generalised and transferred to other ocean island volcanoes such as those in the eastern North Atlantic, where geodynamic conditions, including plate velocity or magma supply rate, differ from those in the Pacific region near Hawaii.

Why Madeira Archipelago?

The Madeira Archipelago, comprising the islands of Madeira, Porto Santo and the three ridge-shaped Desertas Islands (from N to S: Chão, Deserta Grande, Bugio; Fig. 3), is an ideal site to study the evolution of hotspot-related volcanoes and their rift zones in detail. The unique feature of the archipelago is the occurrence of two deeply eroded, well-developed rifts: the E-W trending Madeira rift zone and the NNW-SSE oriented Desertas rift zone. Both are characterised by swarms of steeply dipping collinear dykes, normal faults and graben structures, and abundant cinder cones stacked one on another. Due to deep erosion, the Madeira and Desertas rift zones provide a deep insight into their interior.

The archipelago is situated in the eastern North Atlantic 700 km from the northwestern coast of Africa at the southwestern end of the postulated Madeira hotspot track (Morgan, 1981; Geldmacher et al., 2000). The islands are located on Cretaceous oceanic crust (126-142 Ma; Klitgord and Schouten, 1986; Roest et al., 1992) and rise from about 4000 m water depth up to an elevation of 1896 m above sea level (summit of Pico Ruivo, Madeira Island). The three elongated Desertas Islands form the top of a 60 km long NNW-SSE-striking submarine ridge south-east of Madeira and rise up to 480 m above sea level. The axes of the Madeira and Desertas rift zones intersect at an angle of ~110° near São Lorenço peninsula, the easternmost tip of Madeira (Fig. 3). According to Geldmacher et al. (2000), they form a single volcanic system with a two-armed rift analogous to some Hawaiian volcanoes. Rock ages indicate that Desertas volcanism coincided with a period of volcanic quiescence and erosion on Madeira and that some coupling existed between the two rift arms. Therefore, the Desertas rift was tentatively viewed as a short-lived rift arm of Madeira.

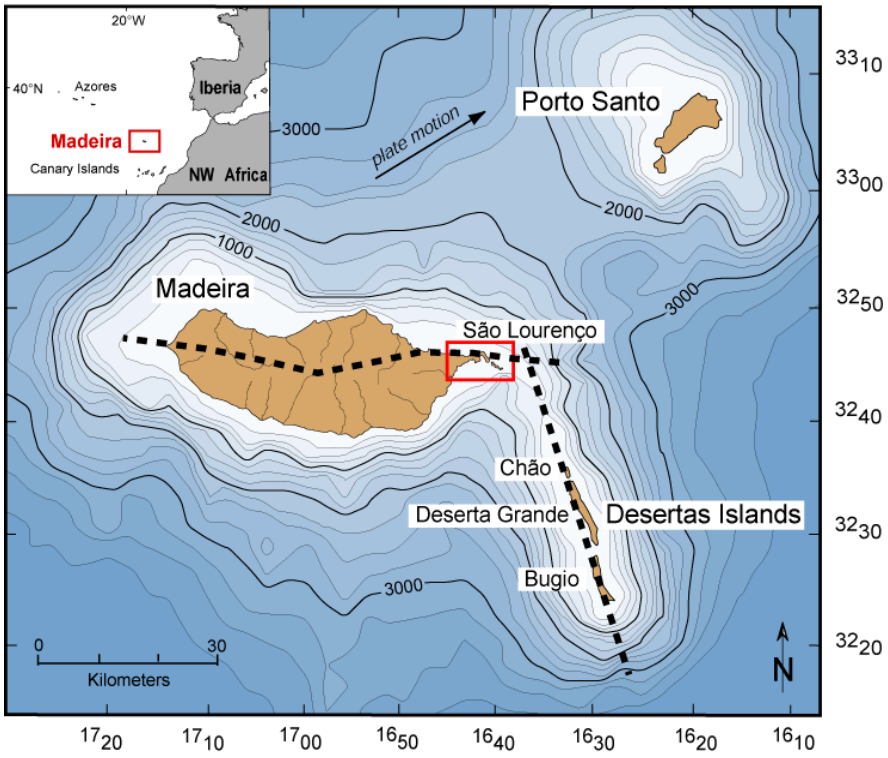

Fig. 3 Bathymetric map of the Madeira Archipelago. Source of bathymetry: TOPEX (Smith and Sandwell, 1997). Near the São Lourenço peninsula, the axes of the E-W oriented Madeira and NNW-SSE trending Desertas rift zones (stippled lines) intersect each other at an angle of 110°.

Apart from the rift geometry, Madeira Archipelago is particularly appropriate for a comparison with rift zones of Hawaiian volcanoes because it has developed under different geodynamic conditions. Both localities can be viewed as two endmembers of hotpot-related volcanism: (1) the endmember Hawaii, being located on the relatively fast-moving Pacific plate (10 cm/a; Clague and Dalrymple, 1987) and related to the most intense hotspot on Earth (buoyancy flux of the Hawaii plume: 8.7 x 10^3 kg/s; Sleep, 1990); and (2) the endmember Madeira Archipelago, having formed on the slow African plate with an average Cenozoic plate motion of ~ 1.2 cm/a near Madeira and being related to a very weak, pulsating or blob-type plume (Geldmacher et al., 2000). Thus, the comparison of these two endmembers allows to make inferences on how external conditions influence the formation and evolution of rift zones.

The main advantage of the Desertas Islands for a rift zone study is the exceptional exposure of its internal structure along the islands' steep cliffs as a result of prolonged erosion. This allows the detailed study and 3-dimensional reconstruction of the interior of this rift. Such a reconstruction combined with geochronological data can provide inferences on the temporal as well as spatial evolution of the Desertas rift. An ideal place to investigate the Madeira rift zone and its geochemical evolution over time is São Lourenço peninsula, the extremely well-exposed easternmost part of Madeira, near the projected juntion of the Madeira and Desertas rift axes. Due to the limited dimension of the area, lithological or geochemical variations can be ascribed to

temporal changes of the magmatic system rather than to spatial variations within the rift itself. The geographic position of São Lourenço may provide key information about the nature of a possible interconnection between the Madeira and Desertas rift systems.

In summary, the Madeira-Desertas complex is suitable for a rift study because of (1) the excellent rock exposures along the Desertas Islands and at São Lourenço, (2) the particular geometric configuration of the two rift systems, (3) the nature of their possible interconnection near São Lourenço, and (4) the geodynamic situation contrasting strongly with that at the Hawaiian Islands.

Aims of the study

The prime aims of this study are as follows:

- to reconstruct the volcanological structures of the Desertas rift zone and the eastern Madeira rift (São Lourenço),
- to clarify if Madeira and the Desertas rift zones were interconnected in terms of a two-armed rift system analogous to Hawaiian rifts or if they represent two distinct volcanoes with separate magma supply systems,
- to obtain information on the nature of a possible interconnection between two adjacent rift zones as exemplified by the Madeira-Desertas rifts,
- to provide insight in the generation and evolution of North Atlantic rift zones based on the examplary study of Madeira Archipelago,
- to compare the Madeira rift systems with those of Hawaiian volcanoes in order to elucidate principal differences between Hawaii, a hotspot with high magma production rates and located on the fast moving Pacific plate, and islands of the North Atlantic, ascribed to weak hotspots and located on the relatively slow-moving African plate,
- to improve our understanding of the formation and internal structure of volcanic rift zones.

In order to achieve these aims, the following methods were applied: detailed field studies on the Desertas Islands and at São Lourenço peninsula, geochemical analyses (major and trace elements, Sr-Nd-Pb isotopes), $^{40}Ar/^{39}Ar$ age determinations, and thermobarometry (fluid inclusion microthermometry and clinopyroxene-melt thermobarometry).

Overview of research

This dissertation comprises a study of volcanic rift zones in Madeira archipelago as a type example of ocean island volcanoes in the eastern North Atlantic. The results are treated in the following three chapters that have been or will be published as separate papers.

Chapter II: Melt extraction pathways and stagnation depths beneath the Madeira and Desertas rift zones (NE Atlantic) inferred from barometric studies, focuses on similarities and differences of the magma plumbing systems beneath São Lourenço/Madeira and the Desertas Islands. Fluid inclusion barometry and clinopyroxene-melt thermobarometry were applied to phenocrysts and xenoliths in order to reconstruct levels of magma stagnation beneath the two adjacent rift zones and to examine a possible genetic relationship during their evolution. The data suggest that Madeira and the Desertas represent separated volcanic systems rather than a two-armed rift and that both root in distinct regions of melt extraction. Magma focusing into the Desertas system is supposed to result from lithospheric bending caused by the load of the Madeira and Porto Santo shields, combined with regional variations in melt production due to an irregularly shaped plume.

Chapter III: Internal structure and evolution of a volcanic rift system in the eastern North Atlantic: The Desertas rift zone, Madeira archipelago, summarises the results of detailed field studies, 40Ar/39Ar age determinations and geochemical analyses from the Desertas Islands. A detailed volcanological map was compiled on the basis of several weeks of field work providing insight into the internal structure and evolution of the Desertas rift. The observed volcanic structures combined with rock ages indicate that a major volcanic centre was located at the southern end of the Desertas ridge and/or near its central part. In accordance with geobarometric data of Chapter II, the model presented in this chapter suggests that the Desertas ridge represents a discrete volcano which presumably became interconnected with Madeira by growth to the north-northwest. The initiation of Desertas volcanism is supposed to result from the combination of a weak pulsating mantle plume, irregular motion of the African plate and flexural stresses within the lithosphere caused by the loads of Madeira and Porto Santo islands.

Chapter IV: Geochemical evolution of volcanic rift systems in Madeira archipelago (NE Atlantic) presents a geochronological and geochemical study of the São Lourenço peninsula, the easternmost part of the Madeira rift zone which is supposed to play a pivotal role as a possible physical connector between Madeira and the Desertas Islands. This peninsula reflects the temporal and geochemical evolution of the Madeira rift since its stratigraphy covers the entire subaerial shield stage of Madeira within a well-confined area. In order to test the models developed in

Chapters II and III, comprising discrete Madeira and Desertas volcanos rather than a single volcanic complex with a two-armed rift, rock ages and geochemical data of lavas from São Lourenço are compared with those from the Desertas Islands. Sr-Nd-Pb isotope compositions and their evolution over time reveal that the two rift systems have not been interconnected. This confirms the hypothesis of Chapters II and III that the Desertas represent a distinct magmatic system which roots in particular regions of melt extraction within the Madeira source. To explain the shift of volcanic activity between Madeira and the Desertas, a revised model takes up the idea of an irregularly shaped Madeira plume causing lateral variations of the melting region and thus of volcanism occurring in Madeira Archipelago.

In summary, all different methods applied lead to the same conclusion, namely, that the Desertas ridge represents a separate magmatic system rather than a temporary rift arm of a single Madeira/Desertas volcanic complex. The new model presented in this study implies that two adjacent volcanoes such as the Madeira and Desertas systems can become interconnected by growth. A conceivable explanation for the formation of the Desertas rift zone is a local gravitative stress field causing preferred extension in-between the Madeira and Desertas edifices as they progressively overlapped. The evolution of the Desertas rift hence differs significantly from that of caldera-centered, two-armed rift systems typical for Hawaiian volcanoes. Models for Hawaiian rift zones are thus not necessarily transferable to ocean island volcanoes in the eastern North Atlantic. The concept of rift zone formation in-between two overlapping volcanic edifices may serve as a prototype to explain other North Atlantic rift zones as well, such as the Cumbre Vieja rift on La Palma or the Southern Ridge of El Hierro (both Canary Islands).

II Melt extraction pathways and stagnation depths beneath the Madeira and Desertas rift zones (NE Atlantic) inferred from barometric studies

Stefanie Schwarz, Andreas Klügel, Cora Wohlgemuth-Ueberwasser

Department of geology, University of Bremen, Germany

Submitted to Contributions to Mineralogy and Petrology:
Received 11.8.2003; accepted 19.12.2003; published online: 17.2.2004

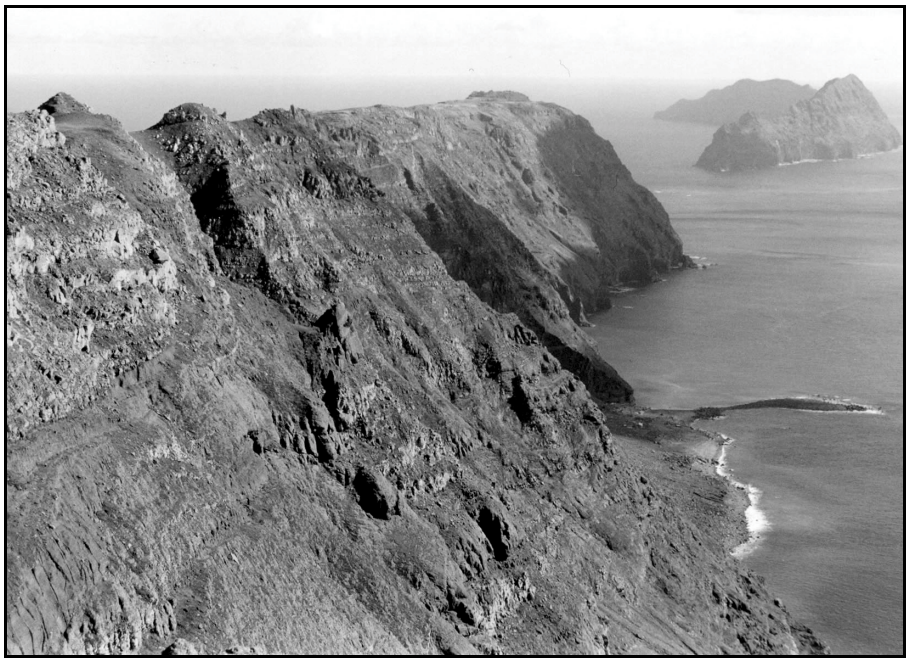

View from Pedregal (Deserta Grande) towards south of the sleeping dragon *Bugio*

Contrib Mineral Petrol (2004) 147: 228 240
DOI 10.1007/s00410-004-0556-4

ORIGINAL PAPER

Stefanie Schwarz · Andreas Klügel
Cora Wohlgemuth-Ueberwasser

Melt extraction pathways and stagnation depths beneath the Madeira and Desertas rift zones (NE Atlantic) inferred from barometric studies

Received: 14 August 2003 / Accepted: 19 December 2003 / Published online: 17 February 2004

Abstract The Madeira and Desertas Islands (eastern North Atlantic) show well-developed rift zones which intersect near the eastern tip of Madeira (São Lourenço peninsula). We applied fluid inclusion barometry and clinopyroxene-melt thermobarometry to reconstruct levels of magma stagnation beneath the two adjacent rifts and to examine a possible genetic relationship during their evolution. Densities of CO_2-dominated fluid inclusions in basanitic to basaltic samples from São Lourenço yielded frequency maxima at pressures of 0.57 0.87 GPa (23 29 km depth) and 0.25 0.32 GPa (8 10 km), whereas basanites, basalts and xenoliths from the Desertas indicate 0.3 0.72 GPa (10 24 km) and 0.07 0.12 GPa (2 3 km). Clinopyroxene-melt thermobarometry applied to Ti-augite phenocryst rim and glass/groundmass compositions indicates pressures of 0.45 1.06 GPa (15 35 km; São Lourenço) and 0.53 0.89 GPa (17 28 km; Desertas Islands) which partly overlap with pressures indicated by fluid inclusions. We interpret our data to suggest a multi-stage magma ascent beneath the Madeira Archipelago: main fractionation occurs at multiple levels within the mantle (>15 km depth) and is followed by temporary stagnation within the crust prior to eruption. Depths of crustal magma stagnation beneath São Lourenço and the Desertas differ significantly, and there is no evidence for a common shallow magma reservoir feeding both rift arms. We discuss two models to explain the relations between the two adjacent rift systems: Madeira and the Desertas may represent either a two-armed rift system or two volcanic centres with separate magma supply systems. For petrological and volcanological reasons, we favour the second model and suggest that Madeira and the Desertas root in distinct regions of melt extraction. Magma focusing into the Desertas system off the hotspot axis may result from lithospheric bending caused by the load of the Madeira and Porto Santo shields, combined with regional variations in melt production due to an irregularly shaped plume.

Electronic Supplementary Material Supplementary material is available for this article if you access the article at http://dx.doi.org/10.1007/s00410-004-0556-4. A link in the frame on the left on that page takes you directly to the supplementary material.

Editorial responsibility: J. Hoefs

S. Schwarz (✉) · A. Klügel · C. Wohlgemuth-Ueberwasser
Department of Geology, University of Bremen, Klagenfurter Straße, Geb. GEO, 28359 Bremen, Germany
E-mail: sschwarz@uni-bremen.de
Tel.: +49-421-2188974
Fax: +49-421-2189460

Introduction

Little is known about magma transport within the lithosphere slowly moving over a hotspot. Although studies of hotspot-related volcanic ocean islands such as Hawaii, the Canary Islands and Iceland have led to a better understanding of magma plumbing systems of ocean island volcanoes (Hawaii: e.g. Eaton and Murata 1960; Duffield et al. 1982; Clague 1987; Ryan 1988; Delaney et al. 1990; Tilling and Dvorak 1993; Canary Islands: e.g. Hansteen et al. 1998; Klügel et al. 2000; Iceland: e.g. Gudmundsson 1995), central questions remain. These include why different magma reservoirs form beneath the volcanoes, their depths, their evolution over time and their control on magma petrogenesis. Moreover, it is not clear how magma supply systems of adjacent volcanoes may be interconnected and which inferences can be made about melt pathways within the lithosphere.

The Madeira Archipelago is an ideal site to study the evolution of hotspot-related volcanoes and their rift zones in detail. The unique feature of the archipelago is the occurrence of two well-developed volcanic rift zones exposed by deep erosion: the E W-trending Madeira rift zone and the NNW SSE-oriented Desertas rift. They have been interpreted to represent a two-armed volcanic

rift system, with activity shifting between both arms (Geldmacher et al. 2000). The possible genetic relationship of the magma supply systems of the two rift arms is, however, still unknown.

Thermobarometry is a suitable approach to address this question. Former studies have shown that depths of magma storage can be estimated from densities of fluid inclusions trapped in phenocrysts and xenoliths (Roedder 1965, 1983; De Vivo et al. 1988; Belkin and De Vivo 1993; Szábo and Bodnar 1996; Hansteen et al. 1998; Andersen and Neumann 2001). In addition, pressure and temperature can be derived from the compositions of glass and coexisting clinopyroxene phenocryst rims to infer depths of magma reservoirs (Putirka et al. 1996).

In this paper, we present fluid inclusion and clinopyroxene-melt thermobarometric data from the Desertas Islands and São Lourenço, the easternmost tip of Madeira located near the projected junction between the two rift arms. Our geobarometric data, combined with geochronological data on the evolution of the islands, provide a first model of magma storage beneath the two rifts. We compare our results with current models of magma transport and storage beneath two-armed rift systems such as Kilauea, and discuss if and how the Madeira and Desertas rifts may have been interconnected. Finally, we show what constraints can be placed on the distribution of volcanism of the Madeira/Desertas complex.

Geological setting

The Madeira Archipelago is located in the eastern North Atlantic, 700 km from the north-western coast of Africa. The archipelago consists of five islands: Madeira, Porto Santo and the three Desertas Islands (from N to S: Ilhéu Chão, Deserta Grande, Ilhéu Bugio; Fig. 1). The island of Madeira is interpreted as the present locus of the Madeira hotspot which can be traced back to 70 Ma (Geldmacher et al. 2000). The main island rises from about 4,000-m water depth to an elevation of 1,896 m above sea level, and the Desertas to an elevation of 480 m. The underlying oceanic crust is about 140 Ma old (Pitman and Talwani 1972).

Madeira and the Desertas Islands are interpreted to represent a single volcanic complex, with a two-armed rift system consisting of the E–W-oriented Madeira rift arm and the NNW–SSE-oriented Desertas rift arm (Geldmacher et al. 2000). Their rift axes intersect at an angle of ~110° near Ponta de São Lorenço, the easternmost tip of Madeira (Fig. 1). The Madeira-Desertas volcanic system is characterised by a shield stage and a post-erosional stage (Geldmacher et al. 2000). The shield stage can be divided into (1) the Early Madeira rift phase (EMRP, >4.6–3.9 Ma), comprising the submarine basement and the oldest subaerial rocks of Madeira, (2) the Desertas rift phase (DRP, 3.6–3.2 Ma), with a shift

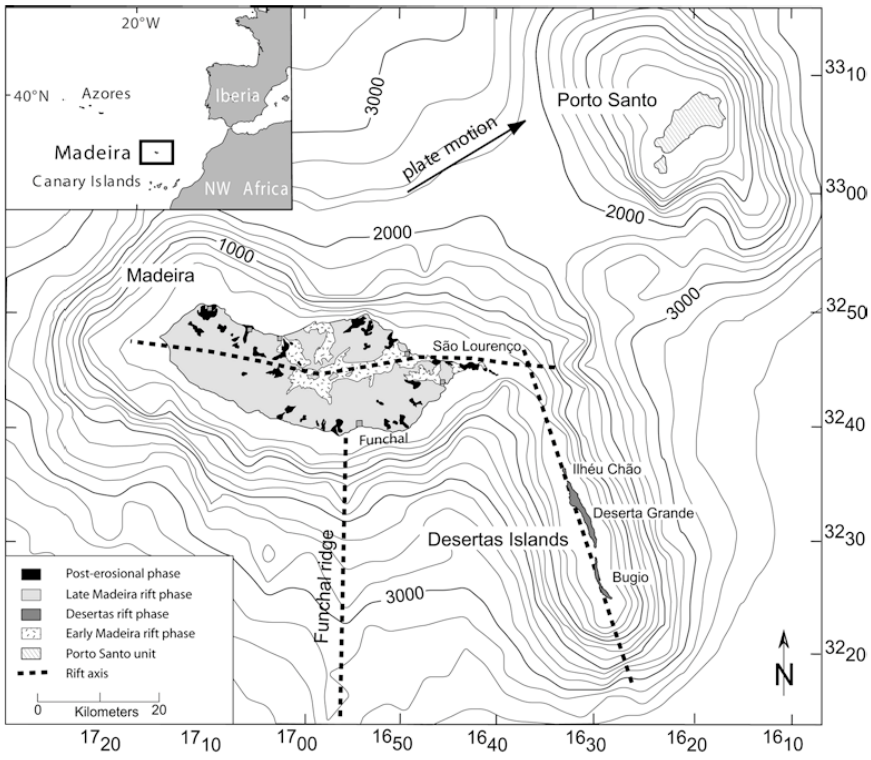

Fig. 1 Bathymetric and geological map of the Madeira Archipelago. Source of bathymetry: TOPEX (Smith and Sandwell 1997); geology modified after Geldmacher et al. (2000). Near São Lourenço, the axes of the Madeira and Desertas rift zones intersect each other at an angle of 110°. The NS-trending submarine ridge south of Funchal is also interpreted as a volcanic rift zone and presumably represents the location of most recent volcanic activity

of subaerial volcanic activity from the Madeira rift to the Desertas rift arm, and (3) the Late Madeira rift phase (LMRP, 3.0–0.7 Ma), during which the activity switched back to Madeira along the E–W-trending rift system. During the post-erosional stage (PE, < 0.7 Ma), cinder cones, tephra layers and intracanyon flows were deposited after a period of inactivity and erosion. New $^{40}Ar/^{39}Ar$ age determinations (van den Bogaard, unpublished data) show that the oldest subaerial rocks on Madeira are exposed on São Lourenço and that the stratigraphic sequence of the peninsula covers the complete Madeira shield stage with ages of 5.1–4.0 Ma (EMRP) and 2.6–0.97 Ma (LMRP). Furthermore, the new data indicate that subaerial volcanism on the Desertas extended from at least 5.07 to 2.7 Ma, and thus partly overlaps with the Early and Late Madeira rift phases.

Another rift arm of Madeira is located to the south of Funchal (Fig. 1) and forms a 50-km-long, submarine ridge with at least a dozen volcanic cones which occur clustered at the southern tip. This structure, hereafter referred to as the Funchal ridge, was discovered, mapped and sampled during cruise M51/1 of the German research vessel Meteor (Hoernle et al. 2001). The freshness of most samples suggests that this rift arm may still be active.

Rock types

Madeira and the Desertas Islands are characterised by alkaline rocks ranging from picrites and basanites to benmoreites (Fig. 2). The main phenocryst phases of alkali basalts and basanites from the Desertas Islands and São Lorenço are olivine and clinopyroxene (Ti-rich augite). Some basalts and hawaiites additionally contain plagioclase phenocrysts. Despite similar whole-rock geochemistry, significant and systematic petrographic differences between São Lorenço and the Desertas Islands can be observed (see Table 1). Olivine and especially clinopyroxene megacrysts (> 1 cm in size) occur commonly on the Desertas Islands but only locally on São Lorenço. Amphibole megacrysts (up to 4-cm diameter) occur exclusively on the Desertas Islands. Basalts with olivine as the only phenocryst phase are abundant on São Lourenço, whereas Desertas basalts usually contain olivine plus clinopyroxene phenocrysts. Fluid inclusions are far more abundant in phenocrysts of Desertas basalts than in those from São Lorenço. These observations suggest distinctive magma chamber processes, magma ascent rates and/or stagnation levels.

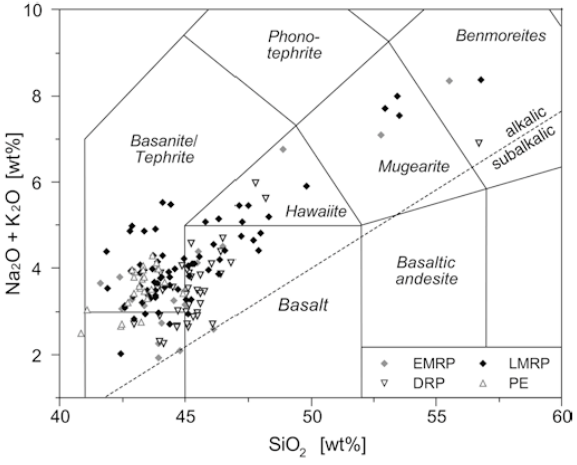

Fig. 2 TAS diagram of basaltic samples from the rift phases of the Madeira/Desertas volcanic complex (Geldmacher and Hoernle 2000), using the field boundaries of Le Maitre et al. (1989). Volcanic rocks are subdivided into alkalic and subalkalic after McDonald (1968). *EMRP* Early Madeira rift phase, *DRP* Desertas rift phase, *LMRP* Late Madeira rift phase, *PE* post-erosional phase on Madeira

Analytical methods

Geobarometric data were obtained by microthermometry of fluid inclusions and by mineral-melt equilibria. Fluid inclusions were observed in 100-μm, doubly polished plates from lavas, dikes and xenoliths from Deserta Grande and Bugio (Desertas Islands), São Lourenço and the Funchal ridge. Microthermometric measurements were carried out on a Linkam THMSG 600 heating-cooling stage calibrated with SYNFLINC synthetic fluid inclusion standards at −56.6 (CO_2) and 0 °C (H_2O). Melting and homogenisation temperatures are reproducible to better than ±0.2 °C. Inclusion densities were derived from Angus et al. (1976), and isochores were calculated using the computer program Flincor (Brown 1989), utilizing the Kerrick and Jacobs (1981) equation of state for the CO_2–H_2O system. In order to determine the possible presence of components other than CO_2, Raman microspectroscopy of two representative samples was carried out at the Institute of Geoscience, University of Leoben.

Mineral and glass analyses were performed on JEOL JXA 8900 electron microprobes (universities of Göttingen, Frankfurt and Kiel) operated at an acceleration voltage of 15 kV. Glasses were analysed with a beam current of 8 nA and a defocussed beam of 10 μm, minerals with 20 nA and a focussed beam. To determine average compositions, at least 15 points per glass sample and four points per clinopyroxene were measured.

Fluid inclusion barometry

All samples studied are porphyritic with 10–15% olivine and clinopyroxene phenocrysts, some containing plagioclase as additional phenocryst phase. Most Bugio basalts are ankaramites with 40–50% phenocrysts up to 1 cm in size. In addition, fluid inclusions in two xenoliths of spinel wehrlite (DES4) and spinel dunite (DGR132) from Deserta Grande and in a harzburgite xenolith from the southern tip of the Funchal ridge were analysed. Petrographic descriptions of xenoliths are given in the Appendix.

Table 1 Lithological and petrographic differences between Desertas and São Lorenço volcanics

		Desertas Islands	São Lourenço EMRP	LMRP
Field observations				
Ankaramites		Abundant as lava flows and tuffs	Rare	Very rare
Phenocrysts > 4 mm		Abundant, especially cpx crystals up to 2-cm diameter	Rare, max. -cm diameter	Very rare
Xenoliths		Some peridotites and few gabbros	None	None
Petrographic observations				
Phenocrysts	Ol and cpx	Nearly always ol plus cpx (~90% of samples)	Commonly ol plus cpx (~75% of samples)	Only ol in ~55% of samples
	Plag	Tabular habit Single crystals	Elongated habit Often glomerocrysts	Very rare
	Amph	Megacrysts up to 4-cm diameter in some lavas and pyroclastics	None	None
Fluid inclusions in phenocrysts		Abundant	Very rare	Rare

Occurrence of fluid inclusions

Several generations of CO_2-dominated fluid inclusions occur abundantly in olivine and clinopyroxene phenocrysts and in the xenoliths. They can be divided into (1) primary inclusions occurring singly or in groups which do not form trails, and (2) secondary or texturally late inclusions forming trails reaching, and sometimes crossing, grain boundaries. Some inclusions which show textural evidence of partial decrepitation with measurable fluid phases were not incorporated. Common inclusion sizes are 3 to 15 μm, seldom >20 μm. In general, fluid inclusions are far more abundant in phenocrysts of samples from the Desertas Islands than from São Lourenço. In the xenoliths, secondary fluid inclusions are the main inclusion type and are common in olivine, but relatively rare in clinopyroxene.

Microthermometry of fluid inclusions

Composition of fluid inclusions

Upon rapid cooling, all fluid inclusions froze to aggregates between −70 and −100 °C of solid CO_2; further cooling to about −190 °C produced no visible phase changes. Upon heating of the inclusions from about −190 °C, the following phase transitions were observed: (1) initial and final melting of CO_2 (Tm) between −57.4 and −56.4 °C, and (2) final homogenisation of liquid and vapour (L + V) into liquid (Th_L) or into vapour (Th_V) at less than 31.1 °C. In many cases, phase transitions of inclusions homogenising into vapour could not be accurately determined due to optical constraints. Therefore, Th_V data do not reveal distinct statistical maxima but, nevertheless, they have to be considered as significant.

Few inclusions show Tm below the triple point for pure CO_2 (−56.6 °C), which most likely results from thermal gradients in the heating-cooling stage. Raman analysis of some of these inclusions revealed no fluid components other than $CO_2$and traces of CO. There is no evidence for the presence of H_2O, although H_2O is expected as a component in fluids exsolved from mafic melts (Dixon et al. 1997). This indicates that diffusive hydrogen loss from fluid inclusions may have occurred at high temperatures (Bakker and Jansen 1991), changing original fluid inclusion compositions. Another feasible process to remove H_2O from the inclusion fluid are hydration reactions between the fluid and the host mineral forming secondary minerals such as amphiboles, sheet silicates or carbonates (Andersen et al. 1984; Andersen and Neumann 2001; Frezotti et al. 2002). We did not observe any sign of secondary products, although this may be related to small inclusion diameters (mostly < 10 μm).

By assuming that the fluid phase coexisting with mafic melt had an $XH_2O = H_2O/(CO_2 + H_2O)$ of 0.1, which is an upper limit for basanitic melts at 1,000 MPa (Dixon et al. 1997; Sachs and Hansteen 2000), all calculated inclusion densities would increase by 4.5%. Because of possible error introduced by such an assumption, we present original rather than corrected density data throughout this study, calculated for pure CO_2, and consider the possible error in the discussion.

Homogenisation temperatures and inclusion densities

The measured homogenisation temperatures of all inclusions and their resulting densities are presented in Figs. 3 and 4. Inclusion densities show distinctive histogram maxima (intervals) in their frequency distribution. For convenience, we subsequently define the limits of each interval such as to comprise 90% of the respective data points.

Basalts and xenoliths from Deserta Grande Both primary and secondary fluid inclusions homogenised into liquid between 12.6 and 30.3 °C in olivine and at 14.8 to 27.8 °C in clinopyroxene. Some measured inclusions in olivine phenocrysts homogenised into vapour at 22 to

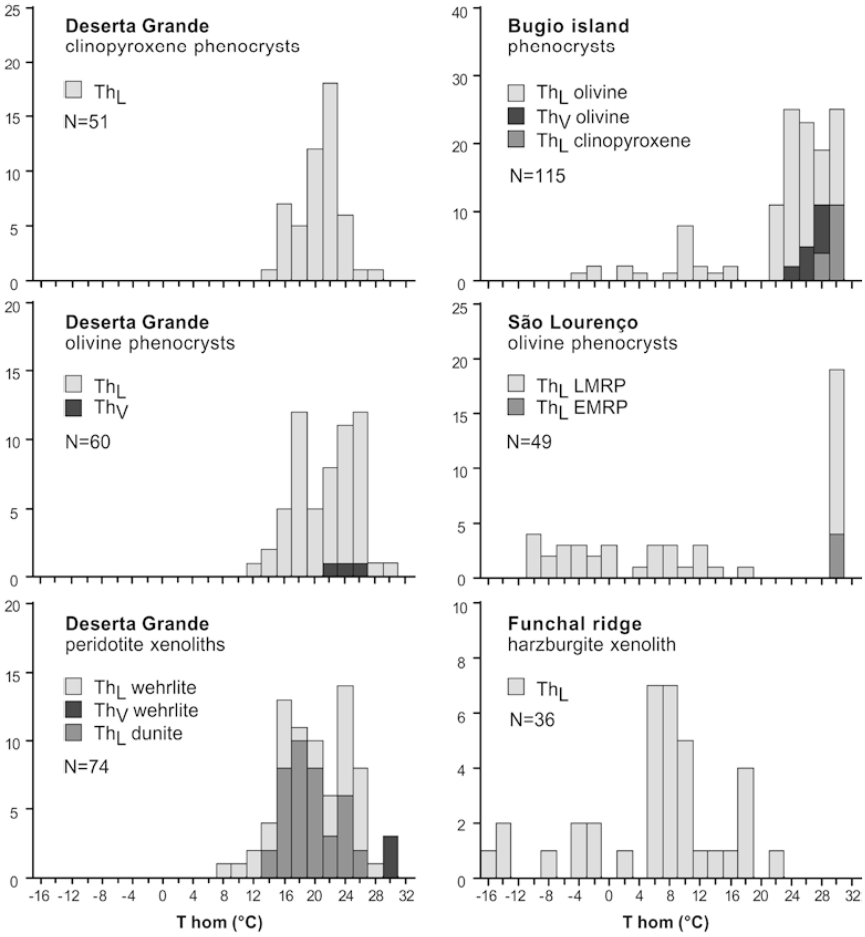

Fig. 3 Distribution of homogenisation temperatures of CO_2-dominated fluid inclusions in phenocrysts of basaltic rocks and xenoliths from the Desertas Islands and São Lorenço. Th_L homogenised into liquid, Th_V homogenised into vapour

25.3 °C (Th_V). These values correspond to densities ranging from 0.22 to 0.83 g cm^{-3} with two maximum intervals: (1) between 0.22 and 0.24 g cm^{-3} and (2) between 0.7 and 0.82 g cm^{-3}. Inclusions in olivine of peridotite xenoliths showed Th_L between 7.5 and 27.9 °C, and some inclusions in wehrlite olivine homogenised at Th_V~29 °C. Resulting density maxima occur at 0.7 to 0.83 g cm^{-3}, overlapping with those of inclusions in phenocrysts, and at 0.31 to 0.32 g cm^{-3}.

Basalts from Bugio Almost all fluid inclusions were observed in olivine phenocrysts, with Th_L ranging from −4.3 to 30.9 °C. Homogenisation temperatures < 15 °C occur exclusively in texturally early fluid inclusions. Some inclusions show vapour homogenisation at 24.1 to 28.2 °C. Inclusions in clinopyroxene homogenised into liquid at 28.4 to 29.8 °C. These Th data give densities ranging from 0.23 to 0.95 g cm^{-3} with three frequency maxima: (1) 0.23 to 0.29 g cm^{-3}, (2) 0.6 to 0.75 g cm^{-3} and (3) 0.83 to 0.93 g cm^{-3}. In summary, the shallow and intermediate density maxima overlap with those from Deserta Grande, but a third higher-density range can additionally be observed.

Basalts from São Lourenço Primary as well as secondary inclusions were observed in olivine phenocrysts in one EMRP sample (SL106) and in three LMRP samples. In general, the inclusions homogenised into liquid at temperatures between −10 and 30.4 °C. Compared with samples from the Desertas Islands, homogenisation temperatures are more dispersed and tend to lower values. No fluid inclusions homogenising into vapour were found. Fluid inclusions in sample SL106 give densities of 0.60 g cm^{-3}. For the LMRP samples, resulting density maxima occur at (1) 0.56 to 0.60 g cm^{-3} and (2) 0.84 to 0.99 g cm^{-3}.

Harzburgite xenolith from the Funchal ridge Primary as well as texturally late fluid inclusions were observed in

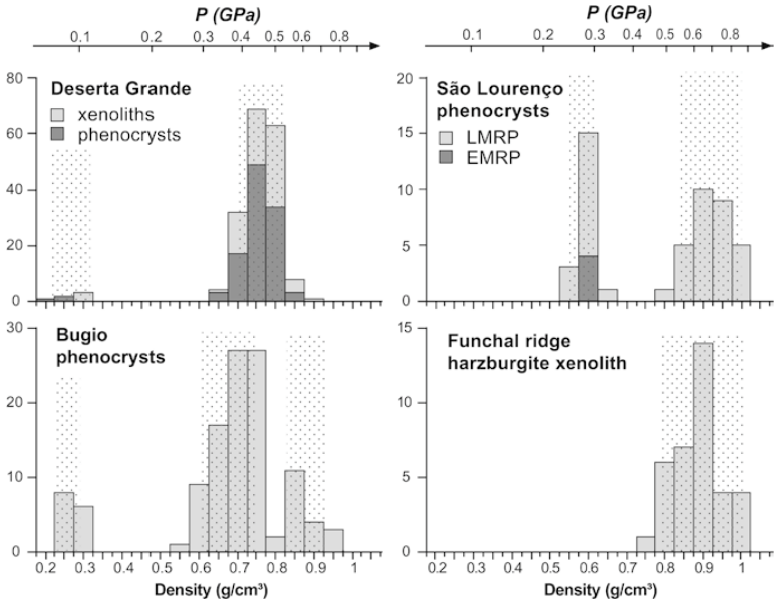

Fig. 4 Density distribution of CO_2-dominated fluid inclusions in basalts and xenoliths from the Desertas Islands and São Lorenço. Densities were derived from Angus et al. (1976). Pressures were calculated for model temperatures of 1,150 °C and pure CO_2, using the Kerrick and Jacobs (1981) equation of state. *Dotted areas* symbolise density intervals comprising 90% of the respective data points

olivine porphyroclasts. All homogenised into liquid between −15.1 and 22.5 °C, comprising the lowest homogenisation temperatures of this study. Resulting densities range from 0.74 to 1.01 g cm^{-3}, with a maximum between 0.78 and 1.01 g cm^{-3} overlapping with the high density ranges of the Desertas Islands and São Lourenço.

Pressures of inclusion formation

Density data of CO_2-dominated fluid inclusions can provide constraints on the pressures at which they were entrapped during crystal growth or crack healing or at which they re-equilibrated (Roedder and Bodnar 1980; Roedder 1984). Pressures of inclusion formation or re-equilibration corresponding to calculated densities were derived assuming a model temperature of 1,150 °C as based on clinopyroxene-melt thermobarometry (see below). Since isochores of CO_2 inclusions have moderately positive slopes (Fig. 6), variations in model temperature have only little effect on calculated pressures.

If one assumed a constant H_2O fraction of 10% rather than pure CO_2 for all inclusions, different isochores would result (Kerrick and Jacobs 1981). For a density range between 0.2 and 1.05 g cm^{-3} for pure CO_2 inclusions, as observed in the present study (Fig. 4), the corresponding pressures would increase from 0.063–1.01 (pure CO_2) to 0.07–1.28 GPa ($X_{H2O} = 10\%$), i.e. by 11 to 26%. These values may be considered as an upper limit of systematic error.

Due to decrease of inclusion densities by diffusive loss of H_2O as well as re-equilibration of fluid inclusions during magma ascent, the following estimates represent *minimum* pressures.

Desertas Islands

Densities indicated by fluid inclusions in phenocrysts from Desertas Grande overlap perfectly with those in xenoliths and yield two intervals corresponding to the following pressures: (1) 0.07 to 0.12 GPa, and (2) 0.4 to 0.53 GPa. Inclusion densities from Bugio samples largely overlap with these ranges (Fig. 4). However, three density intervals can be distinguished whose corresponding pressure limits slightly differ from those of Deserta Grande: (1) 0.075–0.1 GPa, (2) 0.29–0.44 GPa, and (3) 0.55–0.71 GPa.

São Lourenço

EMRP samples indicated pressures of 0.29 GPa, and fluid inclusion data of LMRP samples yield two density maxima corresponding to the following pressures: (1) 0.26 to 0.29 GPa and (2) 0.57 to 0.85 GPa. In contrast to the Desertas Islands, no shallow pressure range around 0.1 GPa could be identified, and no fluid inclusions yielded pressures between 0.32 and 0.49 GPa. The higher pressure range of São Lourenço partly overlaps with the highest pressure range indicated by fluid inclusions in samples from Bugio (Desertas), but tends to higher values.

Funchal ridge

Fluid inclusion densities from Funchal ridge samples yield pressures between 0.48 and 0.9 GPa, overlapping

with data from Desertas Islands and São Lourenço but extending towards higher pressures.

Clinopyroxene-melt thermobarometry

Mineral-melt equilibration pressure (P) and temperature (T) were calculated with the thermobarometer of Putirka et al. (1996) which is based on the exchange of jadeite/diopside/hedenbergite components between clinopyroxene and melt.

Sample description and preparation

Investigated lapilli samples from São Lourenço (SL163, LMRP), Deserta Grande (DGR101, DGR123) and Bugio (DBU101) have glassy to tachylitic groundmass with plagioclase, olivine and augite micro-phenocrysts (up to 300 μm, olivine up to 1 mm). Only sample DBU101 has clinopyroxene and plagioclase phenocrysts up to 4 mm. A submarine basalt (M51/1-447DR-1) from the southern tip of the Desertas ridge was investigated and has a tachylitic matrix with plagioclase, olivine and clinopyroxene phenocrysts and locally some fresh glass at the rim.

Since fresh glassy material was rare, some porphyritic samples were chosen for groundmass separation. These samples have a fresh matrix of plagioclase, clinopyroxene, olivine and Fe Ti oxides in different ratios, and contain euhedral, optically zoned clinopyroxene and olivine phenocrysts. More differentiated samples (e.g. SL151) additionally contain elongated plagioclase phenocrysts. Separated matrix was powdered, fused on an Ir filament and quenched under air at the Institute of Mineralogy (University of Frankfurt).

Data selection

Pressure and temperature data are based on EMP analyses of coexisting augite rim and glass compositions. EMP measurements on sector-zoned clinopyroxenes were generally avoided. Possible equilibrium between clinopyroxenes and melt was tested following the empirical relation of Duke (1976):

$$\log(Fe_{tot}/Mg)_{cpx} = -0.564 + 0.755 * \log(Fe_{tot}/Mg)_{liq}$$

If the deviation between measured and predicted Fe/Mg ratio was significant for several analyses within a single clinopyroxene, the data were rejected. In case of a systematic deviation for all clinopyroxenes within a common sample, the data were incorporated. Such systematic deviations could be ascribed to differing redox potentials and Fe^{2+}/Fe^{3+} ratios which were not considered by Duke (1976).

According to Putirka et al. (1996), the mean prediction errors of the thermobarometer are ±30 K and ±140 MPa. As an independent consistency test of the data, calculated temperatures were compared to those of thermometers based on olivine + liquid equilibria (Roeder and Emslie 1970; Ford et al. 1983; Putirka 1997).

PT-calculations

Desertas Islands

Most samples from the Desertas Islands indicate pressures between 0.57 and 0.82 GPa and temperatures ranging from 1,140 to 1,180 °C (Table 2, Fig. 5). Ol-melt thermometers after Roeder and Emslie (1970), Putirka (1997) and Ford et al. (1983) predict equilibrium temperatures between 1,170 and 1,175 °C which largely agree with the cpx-melt data. Although data obtained by mineral-melt barometry overlap with the highest pressure range indicated by fluid inclusions (Fig. 6b), they generally tend to higher pressures. This difference can be related to re-equilibration of fluid inclusions during magma ascent as well as decrease of inclusion densities by diffusive loss of H_2O.

Pressure predictions of sample K8 from Bugio are exceptional since they scatter over a wide range between 0.13 and 0.89 GPa (Table 2). The values largely overlap with the pressure ranges indicated by fluid inclusions within the prediction error of the clinopyroxene-melt barometer (Fig. 6).

São Lourenço

Mineral-melt thermobarometry applied to EMRP samples yield pressures between 0.45 and 1.06 GPa (Fig. 5). The data can be divided into two PT intervals: (1) from 0.45 to 0.68 GPa and 1,160 to 1,190 °C, and (2) from 0.7 to 1.06 GPa and 1,180 to 1,235 °C (Figs. 5, 6a). Both P intervals overlap with the highest pressure range for fluid inclusions in LMRP samples from São Lourenço (0.56 0.83 GPa; Fig. 6a). Deviations of pressure estimates below the range for fluid inclusions are within the prediction error of the barometer (±0.14 GPa). Compared to data from the Desertas Islands, the range of pressure estimates for São Lourenço tends to higher values, in accordance with results from the fluid inclusion barometry.

The LMRP lapilli sample (SL163) yields temperatures of 1,150 1,160 °C which are in accordance with crystallisation temperatures of peridotite xenoliths from NW and SE Madeira (1,150 1,300 °C; Munha et al. 1990). Calculated pressures range from 0.56 to 0.64 GPa and overlap clearly with the lower P interval indicated by EMRP samples and, additionally, with the highest pressure range for fluid inclusions in LMRP samples (Fig. 6c).

Discussion

Depths of magma fractionation and stagnation

Our thermobarometric data provide the base for a first model of magma plumbing systems beneath the

Table 2 Results of PT calculations after Putirka et al. (1996)

São Lourenço							Desertas Islands							
Sample#	SL2[a]	SL106[a]	SL122[a]	SL150[a]	SL151[a]	SL152[a]	SL163[b]	DGR101	DGR123	DGR29	DBU101	M51/1-447DR-1	K8	
No. of cpx	6	8	9	8	4	9	6	5	6	6	5	5	6	
P range (GPa)	0.5–0.63	0.45–0.68, 1.02–1.06	0.47–0.57, 0.7–0.95	0.75–0.91	0.58, 0.78–1.01	0.79–1.03	0.56–0.64	0.57–0.69	0.57–0.66	0.67–0.82	0.6–0.73	0.58–0.68	0.13–0.15, 0.37, 0.53–0.56, 0.89	
T range (°C)	1,160–1,170	1,170–1,190, 1,220	1,184–1,190, 1,201–1,219	1,195–1,210	1,167, 1,182–1,199	1,215–1,235	1,150–1,160	1,165–1,175	1,145–1,150	1,175–1,185	1,150–1,160	1,150–1,160	1,120, 1,137, 1,150, 1,179	
P mean of range (GPa)	0.55	0.57, 1.04	0.51, 0.85	0.85	0.58, 0.88	0.95	0.61	0.63	0.61	0.76	0.68	0.65		
T mean of range (°C)	1,165	1,180,1,220	1,186,1,214	1,205	1,167,1,190	1,227	1,154	1,147		1,180	1,153	1,153		
Rock type	Basaltic lava flow	Basaltic dike	Basaltic dike	Basaltic dike	Basanitic dike	Basaltic dike	Lapilli	Lapilli	Lapilli	Basanite flow	Lapilli	Basanite	Beach boulder (basalt)	

[a]Early Madeira rift phase
[b]Late Madeira rift phase

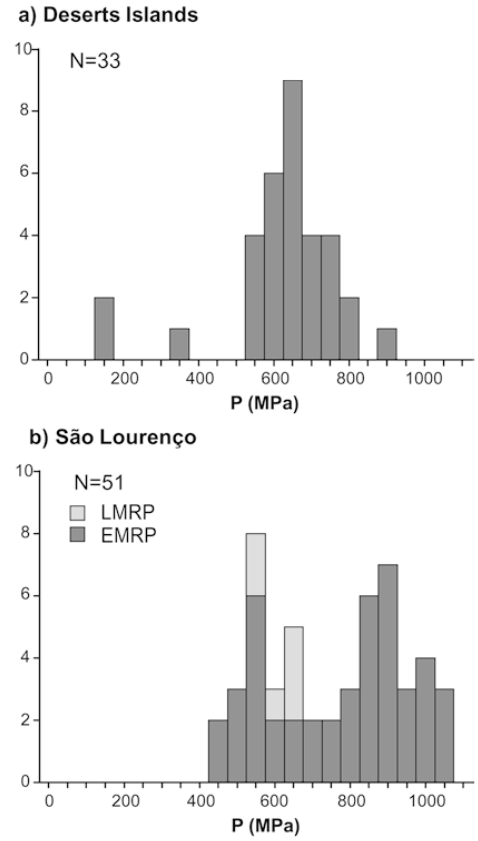

Fig. 5a, b Crystallisation pressures of clinopyroxene phenocrysts in basaltic rocks from **a** the Desertas Islands and **b** São Lorenço, obtained by clinopyroxene-melt barometry after Putirka et al. (1996). Each pressure value represents the conditions of crystallisation for a single clinopyroxene phenocryst

Madeira/Desertas volcanic complex. We interpret the pressure calculations derived from mineral-melt barometry to reflect major levels of crystal fractionation. The pressure data obtained by fluid inclusion barometry were interpreted to imply magma stagnation, degassing and crystal fractionation at a corresponding range of depths. Since inclusion densities may rapidly re-equilibrate during ascent, they additionally indicate depths of temporary magma stagnation at shallower levels.

São Lourenço—Early Madeira rift phase

During the EMRP, major levels of magma fractionation beneath São Lourenço were located at 15–35 km depth, as documented by clinopyroxene-melt barometry (Fig. 6a). Further magma stagnation at about 9 km depth is manifested by few fluid inclusions, but not by clinopyroxene-melt barometry. This observation suggests that magmas stagnated temporarily in the lower oceanic crust.

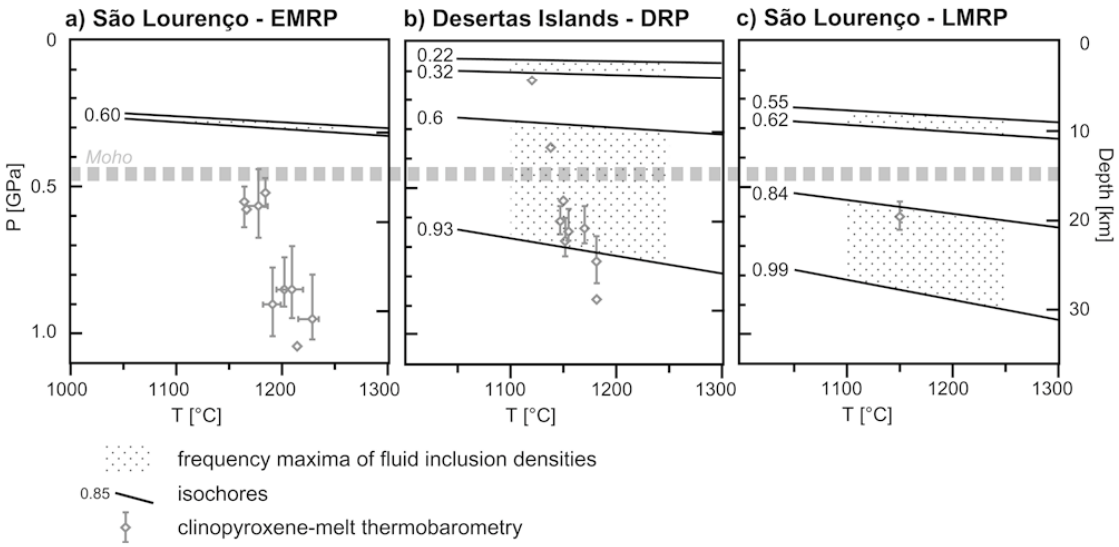

Fig. 6a–c PT diagram summarising fluid inclusion and mineral-melt barometry data applied to basaltic rocks from **a** São Lourenço (*EMRP* Early Madeira rift phase),**b** the Desertas Islands (*DRP*Desertas rift phase) and **c** São Lorenço (*LMRP* Late Madeira rift phase). *Dotted areas* Frequency intervals of fluid inclusion density (see Fig. 4), *shaded symbols* ranges of PT conditions of clinopyroxene fractionation, *quadrangles*mean values of the respective ranges (see Table 2)

Desertas Islands—Desertas rift phase

Clinopyroxene-melt barometry indicates major crystal fractionation of Desertas lavas at 17–28 km depth (Fig. 6b). This range overlaps well with fluid inclusion data from Bugio which yield a density maximum corresponding to pressures between 0.55 and 0.72 GPa (18–23 km depth, Fig. 4). Further magma stagnation, degassing and crystallisation of mafic magmas at 9–17 km depth is manifested by fluid inclusion data from Deserta Grande as well as Bugio (Fig. 6b), and by clinopyroxene-melt barometry (sample K8, Table 2). Fluid inclusions in phenocrysts and xenoliths from Deserta Grande yield a significant frequency maximum at pressures between 0.39 and 0.55 GPa (Fig. 4), corresponding to 12–16 km depth. This range may coincide with the Moho which we suppose to be located at 14–15 km depth, by analogy to the western Canary Islands (Banda et al. 1981) showing a similar age of the underlying oceanic crust (ca. 160 Ma, Roeser 1982). The data may thus reflect a main stagnation and fractionation level near the Moho, possibly a crystal mush zone. This situation is comparable to the Canary Islands where fluid inclusions indicate that primitive melts and their xenoliths may reside at Moho or lower crustal depths prior to eruption (Hansteen et al. 1998).

Finally, both fluid inclusions and mineral-melt barometry indicate a further level between 2 and 4 km depth (Fig. 6b), which demonstrates resetting of fluid inclusions and additional clinopyroxene fractionation at shallower depths during temporary magma stagnation. This stagnation level coincides with a level of neutral buoyancy inferred for the Kilauea volcano, Hawaii (Ryan 1988), and could reflect shallow rift pathways in the upper crust near the base of the volcanic edifice (Fig. 7a).

São Lourenço—Late Madeira rift phase

Main fractionation levels of lavas erupted during the LMRP are located at 18–28 km depth as indicated by fluid inclusion barometry as well as clinopyroxene-melt barometry (Figs. 6c, 7). This range overlaps with fractionation depths during the EMRP and with fractionation levels indicated by Desertas samples.

In contrast, a geobarometric study applied to ultramafic cumulate xenoliths in LMRP units from NW and SE Madeira infers pressures of phenocryst accumulation between 1.2 and 1.5 GPa corresponding to magma reservoirs at 39–48 km depth (Munha et al. 1990). Since our pressure calculations reflect the last equilibration conditions of clinopyroxene prior to eruption and do not preclude deeper magma reservoirs, we believe that the combined data indicate crystal fractionation occurring over a wide depth range.

As is the case for EMRP samples, another shallower pressure range at 0.26 and 0.32 GPa is indicated only by fluid inclusions (Fig. 6c) and suggests temporary magma stagnation at 8–10 km depth in the lower oceanic crust prior to eruption (Fig. 7a).

Funchal ridge

Fluid inclusion densities presented from the southern tip of the Funchal ridge indicate major fractionation between 16 and 28 km depth. Magma stagnation within the upper crust is not indicated by our dataset. Since the

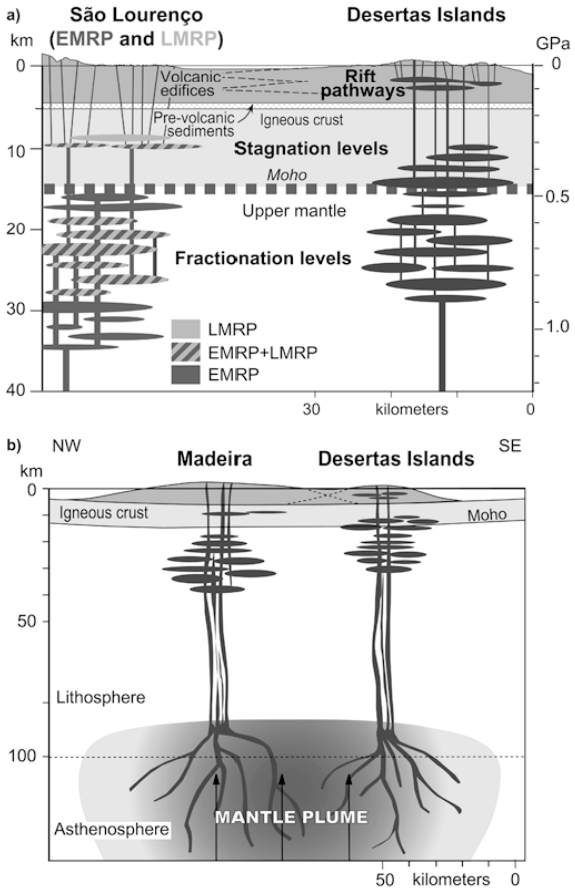

Fig. 7a Section through the oceanic crust and the uppermost mantle illustrating our model of magma transport and storage systems beneath São Lorenço and the Desertas Islands. **b** Sketch of inferred melt extraction pathways. Madeira and the Desertas are interpreted to represent two volcanoes which root in distinct regions of melt extraction within the ascending mantle plume

Funchal ridge is supposed to be the youngest magmatic system of the Madeira Archipelago (Hoernle et al. 2001), shallow stagnation levels may not have developed yet.

Two-armed rift system or separate volcanic systems?

Our data indicate significant differences as well as some similarities between the magma plumbing systems and inferred stagnation levels beneath São Lorenço and the Desertas Islands (Fig. 7). The observations can be explained by two end-member models: (1) the island of Madeira and the Desertas ridge represent two rift arms of a single volcanic system with an interconnection near São Lourenço (Geldmacher et al. 2000), or (2) they represent two separate volcanic systems with independent magma plumbing systems.

Model 1: two-armed rift system

Multiple-armed rift systems are a common feature of oceanic island volcanoes such as Kilauea/Hawaii (Walker 1999) or Tenerife/Canary Islands (Carracedo 1994). Typically, these systems are characterised by a central volcano from which two or three rift arms extend. In the case of Kilauea, the central summit is underlain by a shallow magma reservoir at 2–4 km depth (Ryan 1988) which feeds two rift arms by lateral magma injection mostly along dikes. The following observations point to an interconnection of the Madeira and the Desertas rifts in terms of a two-armed system analogous to Kilauea:

1. Madeira and the Desertas ridge intersect each other near São Lourenço and appear to form a continuous volcanic edifice (Fig. 1), suggesting that both rift arms extend from a centre near the eastern tip of Madeira.
2. The gap in volcanic activity on Madeira during the Desertas rift phase may indicate a close link between the respective magma supply systems, such as an interconnection of magma reservoirs.
3. Mineral-melt barometry as well as fluid inclusion barometry of samples from the Madeira and Desertas rift phases indicate overlapping fractionation levels at 15–28 km depth (Figs. 6, 7a). This may suggest a common magma reservoir and/or lateral magma transport to the rift zones at these depths, possibly along the mantle–oceanic crust boundary where density changes and subhorizontal layering could facilitate such a scenario.
4. Major element, trace element and radiogenic isotope characteristics of shield-stage volcanics from Madeira and the Desertas are broadly similar and show a continuous evolution over time (Geldmacher and Hoernle 2000), which suggests a common magma source for both systems.

Model 2: separate volcanic systems

The alternative model considers Madeira and the Desertas as two discrete, overlapping volcanoes with separate magma supply systems, a situation analogous to, e.g. the adjacent Kilauea and Loihi edifices. The following observations and considerations argue in favour of this hypothesis:

1. There is no petrological or field evidence for a shallow magma reservoir near São Lourenço, arguing against lateral magma transport from a central reservoir into the Madeira and Desertas rift arms. In addition, the inferred depths of shallow magma stagnation beneath São Lourenço during both the Early and Late Madeira rift phases are significantly below those of the Desertas rift phase (Fig. 6). There is thus no progressive evolution of a crustal storage system towards shallower depths as proposed for Hawaiian volcanoes (Clague 1987), which is suggestive of two separate magma plumbing systems.

2. If the magma supply systems of Madeira and the Desertas had been interconnected, lateral magma transport over tens of kilometres must have taken place in the uppermost mantle or near the Moho where fractionation levels overlap (Fig. 7). Lateral transport along dikes is possible only where an appropriate stress field exists, e.g. within a volcanic edifice (Dieterich 1988). Alternatively, if horizontal compressive stresses are higher than the vertical stress, horizontal intrusions may form (Gudmundsson 1995). Both scenarios, however, seem unlikely to provoke lateral magma transport over tens of kilometres in the uppermost mantle beneath Madeira.
3. There are systematic lithological differences between the São Lourenço and Desertas samples (Table 1). Moreover, fluid inclusions in São Lourenço samples are far less abundant than in Desertas rocks, indicating less fluid entrapment during crystal growth or crack healing. This implies either faster magma ascent from the fractionation levels to the surface, less degassing during fractionation, slower crystal growth, or different volatile contents of the parental magmas. These differences are best explained by distinctive magma transport systems beneath São Lourenço and the Desertas.
4. The present morphology is characterized by maximum elevations in the central parts of Madeira and the Desertas and a depression, rather than a rise, near the intersection of both rift axes (Fig. 1). Moreover, units of the EMRP occur up to 1,300 m above sea level in central parts of Madeira (Geldmacher et al. 2000), but only up to 175 m on São Lourenço. Such morphology and stratigraphy are hard to reconcile with a two-armed rift system emerging from a central volcano near São Lourenço.

Inferences on volcano distribution

After considering all arguments discussed above, we favour the model of two separate volcanoes with distinct magma plumbing systems (Fig. 7). As a consequence, the Madeira and Desertas volcanoes should root in distinct regions of melt extraction within the ascending mantle plume (Fig. 7b). The question arises, then, why the spatial and temporal succession of volcanic activity of the Madeira-Desertas complex is not in accordance with that expected from the hotspot track (Fig. 1). We propose the following model to explain (1) the occurrence of volcanism off the hotspot track, (2) the coupling of Madeira and Desertas volcanism, and (3) the concept of distinct regions of melt extraction whilst maintaining geochemical continuity.

Island spacing of hotspot systems can be controlled by lithosphere flexure due to the load of volcanic shields (Ten Brink 1991). At the transition between flexural depression and bulge, where horizontal flexural stresses are approximately zero, magma flow to the surface may be facilitated, forming a new volcano. For a steady source of melt underneath a moving lithospheric plate, this process produces a chain of discrete volcanoes along a single or dual line (Hieronymus and Bercovici 1999). In contrast, the Madeira hotspot track is ascribed to a weak, pulsating plume (Geldmacher et al. 2000), the shape and flow of which may be influenced by mantle convection. It is conceivable that such a pulsating plume becomes irregularly shaped, causing lateral variations of the melting region. Combined with the flexure model of Ten Brink (1991), this effect could result in a disperse volcano pattern, rather than a line. Although data are lacking, a lithosphere flexure beneath the Madeira Archipelago is likely when compared to the analogous situation of the western Canary Islands (Collier and Watts 2001). We thus presume that the Desertas ridge is located at a lithospheric bend caused by the Madeira and Porto Santo loads, a location with a stress field facilitating ascent of magmas through the lithosphere (Fig. 8). Lateral variations of the melting region, combined with slow plate motion and flexural stress, could have initiated the Desertas volcanism off the hotspot track and caused the shift of activity between Madeira and the Desertas (Fig. 8). This model is in accordance with the geochemical continuity of the Madeira/Desertas complex over time (Geldmacher and Hoernle 2000), which requires a common magma source for both.

Conclusions

The results presented in this paper show that thermobarometric data not only provide information about the depths of magma fractionation and stagnation, but additionally allow inferences on relations between adjacent volcanic systems to be made. Fluid inclusion data as well as mineral-melt barometry indicate systematic differences as well as some similarities between the magma plumbing systems beneath the rift zones of São Lourenço/Madeira and the adjacent Desertas Islands. For both systems, levels of magma fractionation and stagnation were identified within both the uppermost mantle and the crust. São Lourenço samples of Early and Late Madeira rift phases indicate similar levels of magma stagnation within the crust which differ from those beneath the Desertas. This observation suggests that there is no common shallow magma reservoir feeding both the Madeira and the Desertas rifts. A deeper interconnection of the two rift systems within the uppermost mantle or the lower crust by lateral magma transport appears unlikely. We propose that Madeira and the Desertas represent two separate volcano systems, rather than a single volcanic complex with two rift arms. Distinctive magma pathways down to at least 35 km depth imply that both volcanoes root in distinct regions of partial melting within the Madeira plume. The shift of volcanic activity between Madeira and the Desertas may be a result of lateral variations of the melting region in an irregularly shaped

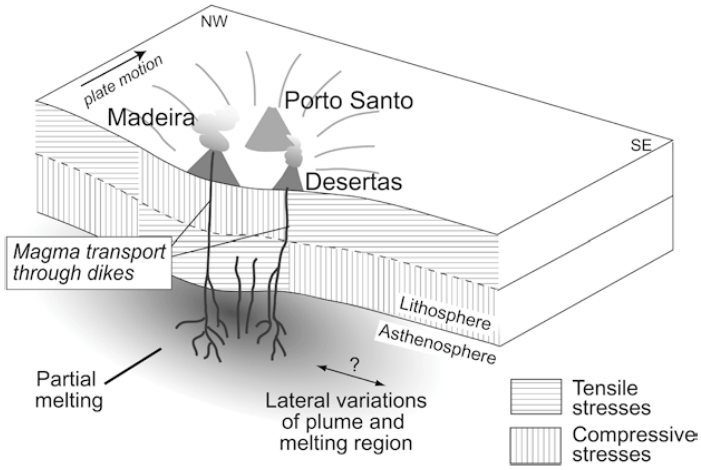

Fig. 8 Schematic section through the lithosphere beneath Madeira perpendicular to plate motion, illustrating the influence of lithosphere flexure on magma ascent (modified after Hieronymus and Bercovici 1999). Hypothetical lithosphere bending due to the load of Madeira and Porto Santo is strongly exaggerated. At the transition between flexural depression and flexural bulge, horizontal stresses are approximately zero, facilitating rise of magma through dikes up to the surface aside the hotspot axis and causing the Desertas volcanism

plume, combined with flexural stresses within the lithosphere due to the loads of Madeira and Porto Santo. This model could explain the shift of volcanic activity between Madeira and the Desertas Islands, and possibly of other hotspot volcanoes as well.

Acknowledgements We thank directors Costa Neves and Susana Fontinha and the staff of the Parque Natural da Madeira for their logistical support during our field studies on São Lourenço and the Desertas Islands. Without their help the study of the islands would not have been possible. Bärbel Kleinefeld is acknowledged for help during microthermometric analysis and for providing Raman measurements. Especial thanks go to Andreas Kronz, Heidi Höfer and Peter Appel for assisting with the EMP measurements. The paper benefited from discussions with Colin Devey, and early versions of the manuscript improved through the critical comments of Kaj Hoernle and the constructive reviews of Thor Hansteen and Tom Andersen. The research was supported by the Deutsche Forschungsgemeinschaft (DFG grant KL1313/2-1).

Appendix

Xenolith petrography

DES4

Spinel wehrlite consisting to about 80% of early-formed olivine up to 3 mm with some kink bands, and 20% of interstitial clinopyroxene with abundant melt inclusions. Cpx is associated with late-formed and smaller, euhedral to subhedral olivines (< 0.5 mm) and small spinels (< 250 μm). Fine-grained spinels (about 20 μm) occur throughout the xenolith. Low intracrystalline deformation and the occurrence of interstitial clinopyroxene with olivine inclusions is evidence for a cumulate origin of the xenolith.

DGR132

Spinel dunite with coarse-grained olivine up to 8 mm in size showing abundant kink bands, melt and fluid inclusions, and euhedral to subrounded spinel up to 0.6 mm in size. Basaltic matrix of fine-grained clinopyroxene, olivine and plagioclase locally occurs in cracks and pockets and is interpreted as host melt which penetrated along grain boundaries and cracks. The dunite xenoliths are interpreted as cumulates.

M51/1-437DR-1

Harzburgite from the submarine Funchal ridge with abundant fluid inclusions. Olivine porphyroclasts (about 80%) from 1 to 6 mm in size show curvilinear grain boundaries and abundant kink bands. Orthopyroxenes porphyroclasts (20%) with clinopyroxene exsolution lamellae show embayments at the xenolith surface, demonstrating that they have reacted with the surrounding melt. No oxide minerals were found. Because of the deformation indicated by kink bands and the resorbed pyroxenes rims, the xenolith is interpreted to represent a fragment of the refractory mantle beneath Madeira.

References

Andersen T, Neuman E-R (2001) Fluid inclusions in mantle xenoliths. Lithos 55:301–320 DOI 10.1016/S0024-4937(00)00049-9

Andersen T, O'Reilly SY, Griffin WL (1984) The trapped fluid phase in upper mantle xenoliths from Victoria, Australia: implications for mantle metasomatism. Contrib Mineral Petrol 88:72–85

Angus S, Armstrong B, de Reuck KM, Altunin VV, Gadetskii OG, Chapela GA, Rowlinson JS (1976) Carbon dioxide (International tables of fluid state, vol 3). Pergamon Press, Oxford

Bakker RJ, Jansen JBH (1991) Experimental post-entrapment water loss from synthetic CO_2-H_2O inclusions in natural quartz. Geochim Cosmochim Acta 55:2215–2230 DOI 10.1016/0016-7037(91)90098-P

Banda E, Dañobeitia JJ, Surinach E, Ansorge J (1981) Features of crustal structure under the Canary Islands. Earth Planet Sci Lett 55:11–24

Belkin HE, De Vivo B (1993) Fluid inclusion studies of ejected nodules from plinian eruptions of Mt. Somma-Vesuvius. J Volcanol Geotherm Res 58:89 100 DOI 10.1016/0377-0273(93)90103-X

Brown PE (1989) FLINCOR: a fluid inclusion data reduction and exploration program. In: Program Abstr Vol 2nd Biennal Pan-Am Conf Fluid Inclusions, 4 7 January 1989, Virginia Polytechnic Institute, State University, Blacksburg, VA, pp 14

Carracedo JC (1994) The Canary Islands: an example of structural control on the growth of large ocean-island volcanoes. J Volcanol Geotherm Res 60:225 241 DOI 10.1016/0377-0273(94)90053-1

Clague DA (1987) Hawaiian xenolith populations, magma supply rates, and development of magma chambers. Bull Volcanol 49:577 587

Collier JS, Watts AB (2001) Lithospheric response to volcanic loading by the Canary Islands: constraints from seismic reflection data in their flexural moat. Geophys J Int 147:660 676 DOI 10.1046/j.0956-540x.2001.01506.x

Delaney PT, Fiske RS, Miklius A, Okamura AT, Sako K (1990) Deep magma body beneath the summit and rift zones of Kilauea Volcano, Hawaii. Science 247:1311 1316

De Vivo B, Frezzotti ML, Lima A, Trigila R (1988) Spinel lherzolite nodules from Oahu island (Hawaii): a fluid inclusion study. Bull Minéral 111:307 319

Dietrich JH (1988) Growth and persistence of Hawaiian volcanic rift zones. J Geophys Res 93:4258 4270

Dixon JE, Clague DA, Wallace P, Poreda R (1997) Volatiles in alkalic basalts from the North Arch volcanic field, Hawaii: extensive degassing of deep submarine-erupted alkalic series lavas. J Petrol 38:911 939

Duffield WA, Christiansen RL, Koyanagi RY, Peterson D W (1982) Storage, migration and eruption of magma at Kilauea Volcano, Hawaii, 1971 1972. J Volcanol Geotherm Res 13:273 307

Duke JM (1976) Distribution of the period transition elements among olivine, calcic clinopyroxene and mafic silicate liquid: experimental results. J Petrol 17:499 521

Eaton JP, Murata KJ (1960) How volcanoes grow. Science 132:925 938

Ford CE, Russell DG, Craven JA, Fisk MR (1983) Olivine-liquid equilibria: temperature, pressure and composition dependence of the crystal/liquid cation partition coefficients for Mg, Fe2 + , Ca and Mn. J Petrol 24:256 265

Frezotti ML, Andersen T, Neumann E-R, Simonsen SL (2002) Carbonatite melt-CO_2 fluid inclusions in mantle xenoliths from Tenerife, Canary Islands: a story of trapping, immiscibility and fluid-rock interaction in the upper mantle. Lithos 64:77 96

Geldmacher J, Hoernle KA (2000) The 72 Ma geochemical evolution of the Madeira hotspot (eastern North Atlantic): recycling of Paleozoic (500 Ma) oceanic lithosphere. Earth Planet Sci Lett 183:73 92 DOI 10.1016/S0012-821X(00)00266-1

Geldmacher J, Bogaard P v d, Hoernle KA, Schmincke HU (2000) The $^{40}Ar/^{39}Ar$ age dating of the Madeira Archipelago and hotspot track (eastern North Atlantic). G3 Geochem Geophys Geosys 1:1999GC000018

Gudmundsson A (1995) Infrastructure and mechanism of volcanic systems in Iceland. J Volcanol Geotherm Res 64:1 22 DOI 10.1016/0377-0273(95)92782-Q

Hansteen TH, Klügel A, Schmincke HU (1998) Multi-stage magma ascent beneath the Canary Islands: evidence from fluid inclusions. Contrib Mineral Petrol 132:48 64 DOI 10.1007/s004100050404

Hieronymus CF, Bercovici D (1999) Discrete alternating hotspot islands formed by interaction of magma transport and lithospheric flexure. Nature 397:604 607 DOI 10.1038/17584

Hoernle KA, Shipboard Scientific Party (2001) Meteor-Berichte, Cruise 51, Leg 1. In: Hemleben C, Hoernle KA, Jørgensen BB, Roether W (eds) Ostatlantik-Mittelmeer-Schwarzes Meer, Cruise No. 51, 12 September-28 Dezember 2001. Universität Hamburg, Meteor-Berichte 03-1

Kerrick DM, Jacobs GK (1981) A modified Redlich-Kwong equation for H_2O, CO_2 and H_2O-CO_2 mixtures at elevated temperatures and pressures. Am J Sci 281:735 767

Klügel A, Hoernle KA, Schmincke H-U, White JDL (2000) The chemically zoned 1949 eruption on La Palma (Canary Islands): petrologic evolution and magma supply dynamics of a rift-zone eruption. J Geophys Res 105:5997 6016

Le Maitre RW, Bateman P, Dudek A, Keller J, Lameyre J, Le Bas MJ, Sabine PA, Schmid R, Sorensen H, Streckeisen A, Wooley AR, Zanettin B (1989) A classification of igneous rocks and glossary of terms recommendations of the International Union of Geological Sciences Subcommission on the Systematics of Igneous Rocks. Blackwell, Oxford, pp 193

MacDonald GA (1968) Composition and origin of Hawaiian lavas. In: Coats RR, Hay RL, Andersen CA (eds) Studies in volcanology: a memoir in honour of Howel Williams. Geol Soc Am Mem 116:477 522

Munha J, Palacios T, MacRae ND, Mata J (1990) Petrology of ultramafic xenoliths from Madeira island. Geol Mag 127:543 566

Pitman W, Talwani M (1972) Sea floor spreading in the north Atlantic. Geol Soc Am Bull 83(3):619 646

Putirka K (1997) Magma transport at Hawaii: Inferences based on igneous thermobarometry. Geology 25:69 72 DOI 10.1130/0091-7613(1997)025<0069:MTAHIB>2.3.CO;2

Putirka K, Johnson M, Kinzler R, Longhi J, Walker D (1996) Thermobarometry of mafic igneous rocks based on clinopyroxene-liquid equilibria, 0 30 kbar. Contrib Mineral Petrol 123:92 108 DOI 10.1007/s004100050145

Roedder E (1965) Liquid CO_2 inlcusions in olivine-bearing nodules and phenocrysts from basalts. Am Mineral 50:1746 1782

Roedder E (1983) Geobarometry of ultramafic xenoliths from Loihi Seamount, Hawaii, on the basis of CO_2 inclusions in olivine. Earth Planet Sci Lett 66:369 379

Roedder E (1984) Fluid inclusions. In: Ribbe PH (ed) Reviews in Mineralogy 12. Mineral Soc Am, Washington, DC

Roedder E, Bodnar RJ (1980) Geologic pressure determinations from fluid inclusion studies. Annu Rev Earth Planet Sci 8:263 301

Roeder PL, Emslie RF (1970) Olivine-liquid equilibrium. Contrib Mineral Petrol 29:275 289

Roeser HA (1982) Magnetic anomalies in the magnetic quiet zone off Morocco. In: Rad UV, Hinz K, Sarntheim M, Seibold E (eds) Geology of the northwest African continental margin. Springer, Berlin Heidelberg New York, pp 61 68

Ryan MP (1988) The mechanics and three-dimensional internal structure of active magmatic systems: Kilauea volcano, Hawaii. J Geophys Res 93:4213 4248

Sachs PM, Hansteen TH (2000) Pleistocene underplating and metasomatism of the lower continental crust: a xenolith study. J Petrol 41:331 356

Smith WHF, Sandwell DT (1997) Global seafloor topography from satellite altimetry and ship depth soundings. Science 277:1956 1962

Szábo CS, Bodnar RJ (1996) Changing magma ascent rates in the Nógrád-Gömör volcanic field Northern Hungary/Southern Slovakia: evidence from CO_2-rich fluid inclusions in metasomized upper mantle xenoliths. Petrology 4:240 249

Ten Brink U (1991) Volcano spacing and plate rigidity. Geology 19:397 400

Tilling RI, Dvorak JJ (1993) Anatomy of a basaltic volcano. Nature 363:125 133

Walker GPL (1999) Volcanic rift zones and their intrusion swarms. J Volcanol Geotherm Res 94:21 34 DOI 10.1016/S0377-0273(99)00096-7

EMS

For electronic supplementary material (**eTable 1** Compositions of glass and fused groundmass (wt.%); **eTable 2** Compositions of clinopyroxene rims (wt.%)) see *Electronic Appendix*.

III Internal structure and evolution of a volcanic rift system in the eastern North Atlantic: The Desertas rift zone, Madeira archipelago

S. Schwarz [a, *], A. Klügel [a], P. van den Bogaard [b], J. Geldmacher [b]

[a] Universität Bremen, Fachbereich Geowissenschaften, Bremen, Germany
[b] IFM-GEOMAR, Kiel, Germany

Submitted to Journal of Volcanology and Geothermal research
Received: 12. 3. 2004

Endemic tarantula of the spider valley on Deserta Grande

Internal structure and evolution of a volcanic rift system in the eastern North Atlantic: The Desertas rift zone, Madeira Archipelago

S. Schwarz [a, *], A. Klügel [a], P. van den Bogaard [b], J. Geldmacher [b]

[a] *Universität Bremen, Fachbereich Geowissenschaften, Bremen, Germany*
[b] *IFM-GEOMAR, Kiel, Germany*

Submitted to Journal of Volcanology and Geothermal Research: 5.3.2004

Abstract

The three elongated Desertas Islands form the top of a 60 km long NW-SE-striking submarine ridge south-east of Madeira (NE Atlantic). The alignment of eruptive centres and parallel dyke swarms indicates that the islands represent a deeply eroded volcanic rift zone. Detailed field studies combined with $^{40}Ar/^{39}Ar$ age determinations and geochemical analyses reveal the internal structure and evolution of this rift, which may serve as a type example of North Atlantic rift zones. We found that bomb- and scoria-rich deposits, dykes and sills increase in frequency towards the south. The northern rift end is composed mainly of lava flows up to several meter thickness and few scoria. The central part is characterised by a 100-200 m thick basal sequence of tuff as a result of explosive eruptions due to magma-sea water interaction during the early subaerial stage. These layers are overlain by subhorizontal lava flows reflecting the change from dominantly explosive to more effusive volcanism during island growth. The southern part is dominated by tuff, scoria and cinder cones, minor lava flows and sills up to 30 m in thickness. $^{40}Ar/^{39}Ar$ ages show that subaerial Desertas volcanism lasted from 1.9 to >5.1 Ma and thus overlaps in age with the shield-building phases of Madeira island. Desertas lavas show no temporal or spatial variation in chemistry, except for samples from the top of the islands, erupted between 2 and ~3.4 Ma, which are strongly REE- and Y-enriched and thus unique in the archipelago. Our combined data suggest that a major volcanic centre was located at the southern end of the ridge and/or near its central part. In contrast to rift systems of Hawaiian volcanoes such as Kilauea, we did not find any volcanological or petrological indication of a central caldera underlain by a shallow magma reservoir feeding the rift. Our model presented suggests that the Desertas ridge represents a discrete volcano that became interconnected with Madeira by growth to the north-northeast. A conceivable explanation for the formation of the elongated Desertas rift is a local gravitative stress field causing preferred extension between the Madeira and Desertas edifices as they progressively overlapped. Our model thus emphasises the importance of edifice amalgamation and gravitative stress in the evolution of large volcanoes and their rift zones. The initiation of Desertas volcanism could be the result of a weak pulsating mantle plume and irregular motion of the African plate, combined with flexural stresses within the lithosphere due to the loads of Madeira and Porto Santo islands. Cessation of volcanism coincides with the exclusive occurrence of REE- and HREE-enriched lavas and may be related to a compositionally changing or exhausting mantle source. Our results indicate that models for Hawaiian rifts cannot necessarily be transferred to hotspot volcanoes associated with weak plumes and/or irregular plate motion.

Keywords: Volcanic rift zones, Desertas Islands, Madeira, $^{40}Ar/^{39}Ar$ age dating

Introduction

Volcanic rift zones are a common feature of ocean island volcanoes, for example: the Hawaiian and the Canary Islands. They define narrow zones along which the islands preferably grow by intrusion and extrusion (e.g. Carracedo, 1994, 1999; Walker 1999) resulting in elongated volcano piles. Along their topographic ridges, volcanic activity accumulates involving linear and parallel oriented dyke swarms, cinder cones stacked one onto another, and lava flows extending from this narrow zone. Many ocean island volcanoes have two- or three-armed rift systems where a central volcano is underlain by a shallow magma chamber feeding the rifts (Wright and Fiske 1971, Duffield 1982, Delaney and Dvorak 1993).

Rift zones play an important role on magma transport and thus influence the evolution and constitution of ocean islands. They localise volcanic hazards and may promote sector collapses. Hence, it is important to understand their internal structure and evolution. The interior of most rift zones, however, is not exposed, and only deeply eroded volcanoes such as Koolau (Oahu, Hawaii) offer an insight into these systems at surface (Walker, 1987, 1992). Studies revealed on Oahu showed that rift zones are generally underlain by coherent dyke intrusions. Since dykes develop as extensional fractures perpendicular to the direction of minimum compressive stress (Anderson, 1951; Nakamura, 1980, Gautneb and Gudmundsson, 1992), the orientation of a coherent dyke complex reflects the stress field of a volcano pile.

Most of the present knowledge about rift zones is based on observations from Hawaiian volcanoes (e.g. Walker, 1987; Dietrich, 1988; Ryan, 1988; Hill and Zucca, 1987). The question arises if and how Hawaiian models can be generalised and transferred to ocean islands such as Madeira and the Canary Islands. For this purpose, Madeira Archipelago is an ideal place to carry out an exemplary study, because it has two well-developed and deeply eroded rift zones, and the islands grew under general geodynamic conditions that differ totally from those of Hawaiian volcanoes. Whereas Hawaii is situated on the relatively fast-moving Pacific plate (10 cm/a; Clague and Dalrymple, 1987), Madeira Archipelago has grown on the slow African plate with an average Cenocoic plate motion of ~ 1.2 cm/a (Geldmacher et al., 2000). Another important difference between both systems is the hotspot intensity: In contrast to Hawaii with a high buoyancy flux of 8.7×10^3 kg/s (Sleep, 1990), the Madeira hotspot is related to a very weak, pulsating or blob-type plume (Geldmacher et al., 2000). The comparison of North Atlantic rift systems such as on Madeira with Hawaii possibly allows us to make inferences on how external conditions influence the formation and evolution of rift zones.

In order to gain insight in the rift systems of Madeira Archipelago, we have undertaken a detailed field study on the volcanological structures and evolution of the deeply eroded Desertas rift zone located south-east of Madeira island. In this paper, we present the results of

volcanological mapping combined with $^{40}Ar/^{39}Ar$ age determinations and new major and trace element data. Based on our field data, we compare the Desertas with the Koolau dyke complex (Oahu, Hawaii) as a prototype of Hawaiian rift zones and reconstruct the former constitution of the Desertas rift zone. Finally, we offer conceivable models to explain the evolution of the Desertas, as a prime example of rift-building processes on volcanic islands in the North Atlantic.

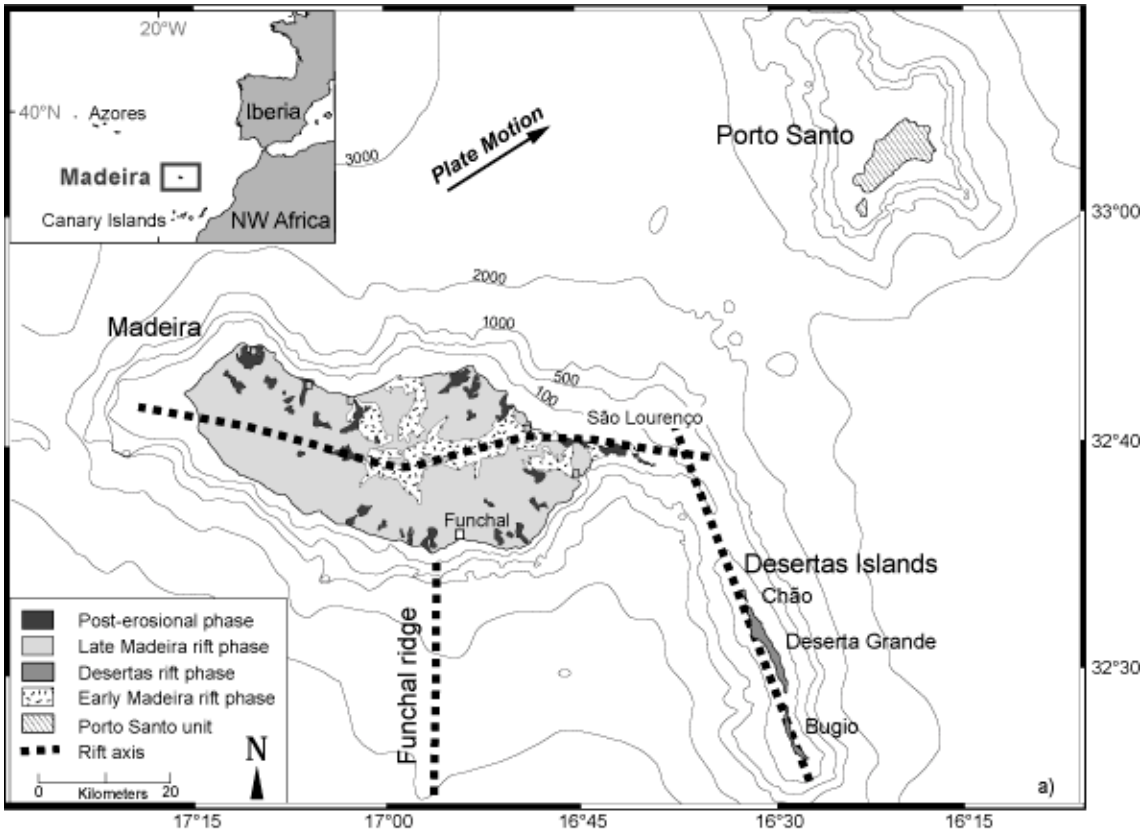

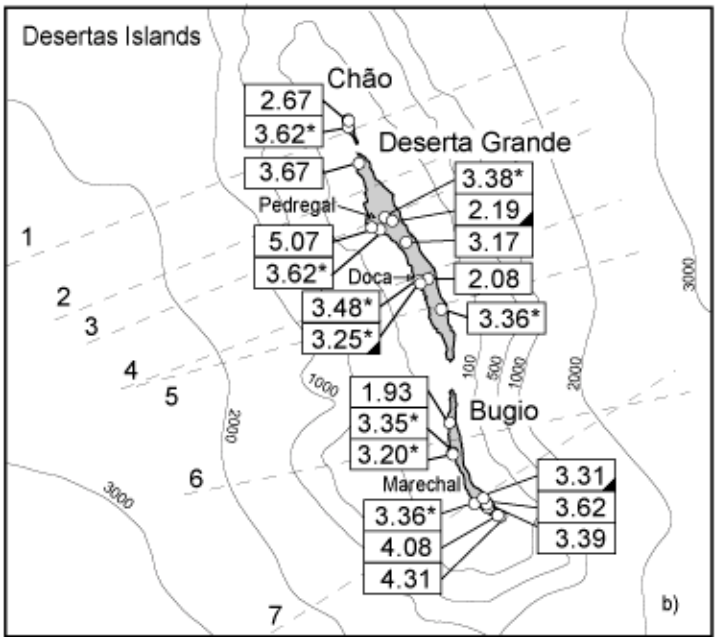

Fig. 1 a) Geological map of Madeira archipelago after Geldmacher et al. (2000) and Zbyszewski et al. (1975), bathymetry based on nautical maps. The three islands Chão, Deserta Grande and Bugio form the top of a 60 km long submarine ridge. b) Enlargement of the Desertas ridge showing the position of topographic sections (stippled lines) in Fig. 2 and 3 and sampling sites for age determination (white circles). Numbers are in million years. Black triangles in the lower right-hand corner of boxes around the age mark samples from dykes. Numbers with one asterisk identify $^{40}Ar/^{39}Ar$ ages in Ma from Geldmacher et al. (2000), all other numbers are $^{40}Ar/^{39}Ar$ age determination from this study.

Geological setting

Madeira Archipelago is situated in the eastern North Atlantic about 700 km off NW Africa (Fig. 1a). It comprises five islands: Madeira, Porto Santo and the three Desertas Islands (from N to S: Chão, Deserta Grande and Bugio; Fig. 1b). Madeira island represents the present location of the >70 Ma old Madeira hotspot that also several seamounts to the north-east (Geldmacher et al, 2000). The main island rises from about 4000 m water depth up to an elevation of 1896 m a.s.l. and the Desertas islands up to 480 m a.s.l. The underlying oceanic crust is about 130-140 Ma old (Roest et al., 1992).

Madeira shows an E-W oriented elongation whereas the Desertas Islands form the top of a NNW-SSE striking, about 60 km long submarine ridge. The islands' elongation reflects the orientation of the respective rift zones, the axes of which intersect at an angle of ~110° near São Lourenço peninsula, the easternmost tip of Madeira (Fig. 1a). Madeira and the Desertas Islands were interpreted to represent a two-armed rift system consisting of the Madeira and the Desertas rift arms (Geldmacher et al., 2000). Recent barometric studies, however, suggest that Madeira and the Desertas may represent two separate volcanic systems (Schwarz et al. 2004).

The temporal evolution of the Madeira-Desertas complex was divided into a shield stage and a post-erosional stage (Fig. 1a; Geldmacher et al., 2000). The shield stage comprises three phases: (1) the Early Madeira rift phase (EMRP, >4.6-3.9 Ma), including the submarine basement and the oldest subaerial rocks exposed on Madeira, (2) the Desertas rift phase (DRP, 3.6-3.2 Ma), during which Madeira was nearly inactive, and (3) the Late Madeira rift phase (LMRP, 3.0-0.7 Ma) with a shift of volcanic activity back to Madeira along the existing E-W oriented rift system. After a period of inactivity and erosion, cinder cones, tephra and intercanyon flows were deposited during the post-erosional stage (PE, <0.7 Ma).

Another recently discovered rift arm of Madeira is located to the south of Funchal (Fig. 1a) and forms a 50 km long, submarine ridge with at least a dozen volcanic cones clustered at the southern tip. This structure, named Funchal ridge, was discovered, mapped and sampled during cruise M51/1 of the German research vessel Meteor (Hoernle et al. 2001). The freshness of most samples suggests that this rift arm may still be active.

Methods used

Mapping and structural geology

Since the existing geological map of the Desertas Islands (Zbyszewski et al., 1973) does not provide volcanological details necessary to infer the internal structure of the rift zone, the nature and distribution of volcanic deposits and structural elements were studied in detail on land and

from the sea. The stratigraphic relations were mapped on the basis of a 1: 25000 topographic map. In addition, the island's steep flanks, only accessible from sea, were studied using a series of photographs taken from all sides of the islands. Detailed volcanological maps are available as electronic supplementary material.

In order to determine the direction of the zones of weakness and hence the orientation of the rift complex, measurements of 127 representative dykes were carried out on the Desertas Islands with all azimuth date being corrected to the IQRF magnetic declination. The measured dyke azimuths are summarised in a separate map (see electronic supplementary material). Faults are mostly exposed in the vertical coast cliffs and their orientation was measured or estimated where possible. Due to intensive weathering and inaccessibility, several faults observed along the steep coasts could not be traced on the top of the islands.

Sample preparation and analytical methods

After removing weathered surfaces, the freshest parts from each sample were crushed and powdered with an agate mill. Samples with altered rims or secondary mineral phases within vesicles were hand-picked under a binocular microscope, washed in distilled water in an ultrasonic bath and subsequently powdered. Whole rock major element data and trace elements Cr, V and Zn were determined by X-ray fluorescence spectrometry (XRF) on fused glass beads (dilution factor = 1:6) using a Philips X'Unique PW1480 X-ray fluorescence spectrometer at GEOMAR and calibrated with international standards. H2O and CO2 were analysed with an infrared photometer (Rosemount CSA 5003).

Additional trace element analyses (Rb, Sr, Y, Zr, Nb, Cs, Ba, Hf, Ta, Pb, Th, U and all rare earth elements (REE)) were carried out from mixed acid (HF-aqua regia) pressure digests which were prepared 210 °C, using a MLS Ethos microwave. About 50 mg of sample were processed and the analyte solution was spiked with 1 ng/ml indium as internal standard. The final dilution factor was 1:5000 corresponding to 0.2 mg/ml of total dissolved solid (TDS). The analyses were carried out using a ThermoFinnigan Element2 inductively coupled plasma-mass spectrometer (ICP-MS) at the Institute of Geosciences, University of Bremen. In order to avoid mass interferences, the REE and Hf were measured at high resolution (10000), the transition metals at medium (4000) and all other elements at low (300) resolution. External precision as determined by repeated analyses of standard reference materials (SRM) is better than 5% for most elements. The accuracy of reference standard material BHVO-2 and BCR-2, analysed along with the samples, is better than 10% except for Ta and Hf with up to 15 % and Cs (up to 20%) with respect to the USGS reference values. Duplicate digestions of samples yield a precision better than 10 % except for Tl and Cs (up to 20 %).

$^{40}Ar/^{39}Ar$ age dating: Sample preparation and analytical techniques

The ages of 10 samples were determined by incremental heating $^{40}Ar/^{39}Ar$ age determinations carried out on microcrystalline, plagioclase-rich groundmass separates and 2 rock ages were determined by single-crystal $^{40}Ar/^{39}Ar$ laser analysis using an Ar-ion laser combined with a MAP-216 mass spectrometer at IFM-Geomar. The mass spectrometer is equipped with a Baur-Signer-type source, a Johnston electron multiplier, and a gas extraction system connected to an ultra-clean gas cleanup line (~600 cc; Zr-Al getters; liquid nitrogen cold trap).

Aphyric as well as porphyritic rock samples from all three Desertas Islands were chosen for age dating: one from Chão, five from Deserta Grande and six from Bugio (Fig. 1b). Compositions range from basanites to alkali basalts, and more evolved samples fall within the field of hawaiites and mugearites. Groundmass and aphyric samples contain mainly plagioclase and clinopyroxene, and minor olivine and Fe-Ti oxides. Olivine and Ti-rich augite are the main phenocryst phases in porphyritic samples. After careful petrographic study, these samples for were chosen age determination with relatively high plagioclase proportion within the groundmass and a low degree of alteration.

After removing altered crusts, selected pieces of the samples were crushed and sieved. Groundmass and aphyric basalt separates were prepared from the 250-500 µm fraction by hand-picking under a binocular microscope. Several samples dated, however, contain secondary mineral phases within the groundmass such as iddingsite, which replaced olivine marginally to completely (DGR115, DGR119, DGR124, DBU103, DBU104, DBU111). Few samples show chlorite from groundmass alteration (DGR104) or zeolithe coatings within vesicles (DGR107). The quantity of zeolithes as vesicle filling was minimised by hand-picking grains free of such alteration products. Prior to irradiation, separates were washed in distilled water in an ultrasonic bath and then dried at <50 °C.

Cd-shielded sample irradiations were carried out using the FRG2 reactor at the GKSS Research Centre (Geesthacht) for 7 days. Irradiated groundmass samples were loaded into aluminium trays with multiple pans holding typically between 5 and 10 mg of material, and baked and pumped within a sample chamber fitted with a quartz glass window transparent to the laser's principal wavelengths (488 and 514 nm).

Incrementally increasing laser power output from 0.15 to 25 Watt, samples were heated from <350 to >1800 °C (IR spectrometry) until complete fusion and partial evaporation of residual silicate melt spheres. Software controlled scanning across samples in pre-set patterns with a defocused laser beam, to more evenly heat the material. Automated step-heating was followed by final fusion at ~25 W with a focused beam to ensure complete degassing (m/z 40 and m/z 39 signals at blank level).

Ion beam currents were measured with the electron multiplier at m/z = 36 to 40 and half-mass baselines with an 7.5 digit integrating HP multimeter. Peak heights were regressed to inlet time, peak decay typically being less than 10% during the analyses. Average extraction line blanks are determined as $2x10^{17}$ mol at m/z = 36 and $4x10^{16}$ mol at m/z = 40. Mass discrimination was monitored using air-fused zero age basaltic glass and pipette air samples (1.0083 ± 0.0006 amu). Correction factors for interfering neutron reactions on Ca and K are determined from co-irradiated CaF_2 and K_2SO_4 crystals ($36/39_{Ca}$ = 0.445±0.005, $37/39_{Ca}$ = 1006±7, $38/39_K$ = 0.0168, $40/39_K$ = 0.004±0.002).

$^{40}Ar/^{39}Ar$ ages were measured relative to the flux monitor standard TCR sanidine (27.92 Ma; Duffield and Dalrymple, 1990; Lanphere and Dalrymple, 2000), uncertainties for the J-values being estimated as ± 0.08% (1σ). Incremental heating plateau ages (and single-particle mean apparent ages) were calculated as weighted mean (Taylor, 1982) and initial $^{40}Ar/^{36}Ar$ isotope ratios and isochron ages as least squares fit with correlated errors (York, 1969) applying decay constants of Steiger and Jäger (1977).

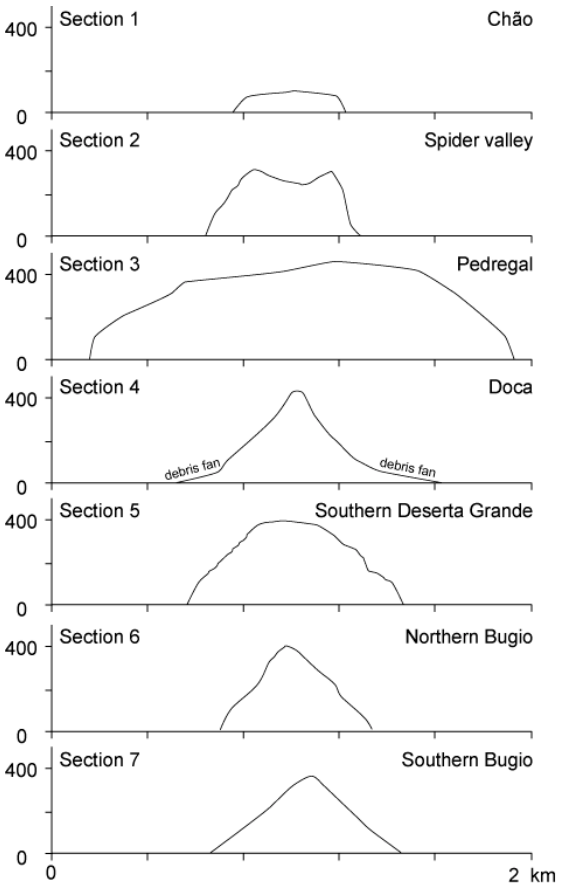

Fig. 2 Subaerial topographic sections of the Desertas Islands without vertical exaggeration based on topographic map. Source: Carta Militar de Portugal, Folhas 10-12: Ilhas Desertas. For position of the sections see Fig. 1b).

Results

Morphology of the islands

The three Desertas Islands align to, and form the top of, the NNW-SSE trending Desertas ridge and represent relics of a deeply eroded rift zone. All three islands are characterised by steep flanks that incline with 45-80° and local plateaus on the top. The northernmost island Chão forms a 1.6 km long and up to 500 m wide plateau at about 80 m a.s.l. bound by subvertical flanks (Section 1, Fig. 2; Fig. 3a). The largest island Deserta Grande is about 11 km long and between 0.5 and 2 km wide showing two main plateaus on top: (1) the Pedregal plateau with an area of about 1 km² at an elevation of 440 m a.s.l. (Section 3, Fig. 2), and (2) the 300 m wide and 2 km long southern plateau with an average elevation of 370 m a.s.l. (Section 5, Fig. 2). The area north of Pedregal plateau is dominated by the asymmetrically V-

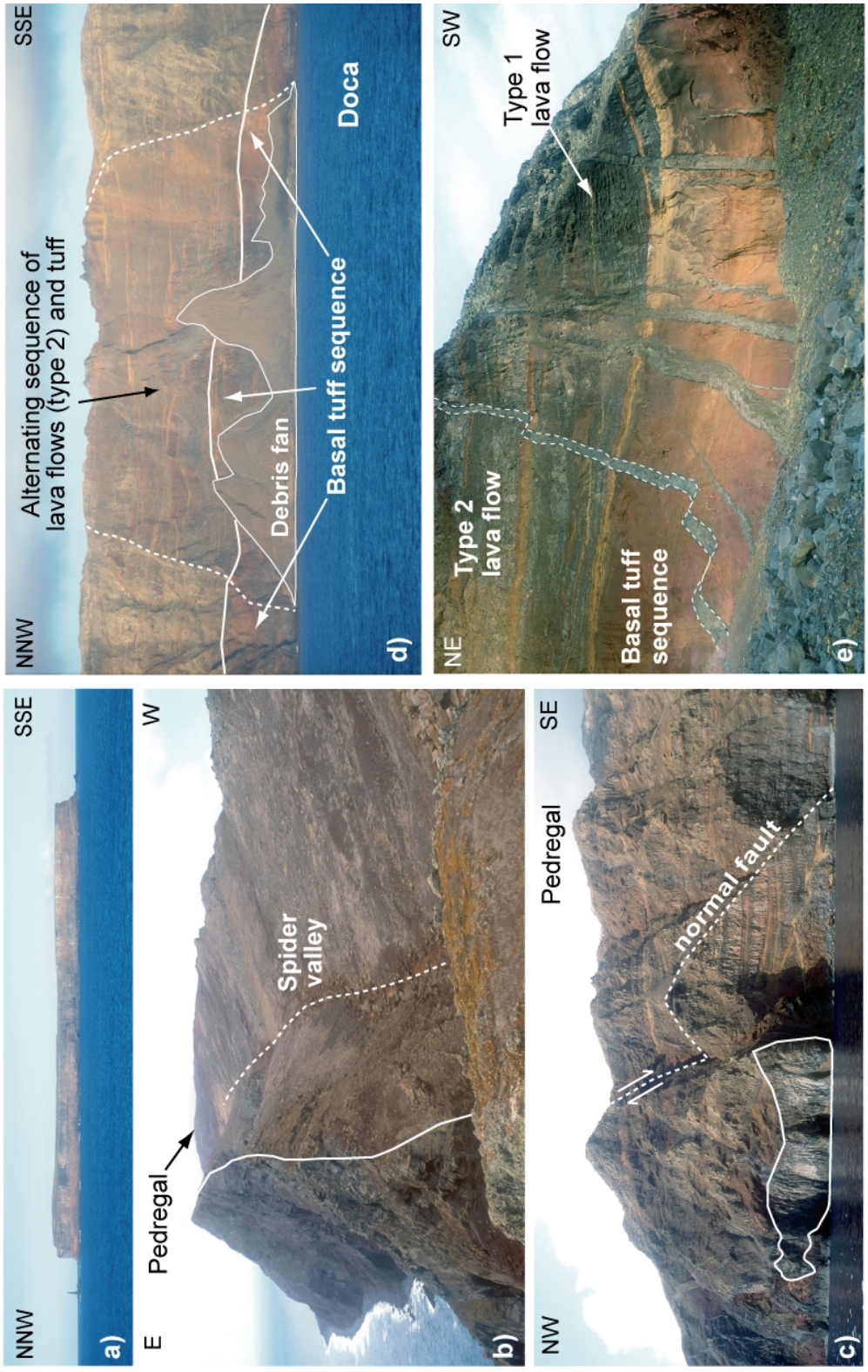

Fig. 3 Photographs illustrating features of the Desertas Islands (for localities, see Fig. 1). a) The northernmost island Chão has steep cliffs crowned by a plateau at ~80 m a.s.l. The dominant facies are type 2 lava flows. b) The morphology of the V-shaped spider valley is unique on the Desertas Islands and supposed to result from tectonic-driven erosion along inferred faults (stippled lines). c) SW-coast of Pedregal: Type 2 lava flows built up the main sequence at Pedregal and are cut by several dykes and normal faults (stippled line). A 5.1 Ma old sill (solid line) crops out at the base. d) A flank collapse ~100 yr. ago created the 400 m high amphitheater at Doca (stippled lines) and a ~1 km wide debris fan (outlined). The basal tuff sequence occurs below 100-150 m a.s.l. and is overlain by subhorizontal type 2 lava flows. NNW-SSE striking dykes cut the entire sequence. e) Southern wall of the Doca amphitheater showing the basal tuff sequence, type 1 lava flows and type 2 lava flows cut by a dyke swarm. Stippled lines mark a segmented dyke indicating horizontal magma transport.

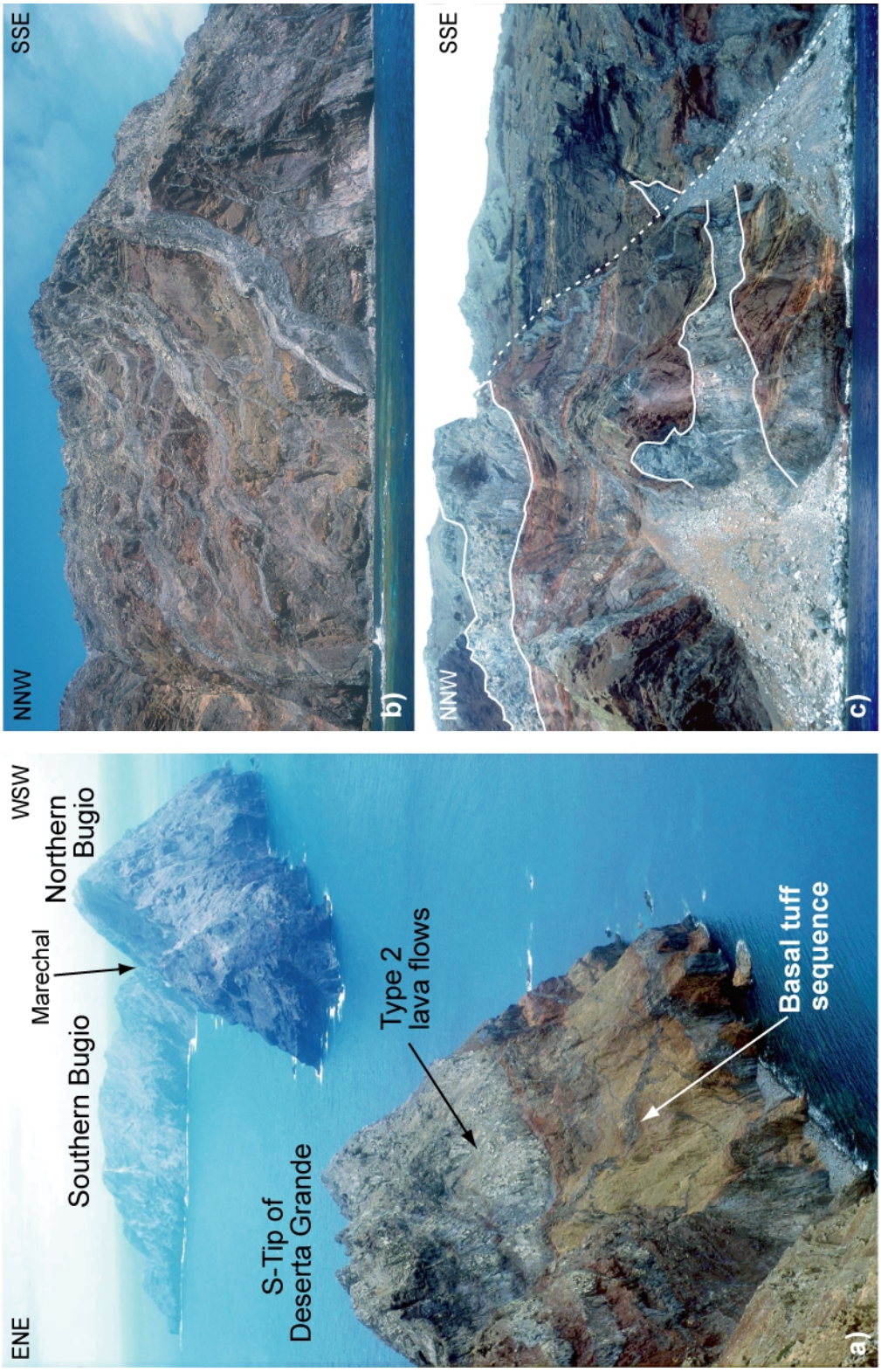

Fig. 4 Photographs illustrating features of the Desertas Islands (for localities, see Fig. 1). a)View from southern Deserta Grande towards Bugio. The southern tip of Deserta Grande exposes the typical stratigraphic sequence of basal tuff overlain by type 2 lava flows. The sickle-shaped island of Bugio is divided into a northern and southern part connected by the narrow Marechal ridge. b) The narrow ridge at Marechal bay (Bugio) consists of tuff, cinder and a dense dyke swarm which strikes parallel to the coast line. c) The south-western coast of S-Bugio predominantly consists of pyroclastic and intrusive rocks. Tuff layers up to 40 m thick and sills with < 30 m thickness (outlined) are exposed. The stippled line marks a normal fault with a strike of about 140° and a downthrow of at least 60 m towards the lower left.

shaped so-called “Spider valley”, the only valley on the Desertas Islands (Section 2, Fig. 2; Fig. 3b). The southernmost island Bugio has a maximum width of 800 m and consists of a northern and southern part connected by a narrow ridge (Fig. 4a). Its northern part rises up to an elevation of 384 m a.s.l. and the southern part up to 330 m (Sections 6 and 7, Fig. 2). The top of southern Bugio shows a 100 m wide and 1 km long plateau which is slightly inclined to the west.

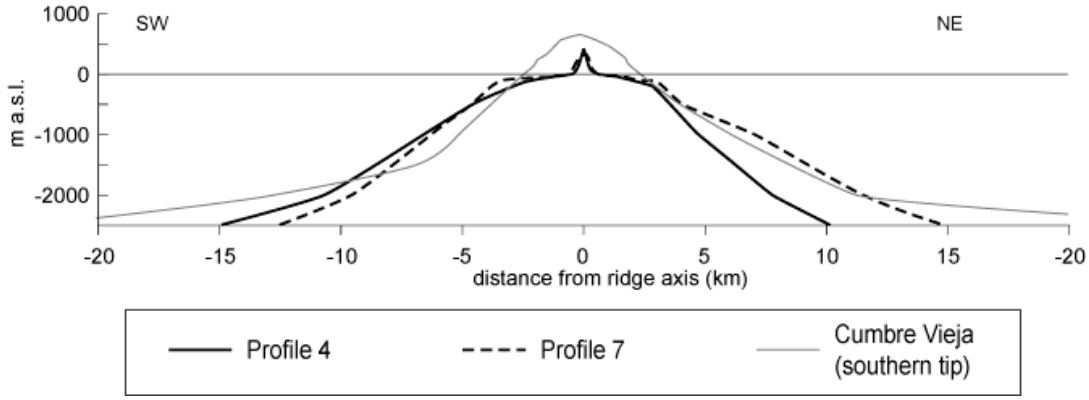

Fig. 5 Topographic sections through the Desertas ridge along lines 4 and 7 of Fig. 1b (vertical exaggeration is 2.5). To each side of the islands, ~ 1-2 km wide submarine abrasion platforms occur which extend down to 150 m below sea level. For comparison, a section through the southern tip of the Cumbre Vieja rift (La Palma, Canary Islands) is shown represented by the black line. Scaling the La Palma ridge to the former coast line of the Desertas shows that these may have had a height of 700-800 m a.s.l.

The wedge-like shape of the Desertas Islands is remarkable (Fig. 4a). The subaerial aspect ratios (height/width) lie between 0.2 and 0.6 and are higher than the mean aspect ratio of 0.12 of the submarine Desertas ridge. Moreover, the aspect ratios of the islands are higher than those of other rift zones, including the Cumbre Vieja ridge (La Palma, Canary Islands) or Pico (Azores) which range between 0.1 and 0.2. Such high aspect ratios indicate strong erosion.

The submarine flanks of the Desertas ridge have slopes between 10° and 30° and the eastern flanks appear to be steeper than those to the west (Fig. 5). To each side of the islands occur 1-2 km wide submarine abrasion platforms that have formed extending down to 150 m below sea level. These indicate that large parts of the islands were removed by repeated collapses combined with marine abrasion which resulted in the steep flanks observed today. These platforms have a tendency to extend further to the west than to the east of the Desertas (Fig. 5). The narrow part at the centre of Deserta Grande (Doca) is characterised by debris fans with lateral extension up to 1 km as a result of a historic flank collapse at the beginning of the 20th century (Section 4, Fig. 2; Fig. 3d).

Rock types and volcanic structures

The Desertas Islands are characterised by alkaline rocks ranging from picrites and basanites to mugearites (Fig. 6). The main phenocryst phases are olivine and Ti-rich augite with less than 0,5 cm in size, yet ankaramites with phenocrysts up to 1 cm are also common. Some basalts and hawaiites additionally contain plagioclase and minor amphibole phenocrysts. Olivine and especially clinopyroxene megacrysts (> 1 cm in size) are common on all three islands and are most abundant on Bugio. In some lapilli tuffs and scoria on Deserta Grande and Bugio, amphibole megacrysts with up to 4 cm diameter occur.

Mapped volcanic units

The following volcanological units were subdivided and mapped: (1) pyroclastic deposits in terms of tuff and lapilli tuff as well as scoria or cinder partly with volcanic bombs, (2) lava flows, and (3) dykes and sills. The general distribution of volcanic units is summarised in Fig. 7. A detailed geological map including volcanic as well as sedimentary units is available as download (electronic supplementary material).

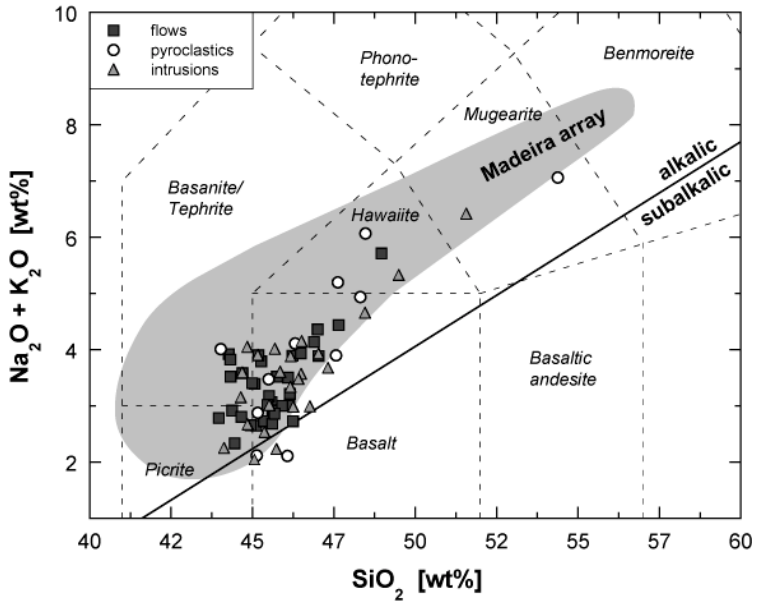

Fig. 6 TAS diagram of samples from the Desertas Islands including Desertas samples from this study and Geldmacher and Hoernle (2000) using the field boundaries of Le Maitre et al. (1989).Volcanic rocks are subdivided into alkalic and subalkalic after McDonald (1968). Field for Madeira is from Geldmacher and Hoernle (2000).

Pyroclastic deposits:

- *Tuff and lapilli tuff*: Yellowish to reddish-brown tuff and lapilli tuff often form uniform layers with up to 2 m thickness which alternate with lava flows. These layers clearly represent fallout layers deposited distal to the source. Locally, thickness of tuff layers increases and the portion of lava flows decreases resulting in tuff sequences up to 200 m thickness (Figs. 3d, 3e, 4a).

Such tuff sequences, within which relics of tuff and/or scoria cones can be found, are interpreted to indicate clustered eruptive sites and thus proximity to the rift axis. We did not find any evidence for submarine pyroclasts such as blocky clast shapes, hyaloclastites or marine algae.

Thick tuff deposits typically form the base of Deserta Grande and of northern Bugio up to an elevation of 200 m a.s.l., further on referred to as basal tuff sequence. This basal tuff sequence was interpreted to represent the result of explosive volcanism due to magma-sea water interaction during the early subaerial shield stage. In the central and southern part of Bugio, tuffs are the dominant deposit type and form sequences with single layers up to 50 m thickness (Fig. 4c).

- *Scoria, cinder and spatter*: Deposits mapped as scoria include cinder and welded spatter that are strongly solidified and mostly reddish-brown to violet because of alteration and oxidation of Fe-bearing minerals, matrix or glass. They contain minor ash, scoriaceous lapilli and locally volcanic bombs with up to 1 m diameter. Their occurrence was interpreted as a criteria of close proximity to eruptive centres. Such deposits are regarded as relics of former cinder or scoria cones being ascribed to hawaiian to strombolian eruptions and are prevalently associated with tuff.

  Relics of former scoria cones containing volcanic bombs occur at the northern tip of Chão, as clusters on the top of Deserta Grande south of Pedregal, locally within the basal tuff sequence on Deserta Grande (e.g. at Doca), and are generally abundant on southern Bugio.

Lava flows:

Based in their occurrence on the islands, we distinguish two types of lava flows:

- *Type 1* forms up to 20° inclined and layered lava flow sequences with each layer of ≤ 0.5 m thickness (Fig. 3e). Individual lava flows are separated from each other by a basal or top breccia, but not by widespread tuff layers. We interpret these thin lava flows as rootless flows or lava tongues being deposited near scoria or spatter cones or strombolian vents.

  These lava flows occur at the northern tip of Deserta Grande and partly within the basal tuff sequence of central Deserta Grande, and they are common at the west coast of northern Bugio and within the tuff sequence of southern Bugio.
- *Type 2* forms sequences of subhorizontal lava flows up to several hundred meters thickness (Fig. 3). Individual flows generally reach a thickness of up to 5 m, locally > 20 m, and are separated from each other by fallout layers of tuff or lapilli tuff up to 2 m thick. These sequences are interpreted as distal flows that may have extended for several kilometres from their source and which characterise the flanks of a rift zone.

Type 2 lava flows are best developed on Chão where flows may reach a thickness up to 30 m (Fig. 3a). On Deserta Grande and northern Bugio, they occur above the basal tuff sequence and form the top of the islands (Figs. 3c, 3d, 4a). Generally, the occurrence of this unit decreases towards south and is absent on southern Bugio.

Intrusives:

- *Dykes:* Basanitic, basaltic or hawaiitic dykes occur single or as partly sheeted swarms. They are observed all along the coasts of Deserta Grande and Bugio (Figs. 3d, 4b), but are absent on Chão. Locally, dykes cut the entire stratigraphic sequence and can be traced up to the top of the islands. A systematic structural study on dyke dip, azimuth and their width was carried out by the authors and is further discussed below.
- *Sills* or several irregularly shaped intrusive bodies of basaltic composition crop out at the base of Pedregal, within the basal tuff sequence of southern Deserta Grande and especially on southern Bugio. In general, an increasing density of sills and dykes is interpreted as a criteria of proximity to the rift axis or to a central volcano.

General distribution of volcanic units:

Since we could observe systematic variations in the distribution of volcanic units along the rift, we describe the islands' structures from N to S, i.e. from Chão to Deserta Grande to Bugio (Fig. 7). The northernmost island *Chão* is composed mainly of subhorizontal type 2 lava flows (Figs. 3a, 7). At the base of the southern part, lava flows have a thickness between 1 and 5 m and dip to the north. These are discordantly overlain by subhorizontal flows with > 5 m thickness. The flow thickness increases towards N and locally reaches 40 m. On top of the island and at its northern steep coast occur subordinate layers of scoria with bombs indicating close proximity to eruptive centres.

The base of northernmost *Deserta Grande* (below 20 m a.s.l.) is characterised by distal flows of < 5 m thickness, representing the prolongation of the lava flow sequence at the southern end of Chão. The basal flows are overlain by a series of slightly N-dipping thin lava flows (type 1). Towards the south and around the Spider valley, tuff, cinder, spatter and spindle bombs are the dominant facies passing into a strongly altered, alternating sequence of type 2 lava flows and tuff at Pedregal. On the island's top plateau south of Pedregal, clusters of cinder and spatter partly with spindle bombs indicate concentration of eruptive centres. The central and southern parts of the island is mainly composed of thick tuff deposits and subordinate scoria at the bottom and sub-horizontal sequences of type 2 lava flows towards the top. The latter locally show a slight eastward dip (Fig. 7), form conspicuous plateaus and are generally less dominant in the West than in the

East. At the west coast of central Deserta Grande (Doca), volcanic structures are best exposed due to a historic flank collapse (Fig. 3d). Below 100-150 m a.s.l., the eroded flank shows a thick basal tuff sequence containing remnants of tuff and scoria cones and proximal type 1 lava flows. Towards the top, the portion of pyroclastics decrease and subhorizontal type 2 lava flows alternating with tuff layers become the dominant facies. A distinctive dyke swarm crosscuts the entire stratigraphy. The island's southern tip, which structurally represents the transition to Bugio, consists mainly of tuff below 100 m a.s.l. and type 2 lava flows above, and is cut by numerous dykes which strike subparallel to the coast line. In general, steeply dipping dykes are abundant all along the steep coasts of the island. Distinct dyke swarms occur at the western flanks of Pedregal, at Doca and the southernmost part of Deserta Grande. Several sills crop out along the west coast at Pedregal and southern Deserta Grande.

In contrast to Deserta Grande, *Bugio* consists mainly of pyroclastic and intrusive rocks and dominant sequences of type 2 lava flows are rare. Bugio's northern part exposes a basal tuff sequence alternating with type 1 lava flows up to 200 m a.s.l. continued by type 2 lava flows towards the top. The northern part thus resembles the southern end of Deserta Grande with predominantly pyroclastics at the base, distal lava flows on top and abundant dykes. Unlike Deserta Grande and northern Bugio, the southern part of Bugio is composed predominantly of units deposited proximal to eruptive sites such as tuff layers tens of m thick, scoria, spatter, volcanic bombs, minor sequences of type 1 lava flows, dykes and sills (Figs. 4b, 4c). and distal type 2 flows are absent. Sills up to 30 m thickness are most abundant at the southern tip of Bugio. Plenty of dykes and coherent dyke swarms occur all along the island and directions of strike and inclinations are similar to those from Deserta Grande (see below). The most distinctive dyke swarm of the Desertas Islands is found at Marechal, the deeply eroded central part of the island (Figs. 1b, 4c, 7).

In summary, deposits which point to the occurrence of former eruptive centres are not evenly distributed along the islands, but appear to be concentrated in southern Bugio and also, to a lower degree, on the top of central Deserta Grande. The stratigraphy of Deserta Grande and northern Bugio, with a basal tuff sequence overlain by type 2 lava flows, reflects a change from explosive to more effusive volcanism with increasing height of the islands, i.e. during the subaerial shield stage.

Sediments

Sediments are found all along the strongly eroded islands. We distinguish three types of sediments: (1) scree deposits as a product of rock falls and flank collapses, (2) reworked material and (3) fluvial sediments. In the schematic map of Fig. 7 only scree deposits are shown, whereas in our detailed geological map all sediment types appear.

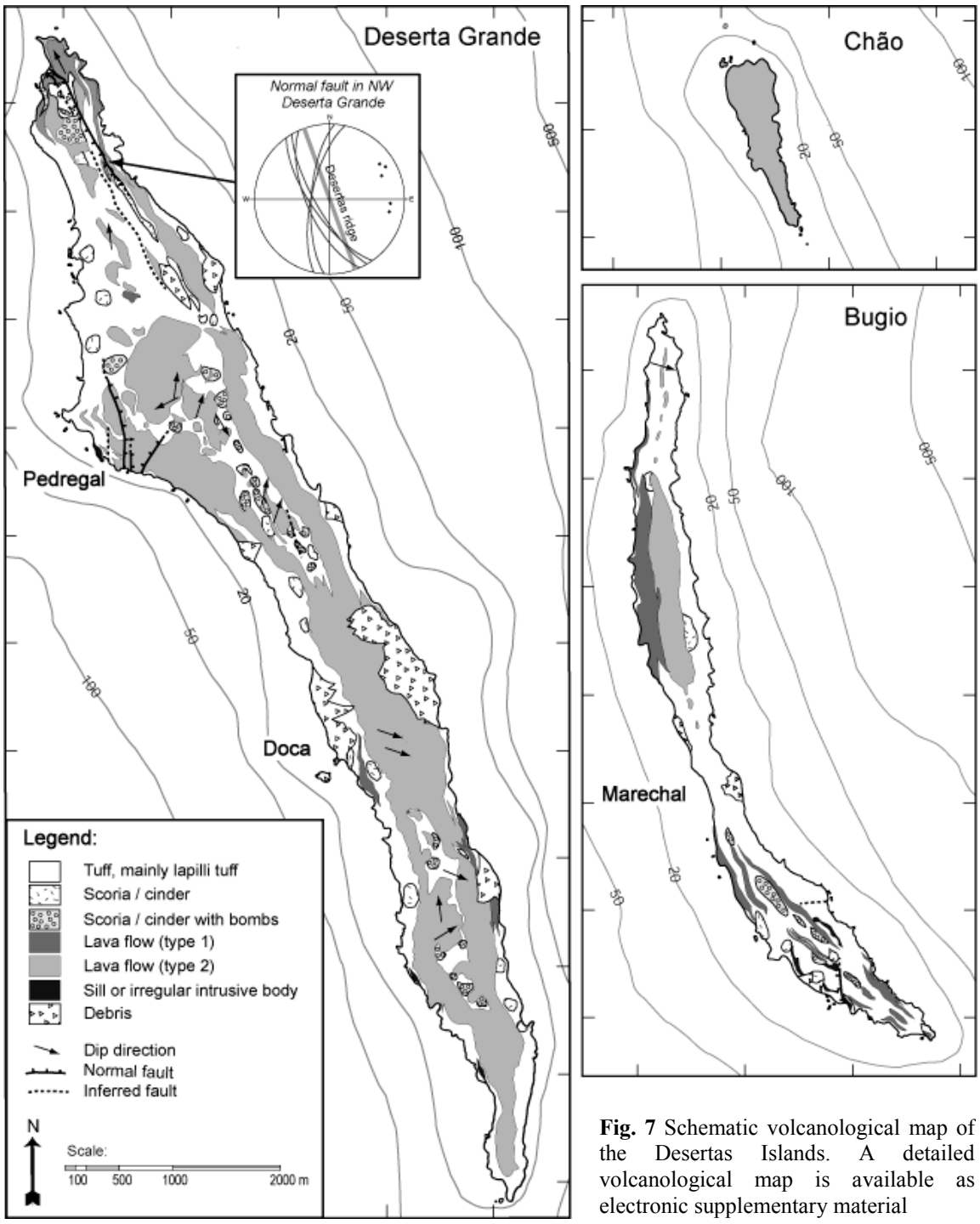

Fig. 7 Schematic volcanological map of the Desertas Islands. A detailed volcanological map is available as electronic supplementary material

Scree deposits:

Flank collapses and rockfalls produce debris fans of 100 m to 1 km width. The material deposited is badly sorted and consists of angular fine-grained to blocky components up to 2 m in size that represent eroded volcanics. Particle size is positively correlated with transport distance, i.e. blocks are deposited distal whereas smaller fragments are deposited proximal. Such scree deposits were found all along the coasts of Deserta Grande and Bugio. The most distinctive debris fans occur in the central part of Deserta Grande (Doca) to both sides of the island (Fig. 7).

Reworked material:

The material mapped is reddish brown and layered without gradation within discrete layers. It is badly sorted and contains subrounded fragments from sand to granule fraction. This kind of deposits represents reworked volcanic material transported and deposited by alluvial processes. They occur on the top plateaus of Deserta Grande and southern Bugio and partly along the eroded steep flanks.

Fluvial units:

Fluvial deposits were found at the bottom of the Spider valley, i.e. in dry river channels which carry water only during raining season from autumn till spring. Particles are rounded, moderately sorted and range from sand to gravel in size.

Structural geology

Dykes

The orientation of dykes and normal faults, usually rift-parallel, reflects the direction of maximum principal stress σ1 at the time of their intrusion and thus retains information about the volcano's stress field (Anderson, 1951; Nakamura, 1980). The density of dyke swarms typically increases with depth and towards the rift core. Such coherent dyke complexes are characterised by symmetrical downbowing of stress trajectories and thus an outward dip of the dykes at the margins on either side of a complex (Walker, 1992). Therefore, dyke azimuths and dip directions can be used to infer the orientation and former location of the rift axis.

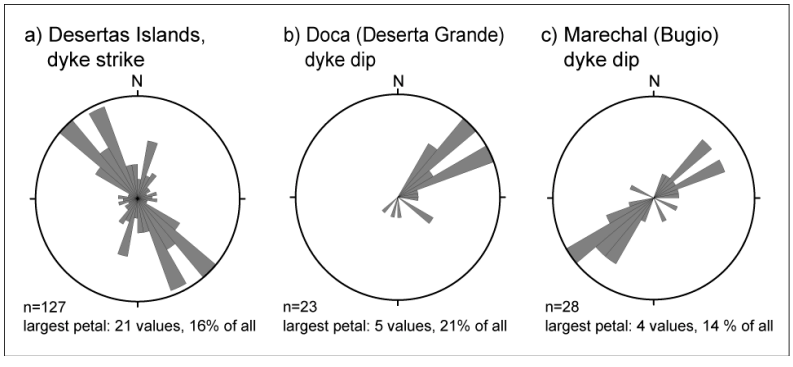

Fig. 8 Trends of 127 Desertas dykes illustrated by rose diagrams (constructed using 10° intervals). a) Rose diagram of strike direction. Note two major directions, one oblique to the Desertas ridge with 135° and another nearly ridge-parallel at 155°. b) Dip direction at Doca, Deserta Grande, where most dykes dip to the NE. c) Dip directions on Bugio, where dykes show opposing dips to the SW as well as the NE.

Based on field observations and photographs, we estimate the overall dyke proportion of the islands to be less than 30 % (Figs. 3, 4). Dyke measurements on Deserta Grande and Bugio showed that 90% of all measured dykes strike between 120 and 170° NW/SE with a near-Gaussian

distribution within this range (average = median = 145°; Klügel and Walter, 2002; Fig. 8). Whereas the dyke azimuths do not show any systematic spatial change along the ridge axis, dip directions reveal an apparent asymmetry: Most of the Deserta Grande dykes dip eastward, whereas on Bugio opposing dips dominate, i.e. to the south-west and the north-east (Fig. 8). The majority of all dykes is steeply dipping between 90° to 43° (median = 80°; Fig. 9). Dyke thickness ranges from 0.1 to 20 m (average = 2.1 m) and 90 % of all dykes are thinner than 5 m (Fig. 10).

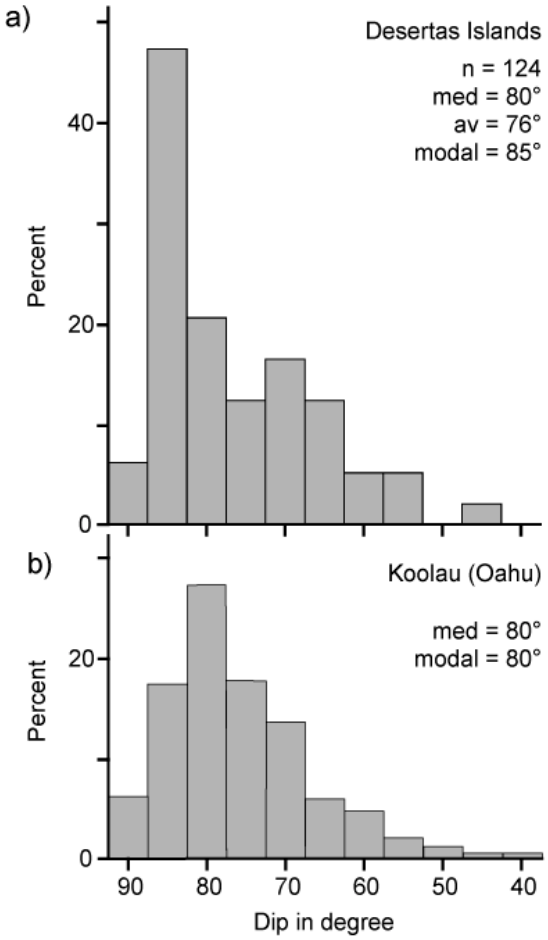

Fig. 9 Dip angles of a) Desertas dykes and b) in Koolau dyke complex (data: Walker, 1987). In both volcanic rift zones dykes are non-vertical with most dips between 65° and 85°

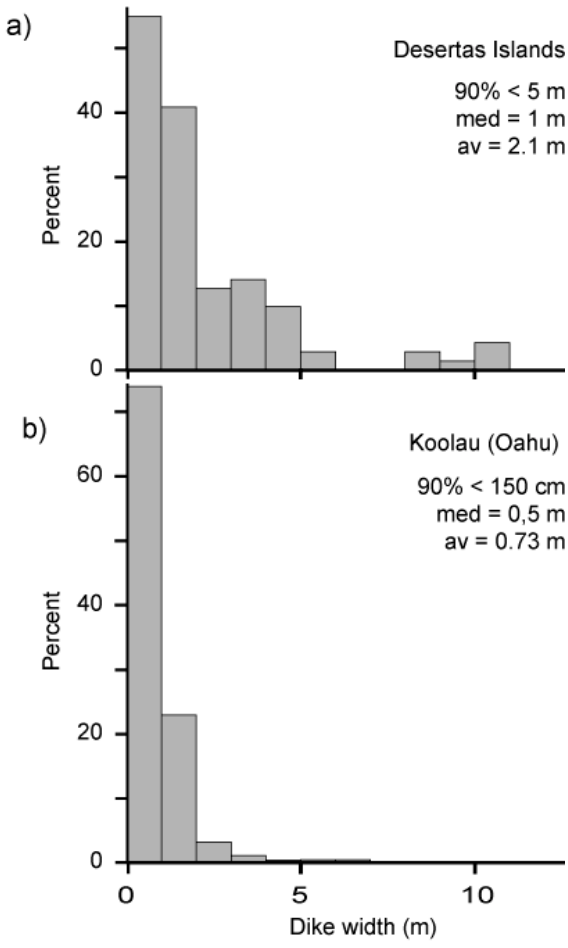

Fig. 10 Dyke widths at the a) Desertas Islands compared with b) Koolau dyke complex (data: Walker, 1987). Dike widths on the Desertas are more variable than those on Oahu. Average values show that Desertas dykes (av. = 2.1 m) are wider than Koolau dykes (av. 0.73 m).

Faults

Several W-dipping normal faults are exposed along the cliffs in the northern part of Deserta Grande (Fig. 7). The conspicuously V-shaped spider valley in the north of Deserta Grande (Section 2, Fig. 2) is assumed to represent the result of tectonic-dominated erosion along a NNW-SSE striking normal fault for the following reasons: (1) the geomorphologic structure is unique on the

islands, and (2) rock types exposed at the western valley flank were found to differ from those exposed on the eastern flank. Yet, only one normal fault with a mean strike of 165° and a dip between 65 and 75° was found along the crest of the eastern flank of the spider valley. The NS-striking northern faults which are aligned to the spider valley, can be followed along a distance up to 2 km.

The steep coast of Pedregal exposes a graben structure, whose inaccessible faults were estimated to be ridge-parallel with about 165-170° and a dip of at least 60°. Because horizons could not unequivocally be correlated across the faults, vertical displacements cannot be estimated. Additional minor faults were also observed along the coast of Desertas Grande, e.g. to the east of Pedregal (Fig. 7) where a WNW-dipping normal fault with a minimum downthrow of 20 m occurs.

Due to strong surface weathering and very limited accessibility, we could observe only few faults on Bugio. In the southern part, one major normal fault has an estimated strike around 160° and vertical displacement of about 60 m (Fig. 4c).

$^{40}Ar/^{39}Ar$ age determinations

From field observations and existing age determinations (Geldmacher et al., 2000), it seems that the three Desertas Islands formed simultaneously. In order to better understand the islands' evolution and their setting within Madeira Archipelago, we sampled and dated additional rocks of various locations (Fig. 1b). 10 samples ranging from basanitic to mugearitic composition were analysed using $^{40}Ar/^{39}Ar$ incremental heating techniques. Two more samples (DBU60 and K16) were previously analysed by single-particle total fusion. Results are displayed in age plateau diagrams in Fig. 11 and compiled in Table 1.

Most of the high-resolution incremental heating analyses yield well-defined age plateaus, in the sense that numerous consecutive gas release steps in the mid temperature ranges comprise a significant fraction (>60%) of the cumulative ^{39}Ar yield and apparent ages identical within error (2 sigma; excluding uncertainties in J).

Uncertainties in the apparent ages of gas released during individual incremental heating steps are relatively large because all matrix samples are highly contaminated with atmospheric Ar (i.e. $^{40,36}Ar$). Atmospheric contamination of basalt matrix may be significantly reduced by etching and partial dissolution of samples in diluted HCL and HNO3, preferentially removing alteration products on grain boundaries without affecting inherited and radiogenic $^{40,36,38}Ar$ components from primary Ar reservoirs (Koppers et al., 2000). Samples in this study, however, were only washed in ultraclean water and ultrasonic baths, and dried at <50° C prior to irradiation and analysis. Atmospheric ^{40}Ar contents therefore approach 100% in the low-temperature heating steps, and only decrease to 60-70 % in the mid and high-temperature ranges.

Small fractions with increased apparent ages in the low and highest temperature ranges indicate the presence of at least two distinct isotopically disturbed Ar reservoirs within the matrix grains, interpreted to reflect ^{39}Ar recoil of secondary phases (low-temperature alteration), and an inherited Ar component with $^{40}Ar/^{36}Ar_i >> 295.5$ derived from groundmass mineral phases degassing preferentially at high temperatures (i.e. olivine, clinopyroxene). Some scatter is also observed within the age plateau ranges, indicating that the different Ar reservoirs are not evenly and selectively degassed during narrow laser power (and heating temperature?) intervals. Isotope correlation yields initial $^{40}Ar/^{36}Ar$ ratios identical to modern atmosphere within uncertainties (~295.5), or rarely slightly higher (DGR115-2 and DBU103-2 only), and isochron intercept ages identical to plateau ages within error.

Duplicate incremental heating analyses with varied sample masses and/or heating schedule were carried out on samples which initially produced only small plateaus (DGR115: 54% ^{39}Ar, DBU103: 69% ^{39}Ar, and DBU104: 85% ^{39}Ar). These generally improved the plateau sizes (57%, 97%, and 99% respectively) and uncertainties, and either replicated the plateau age results within error (DBU103) or yielded significantly lower (DGR115: 2.2±0.1 Ma vs. 2.9 ± 0.2 Ma) or higher plateau ages (DBU104: 3.62 ± 0.07 Ma vs. 2.7 ± 0.2 Ma). Repeated analysis series on samples with initially well-constrained plateaus (DGR104: 99% ^{39}Ar; DGR119: 92% ^{39}Ar), in contrast, yielded slightly smaller plateaus (86%) and plateau ages identical within error (DGR104: 3.8 ± 0.1 Ma), or more disturbed spectra with significantly smaller plateaus (51%) and higher apparent plateau ages (DGR119: 4.7 ± 0.2 Ma). This indicates considerable sample heterogeneity especially with respect to the amount and composition of secondary phases.

In order to derive a single age estimate for each sample, plateau age results from identical analysis series are polled and the inverse-variance weighted mean is calculated (DGR104: 3.67 ± 0.10 Ma; DBU103: 3.31 ± 0.12 Ma). For replicate analysis series with deviating results, age estimates are based on the larger plateau analyses only (DGR115, DGR119, DBU104). Internal errors on the $^{40}Ar/^{39}Ar$ plateau ages are reported at the 1σ confidence level.

Picked groundmass separates yielded ages between 5.07 and 1.93 Ma (Table 1) and thus greatly extend the published Desertas ages (3.2-3.6 Ma; Geldmacher et al., 2000). The oldest age comes from a sill-like intrusive body at the Ponta de Pedregal on Desertas Grande with an age of 5.07±0.06 Ma (DGR104; all reported errors are 1σ) and thus clearly overlap with the Early Madeira rift phase (EMRP). Further ages, falling clearly within the EMRP, were obtained for lava flows at the southern tip of Bugio with 4.31±0.20 Ma (DBU111) and 4.08±0.21 Ma (DBU113). Two samples from the top of the islands yielded ages less than 3 Ma: A hawaiitic bomb from the uppermost unit on Chão (2.67±0.11 Ma; K16) and a dyke sampled on the top of Deserta Grande (2.19±0.13 Ma; DGR115). The youngest samples were found on the top of the stratigraphic profile

Table 1
Incremental heating and single-particle total fusion 40Ar/39Ar analyses on groundmass separates from Desertas Island volcanics.

Sample	UTM coordinates	Type	Rock type	Analysis type	Age spectrum plateau age: Age ± 1σ Ma	^{39}Ar %	MSWD	n (N)	Integrated age: Age ± 1σ Ma	Inverse Isochron analysis: Age ± 1σ Ma	^{40}Ar/^{36}Ar ± 1σ intercept	MSWD
Chao												
K16	355250 / 3606500	Flow	H	MSP-TF	**2.67 ± 0.11**		1.2	12 (12)		2.98 ± 0.58	293 ± 5	1.3
Deserta Grande												
DGR104	356490 / 3600650	Sill	AB	HR-IHA	**5.07 ± 0.06**	99	0.9	15 (20)	5.60 ± 0.08	4.75 ± 0.30	302 ± 3	21.5
DGR107	355830 / 3604230	Volcanic bomb	AB	HR-IHA	3.46 ± 0.17	91	0.7	16 (20)	3.81 ± 0.19	3.56 ± 0.17	298 ± 1	0.9
				Repeat	3.81 ± 0.11	86	0.9	12 (20)	1.20 ± 0.80	3.69 ± 0.27	297 ± 3	2.8
				Combined	**3.67 ± 0.10**							
DGR115	357330 / 3601275	Dyke	AB	*HR-IHA*	*2.90 ± 0.18*	*54*	*0.7*	*8 (20)*	*3.66 ± 0.19*	*3.30 ± 0.32*	*300 ± 4*	*2.2*
				Repeat	**2.19 ± 0.13**	57	1.5	8 (20)	3.25 ± 0.12	1.18 ± 0.26	303 ± 1	2.9
				Combined	*2.49 ± 0.11*							
DGR119	358140 / 3599950	Scoria	AB	HR-IHA	**3.17 ± 0.16**	92	0.9	15 (20)	3.46 ± 0.20	3.30 ± 0.18	295 ± 2	1.3
				Repeat	*4.66 ± 0.17*	*51*	*1.5*	*8 (20)*	*2.36 ± 1.12*	*4.21 ± 0.33*	*303 ± 7*	*3.7*
				Combined	*3.89 ± 0.12*							
DGR124	358980 / 3598070	Flow	AB	HR-IHA	**2.08 ± 0.09**	98	1.2	16 (20)	2.26 ± 0.11	1.89 ± 0.15	298 ± 1	1.1
Bugio												
DBU103	361650 / 3586750	Dyke	AB	HR-IHA	3.41 ± 0.23	69	1.1	12 (20)	3.36 ± 0.21	2.50 ± 0.26	300 ± 2	1.6
				Repeat	3.27 ± 0.09	97	1.1	15 (20)	3.65 ± 0.14	2.91 ± 0.13	305 ± 2	0.9
				Combined	**3.31 ± 0.12**							
DBU104	361825 / 3586575	Scoria	AB	*HR-IHA*	*2.71 ± 0.19*	*85*	*1.2*	*9 (20)*	*3.52 ± 0.33*	*2.97 ± 0.37*	*295 ± 4*	*3.2*
				Repeat	**3.62 ± 0.07**	99	1.5	16 (20)	3.92 ± 0.12	3.55 ± 0.09	300 ± 2	1.3
				Combined	*3.38 ± 0.11*							
DBU106	362025 / 3586325	Scoria	M	HR-IHA	**3.39 ± 0.09**	90	0.7	16 (20)	3.58 ± 0.12	3.38 ± 0.14	298 ± 2	1.2
DBU111	362600 / 3585900	Flow	B	HR-IHA	**4.31 ± 0.20**	78	0.9	14 (20)	4.68 ± 0.21	3.61 ± 0.61	299 ± 2	1.6
DBU113	362700 / 3585750	Flow	AB	HR-IHA	**4.08 ± 0.21**	100	1.0	18 (20)	4.19 ± 0.25	3.83 ± 0.42	297 ± 3	0.9
DBU60	358140 / 3599500	Sill	AB	MSP-TF	**1.93 ± 0.12**		1.5	11 (11)		1.91 ± 0.43	296 ± 11	1.6

HR-IHA = High-resolution incremental heating analyses; MSP-TF = multiple single-particle total fusions. Repeat = duplicate step-heating analyses on same sample. Combined = weighted average of duplicate runs. Reported 40Ar/39Ar dates are weighted age estimates and errors (1s) including uncertainties in the J value (~0.08%). MSWD = Mean Square Weighted Deviates for plateau ages and inverse isochrons calculated for N-1 df. N = total number of heating steps. n = number of heating steps in plateau comprising percent fraction of cumulative 39Ar release. Boldface: accepted ages based on single incremental heating analysis plateaus or weighted means from two duplicate runs. Oblique: results rejected because of plateau size deficiency. disturbed spectra or significant differences at 2sigma level (Combined data). Rock types: AB = alkali basalt, B = basanite, H = hawaiite, M = mugearite.

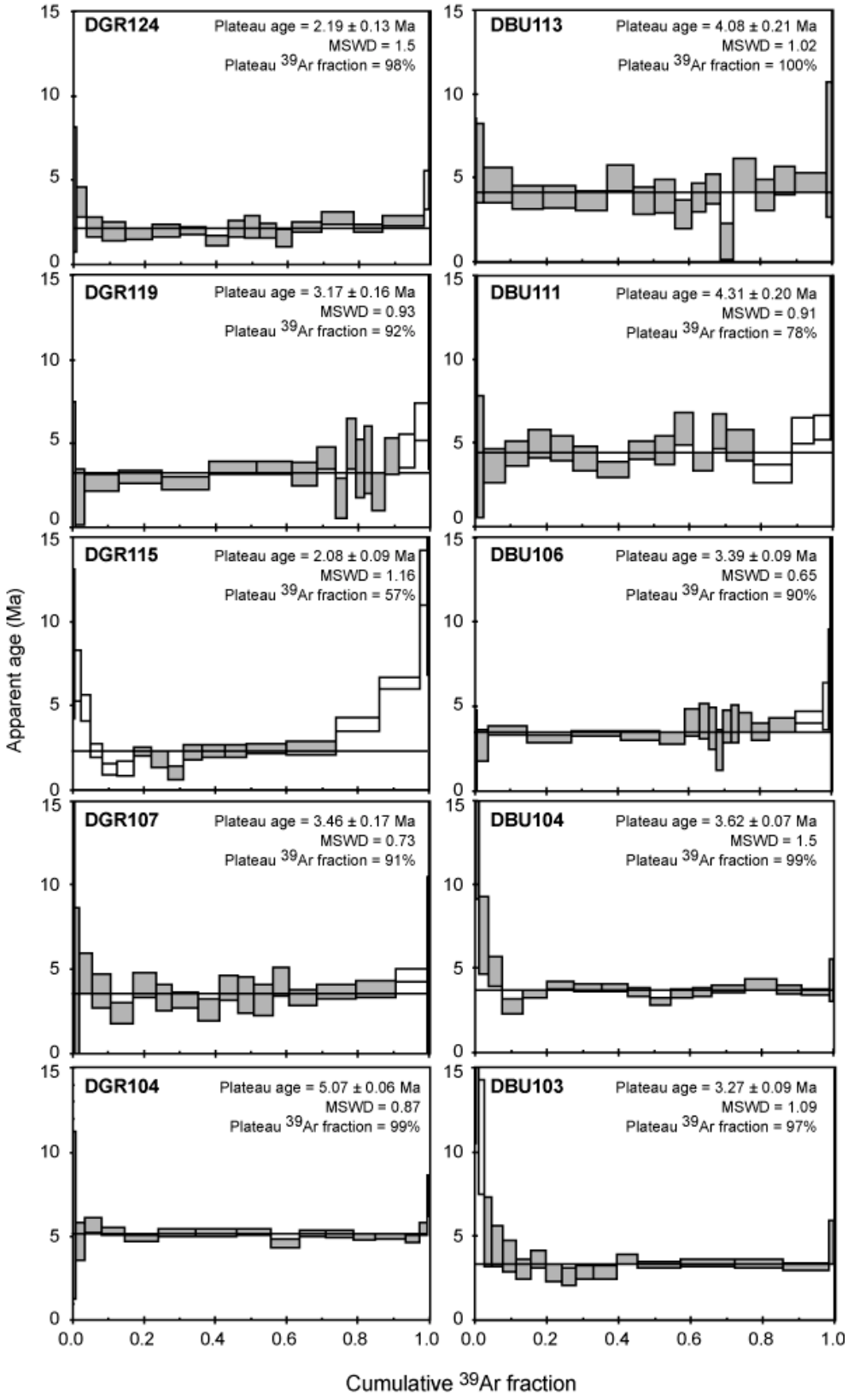

Fig. 13 Variations of ratios of incompatible trace elements versus elevation above sea level for samples from Deserta Grande. The elevation is supposed to represent the best approximation for the stratigraphic sequence of the island. Grey symbols mark dated rocks and numbers give ages in Ma. The diagrams show enrichment of the REE over other incompatible elements, and enrichment of the heavy relative to the light REE, for the youngest samples occurring above 350 m a.s.l.

at Doca on Desertas Grande (2.08±0.2 Ma; DGR124) and from a basaltic layer within a scoria cone at the base of N-Bugio (1.93±0.2 Ma; DBU60).

Remaining rock ages of pyroclastics and a dyke from Deserta Grande and Bugio fall within a range of 3.2-3.7 Ma consistent with published data from Geldmacher et al. (2000; see Table 1). A volcanic bomb sampled at the base of northernmost Deserta Grande yielded an age of 3.67±0.10 Ma (DGR107) and scoria from the top of Deserta Grande shows 3.17±0.16 Ma (DGR119). Two scoria samples from the top of southern Bugio give ages of 3.62±0.07 (DBU104) and 3.39±0.09 Ma (DBU106) and are cut by a dyke with an age of 3.31±0.12 Ma (DBU103).

Major and trace elements

In order to examine if the Desertas volcanism shows systematic geochemical variations over time or along the ridge, whole-rock analyses of major and trace elements were carried out extending the data set of Geldmacher and Hoernle (2000). Major and trace element data for whole rock samples are given in Tables A1 and A2.

In general, the Desertas samples largely overlap in major and trace elements with those from the early and late Madeira rift phases (Geldmacher and Hoernle, 2000). CaO/Al_2O_3, Cr, Co and Ni decrease with decreasing MgO consistent with olivine and clinopyroxene fractionation observed. Likewise, Al_2O_3, alkalis, P_2O_5 and incompatible trace elements (e.g. Rb, Nb, Zr, Ba and Sr) increase with decreasing MgO. Below 5 wt.% MgO, FeO and TiO_2 decrease consistently and SiO_2 increases which indicates fractionation of Ti-Fe oxides and augmented Ti-augite relative to olivine. On a primitive mantle-normalised incompatible element diagram, primitive samples show features characteristic for HIMU ocean island basalts which include enrichment in Nb and Ta and negative anomalies of K and Pb (Fig. 12a). In addition, Desertas samples show typical HIMU trace element ratios such as high Ce/Pb (18-65) and Nd/Pb (10-36), but relatively low Ba/Nb (3.4-7.6), K/Nb (99-199) and La/Nb (0.5-1.2) (Weaver, 1991). This HIMU character is interpreted to reflect recycled oceanic crust in the mantle source (Geldmacher and Hoernle, 2000). The concentrations of the rare earth elements (REE) normalised to C1-chondrite decrease strongly with increasing atomic number ($(La/Yb)_N$ ~ 6-19, $(Sm/Yb)_N$ ~ 2.4-9.8; Fig. 12b) indicating residual garnet source typical for most oceanic island basalts (OIB). Some samples from the top of Deserta Grande and Bugio, however, show a strong enrichment of the REE and Y relative to other incompatible elements, and a few samples show conspicuously flat REE spectra (e.g. DGR 46: $(La/Yb)_N = 2.4$, $(Sm/Yb)_N = 1.5$; DGR 125: $(La/Yb)_N = 3.1$, $(Sm/Yb)_N = 1.7$). These unusual geochemical signatures are unique on Madeira archipelago and were verified by replicate analyses. The most extreme REE enrichment, up to three times higher than the average of all Desertas samples, is found in samples from late dykes cutting the entire Desertas stratigraphy (DGR115, DGR121, DGR143) . These samples have

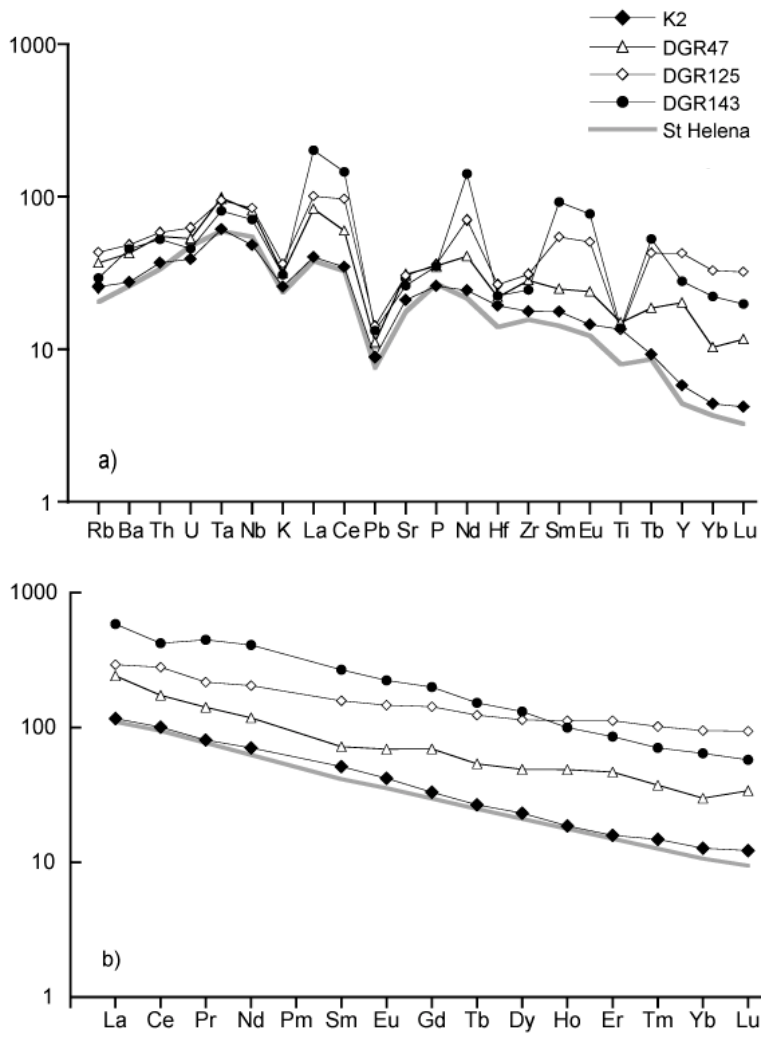

Fig. 12 a) Incompatible trace element concentrations normalised to primitive mantle after Sun and McDonough (1989) of a representative primitive Desertas sample (K2), two HREE-enriched samples (DGR47, DGR125) and one REE-enriched sample (DGR143) compared with HIMU basanite from St. Helena (sample 68 from Chaffey et al., 1989)).The REE- and HREE-enriched samples show negative "anomalies" for Sr, Hf, Zr and Ti. b) REE patterns (normalised to C1 chondrite after Sun and McDonough, 1989) of the same Desertas samples as in a). Note the flat patterns of the HREE-enriched samples compared to the normal Desertas and St. Helena basanites.

extremely high Ce/Pb (81-135) and La/Nb (1.1-5.1) and very low Sr/Nd (1.7-7.1), Zr/Sm (4-16), Zr/Yb (17-25) and Hf/Sm (0.11-0.61). To test whether these REE, HREE and Y enrichments correlate with rock ages, we plotted $(La/Sm)_N$, $(Sm/Yb)_N$, Sr/Nd, Zr/(Yb,Y) and Hf/Sm of lava flows, pyroclastic layers and dykes cutting the entire stratigraphic sequence against elevation above sea level, which is supposed to represent the best approximation for the age succession (Fig. 13). Whereas most other geochemical parameters remain constant, these ratios show no variation below 350 m a.s.l., but then decrease conspicuously. This indicates a systematic geochemical variation of the late Desertas lavas. To test if these REE enrichments are also reflected in isotopic composition, Sr, Nd and Pb isotopes of the HREE-enriched sample DGR46 have been analysed. The isotope ratios, however, show no anomalies and fall perfectly within the range of other Desertas samples (Geldmacher and Hoernle, 2000; Schwarz, unpubl. data).

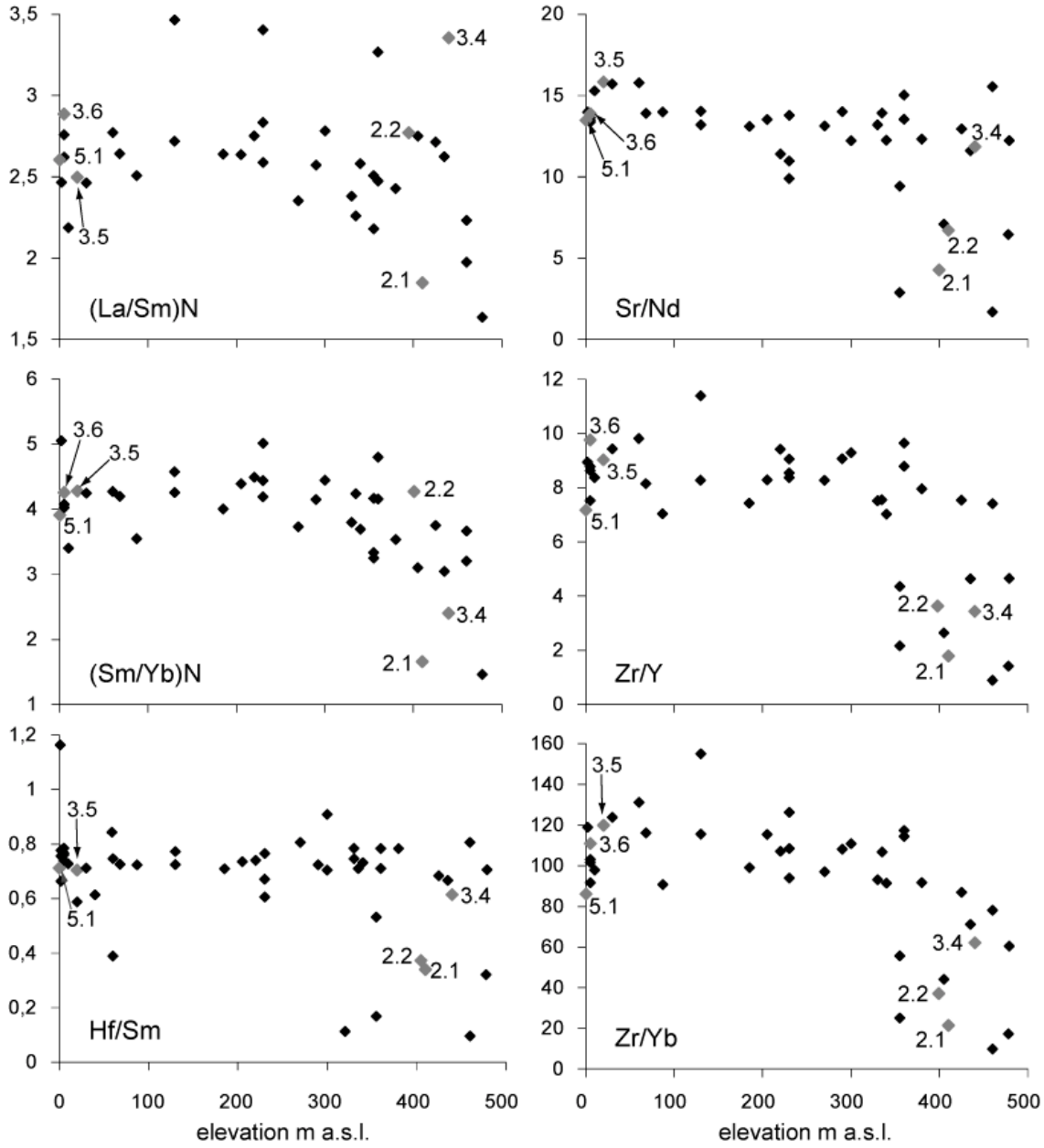

Fig. 13 Variations of ratios of incompatible trace elements versus elevation above sea level for samples from Deserta Grande. The elevation is supposed to represent the best approximation for the stratigraphic sequence of the island. Grey symbols mark dated rocks and numbers give ages in Ma. The diagrams show enrichment of the REE over other incompatible elements, and enrichment of the heavy relative to the light REE, for the youngest samples occurring above 350 m asl..

Discussion

With detailed mapping and age determinations, we studied the volcanic structures and the stratigraphy of the Desertas Islands. We can distinguish between (1) rift axis facies indicated by thick tuff layers, cinder, spatter and/or volcanic bombs, dyke swarms and sills, and (2) rift flank facies comprising sequences of thick lava flows and distal fallout. The distribution of volcanics shows that rift axis facies generally becomes prevalent towards south and east. Most rock ages fall

between 3 and 4 Ma indicating the phase of main subaerial activity. The oldest dated rock (5.07 Ma) comes from a sill-like intrusion at the western coast of Deserta Grande (Pedregal) and the youngest dated rocks with an age around 2 Ma were sampled on the top of Deserta Grande and from a sill at the base of Bugio.

In order to better understand and interpret the observed structures, we compare the Desertas Islands with rift zones on Hawaii which are the best described systems. The well-exposed Koolau dyke complex (Oahu / Hawaii), a prototype of the interior of Hawaiian rift zones (Walker, 1987), is most suitable to find out similarities as well as differences between the Desertas and Hawaiian systems. This comparison allows us to estimate the former morphology of the Desertas rift and to make some inferences on its evolution.

Comparison of the Desertas with Koolau volcano

The Koolau dyke complex on Oahu is the best exposed rift zone on the Hawaiian islands and is supposed to represent the analogue to subsurface regions of other Hawaiian rift zones such as the east rift zone of Kilauea (Walker 1987, 1992). The similarities and differences between the Desertas rift zone and the Koolau dyke complex are summarised in Table 2.

Both are strongly elongated structures with a single dominant rift zone, the dyke complex of which is exposed by erosion and flank collapses. Instead of being buttressed by an older, parallel volcano pile as is the case for Koolau, the Desertas ridge is situated at the lower flank of Madeira and is oriented obliquely to it. Another important difference is the absence of a collapse caldera or central volcano from which the Desertas rift extended. In contrast, the Koolau dyke complex was associated with a caldera indicated by radial oriented dyke swarms and younger, subsidenced lava infill in terms of thick massive lava flows.

In both rift complexes, most dykes are non-vertical with opposing dips between 65° and 85° (median for both localities is 80°, Fig. 9). In some parts of the Desertas, however, dyke dips are not opposed, but tend to be inclined eastward (Fig. 8). This asymmetry of dyke dips places the former rift axis to the west of the islands, since the margins on either side of a wedge-shaped dyke complex are characterised by an outward dip. Dykes at Koolau are generally oriented parallel to the rift axis except around the Kailua caldera. In contrast, the main dyke swarm of the Desertas rift strikes oblique to the morphological ridge (Klügel et al., 2002). A systematic change of dyke azimuths along the Desertas ridge was not observed.

Dyke density is much higher at the Koolau complex where dykes constitute 50-70 % of total rock than on the Desertas where we estimate the dyke portion to be less than 30 %. Since dyke density increases with depth within the dyke wedge which underlies a rift zone, this observation

might be ascribed to the fact that the Koolau dyke complex with maximum degradation depths up to 900 m is deeper eroded than the Desertas rift with estimated erosion of 300-400 m (see below).

Desertas dykes have an average width of 2.1 m and are thus wider than Koolau dykes with an average width of 0.73 m (Fig. 10). This might reflect a higher viscosity of the Desertas magmas or a greater distance from the volcanic centre (Walker, 1987). However, the width of Desertas dykes is not correlated with increasing phenocryst contents or differentiation degrees. In addition, we did not find any systematic variation in width on the Desertas, whereas the width of Koolau dykes increases with distance from the Kailua caldera.

Table 2 Comparison of the Desertas dyke complex with Koolau (Oahu/Hawaii; Walker, 1987))

	Koolau	Desertas
Tectonic setting	buttressed by older parallel volcano pile	elongated volcano pile which intersects the elongated and obliquely oriented island of Madeira
Caldera	Caldera in the southern part of the dyke complex	no indications of a caldera
Dyke density	dykes constitute 50-70% of total rock --> deep levels of the dyke complex are exposed (up to 900 m depth)	dyke complex less dense, dykes constitute less than 50% of total rock, i.e. higher levels of complex are exposed (estimated depth max. 400 m below former surface)
Sheeted dykes	abundant	partially in the central parts of Desertra Grande and Bugio
Dyke trends	parallel to elongation and radially around the caldera	slightly oblique to elongation (10-20°; Klügel et al., 2002)
Median dip	80°	80°
Dyke width	90% < 1.5 m median ~0,5 m mean ~0,73 m dyke width increases with distance from caldera	90% < 5 m median 1 m mean ~ 2,1 m no systematic change in dyke width along the rift axis

Reconstruction of the Desertas rift morphology

The high aspect ratios of the eroded subaerial flanks and the occurrence of plateau-forming, subhorizontal lava flows evidence that the islands must have been far wider than at present. This is in accordance with the pronounced submarine abrasion platforms around the Desertas, supposed to roughly trace the former coastline. Based on the width of these platforms (Fig. 5), we suggest that the Desertas must have been 1-2.5 km wider to each side of the islands which transforms into an original width of the subaerial ridge between 3 and 6 km. If we assume a maximum aspect ratio of 0.13, as is representative of subaerial parts of recently active and steep rift zones such as the Cumbre Vieja (La Palma/Canary Islands) and Pico (Azores), we conclude that the Desertas might have been up to 300-400 m higher than at present (Fig. 5).

Based on the morphology, the distribution of volcanics and intrusions as well as fault orientations, we reconstructed the approximate trend of the former rift axis. The following

observations suggest that the axis was oriented sub-parallel to the Desertas ridge crossing the western parts of Pedregal and the island of Bugio (Fig. 1a):

1. Ridge-parallel normal faults and graben structures indicate an overall azimuth around 160° of the former rift axis (Fig. 7).
2. Due to the paucity of proximal pyroclastics and the abundance of type 2 lava flow sequences, Chão island must be located at some distance to the rift axis to a central volcano, respectively.
3. Deserta Grande represents the eastern margin of the rift zone as suggested by (1) an eastward decrease of proximal pyroclastics (cinder, spatter, bombs) associated with an increase of type 2 lava flows (Fig. 7); (2) mainly E-dipping dykes in the central part of Deserta Grande (Fig. 8); (3) E-dipping distal lava flows in the central and southern part; and (4) shallow abrasion platforms which are wider to the west than to the east of the islands. In addition, graben structures to the west of Pedregal and at northern Deserta Grande may indicate close proximity to the rift axis.
4. Southern Bugio is supposed to represent the deeply eroded rift core as is reflected by (1) the concentration of former eruptive centres; (2) the paucity of lava flow series; (3) numerous sill-like intrusions; and (4) the overall high dyke density. Moreover, dyke dips are opposed as is typical for the inner parts of a coherent dyke complex (Fig. 8).

Geochemical evolution of the late Desertas stage

The subaerially exposed rocks of the Desertas rift overlap in major and trace element compositions with those from the Madeira shield phase (Geldmacher and Hoernle, 2000). There is no systematic variation in chemistry along the rift or within the stratigraphic sequence except for young lavas exposed on the top of Deserta Grande and Bugio. These samples having ages between 2.1 and 3.4 Ma show strongly enriched Y and HREE or REE contents unique on the archipelago. Since these rocks occur on the strongly weathered top of the island, one may suspect that enrichment of specific elements is related to secondary processes or anthropogenic contamination. Ratios of mobile to immobile incompatible elements, however, fall into the range of other Desertas samples (e.g. Rb/Nb = 0.30-0.49, Ba/Nb = 5.3-7.5, K/Nb = 146-197). Given that mobile elements appear to be unaffected and that only the relatively immobile REE and Y are enriched, alteration or contamination seem an unlikely explanation. Thus, the unusual geochemical composition of the late Desertas lavas must be associated with primary magmatic processes such as (1) variations in melting degree, (2) varying source composition or (3) contamination of the ascending melts by assimilating highly REE-enriched phases.

Possibility (1) can be ruled out because an increasing degree of partial melting would not only decrease the LREE/HREE ratios but also those of other highly to moderately incompatible

elements, which is not observed. As possibility (2), garnet exhaustion during melting of a peridotitic mantle source would cause release of HREE, compatible in garnet, and thus their enrichment relative to LREE, explaining the flat REE spectra of late Desertas lavas. Whilst this hypothesis appears plausible at first sight, garnet exhaustion is not indicated by other geochemical parameters and does not explain the strong enrichment of all REE in some late stage Desertas rocks associated with extremely high ratios of e.g. Ce/Pb, Sr/Nd and Zr/Sm and low Nb/La. Alternatively, the strong decrease in Hf/Sm and Zr/Yb of these lavas could indicate a change from pyrope to Ca-rich garnet, i.e. from a peridotitic to a more eclogitic mantle source (van Westrenen et al., 2001). This scenario, however, seems unlikely because (1) it would result in an increased melt production rather than cessation of Desertas volcanism, and (2) because it does not explain the relative HREE enrichment of some lavas. Moreover, a change to a more eclogitic source would be the opposite of the model of Geldmacher and Hoernle (2000) requiring progressive exhaustion of the eclogitic component of recycled oceanic crust within the Madeira/Desertas mantle source.

Finally, the observed REE enrichment might result from melting of a REE-rich mineral such as chevkinite (Troll et al., 2003) either within the source or, as possibility (3), during reactive flow or shallow level assimilation. Such high REE concentrations as observed, however, would require selective melting and assimilation of a refractory REE-rich mineral without involving its host rock, which appears highly unlikely. In addition, chevkinite prefers the LREE over the HREE, wich is not in accordance with our data, and there is no isotopic evidence for crustal contamination of the late Desertas lavas (Geldmacher and Hoernle, 2000; Schwarz, unpubl. data).

In summary, it is difficult to reconstruct any secondary process, contamination scenario or source component that has provoked the observed REE enrichment. Although we cannot provide a final model, we speculate that this remarkable trace element distribution reflects mantle processes causally related to the cessation of Desertas volcanism while volcanic activity on Madeira continued during the Late Madeira shield stage.

Evolution of the rift zone

The emergence and conspicuous morphology of the Desertas ridge and its rift orientation cannot be explained simply by regional stresses or plate motion. One current model to explain the formation of the Desertas rift is an interconnection with Madeira in terms of a two-armed rift system analogue to Hawaiian volcanoes such as Kilauea (Fig. 1; Geldmacher et al., 2000). If this were the case, one would expect a central volcano at the projected intersection of the Madeira and Desertas rift axes from where the two rifts would emanate, i.e. near São Lourenço, the easternmost tip of Madeira. However, there is no volcanological or morphological evidence for such a central volcano connecting Madeira and the Desertas. In fact, the thickness of the stratigraphic sequence

on Madeira increases westward from São Lourenço to the central part of the island where the main activity took place during the Early as well as Late Madeira rift phases (Geldmacher et al., 2000; Schwarz et al., 2004). Additionally, well-preserved submarine volcanic cones at 700-1000 m water depths, discovered and sampled during the R/V Meteor cruise M51/1 in-between São Lourenço and the Desertas (Hoernle et al., 2001), indicate that this part never emerged above sea level and thus was never as productive as the Desertas and Madeira rifts.

Petrographic and geobarometric differences between rocks from São Lourenço and the Desertas (Schwarz et al., 2004) combined with our volcanological observations rather point to two discrete volcanic systems. This hypothesis is supported by the exclusive occurrence of strongly REE- and Y-enriched lavas on the Desertas during the late subaerial stage and their absence on Madeira. We conclude, therefore, that the Desertas ridge represents a separate volcano whose period of subaerial activity lasted from at least 5.1 Ma to 2 Ma and thus partly overlapped with that of Madeira. Then, the question arises why growth of the Desertas volcano resulted in a strongly elongated ridge rather than a roughly circular edifice. It is conceivable that in the absence of a suitable regional stress field, the rift orientation and morphology were most likely caused by local gravitative stress. We propose that during the early submarine shield stage of Madeira, one or more proto-Desertas seamounts formed and grew. When these volcano piles overlapped with the lower flank of Madeira, the resulting gravitative stress field became such that preferred extension occurred in-between the Desertas and São Lourenço. The working of this particular scheme of volcano spreading has been demonstrated experimentally (Klügel et al., 2002; Walter, 2003; Klügel and Walter, 2003) and is facilitated by a ductile sediment layer underlying the archipelago.

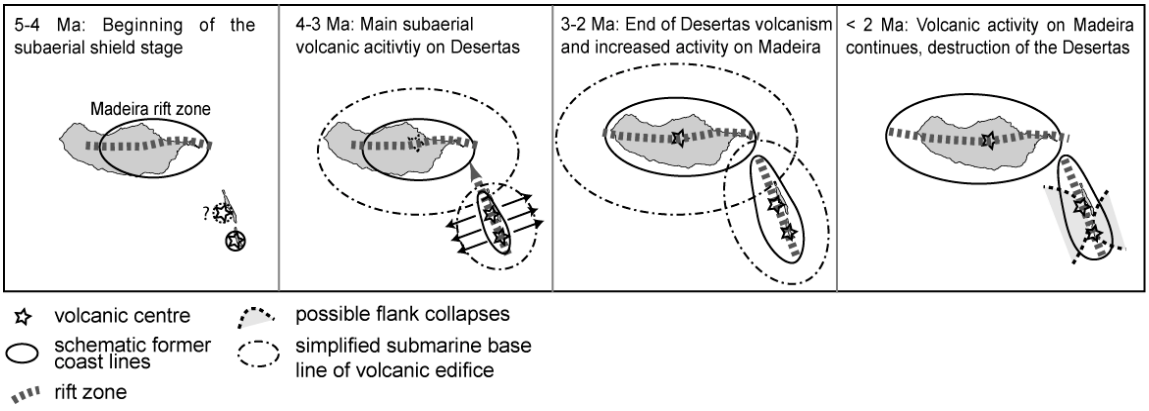

Fig. 14 Evolution model of the Madeira/Desertas volcanic complex. The Desertas ridge represents a separate volcanic systems which became interconnected with Madeira by growth. The volcanic centre of the Desertas ridge was located either to the south-west of Pedregal (Deserta Grande) or at the southern tip of the ridge (Bugio). When the proto-Desertas overlapped the flank of Madeira, the resulting stress field became such that preferred extension occurred in-between the two overlapping edifices triggering the formation of a distinctive rift zone and the elongation of the Desertas volcano. Marine erosion and repeated flank collapses probably removed a central volcano south-west of Deserta Grande and/or great parts of the volcano's southern end where Bugio is located at present.

Although our hypothesis cannot be verified, it is supported by our field data and age determinations which allow to place constraints on the locality of the presumed proto-Desertas volcano. One possible locality is south-west of Pedregal, the widest part of Deserta Grande and the central part of the ridge, from where two rifts propagated north- and southwards (Fig. 14). This model is supported by the following observations: (1) The oldest dated rocks of the Desertas Islands are derived from an intrusion located at sea level near the base of Pedregal which may represent an old core of the rift (Fig. 15); (2) the thickness of stratigraphic sections between 3.6 and ~3 Ma increases from Chão and Bugio towards Deserta Grande, i.e. towards the central part of the rift (Fig. 15); and (3) the occurrence of proximal deposits such as bombs and thick tuff layers decrease and massive sequences of type 2 flows increase from Pedregal towards north and east. This model is somewhat comparable with two-armed rifts of Kilauea or Mauna Loa, yet the important difference is the lack of any evidence for a collapse caldera or a shallow magma reservoir beneath Pedregal (Schwarz et al., 2004). However, it is conceivable that a former central caldera near Pedregal became removed by marine erosion and/or flank collapses.

Alternatively, a central volcano may have been located at the present island of Bugio, from where the rift successively developed northward towards Madeira (Fig. 14). Such an evolution of the Madeira/Desertas complex would differ significantly from that of a two-armed rift system. The extreme concentration of eruptive sites and intrusions at Bugio, particularly in its southern part, indicate proximity to the rift axis and argue in favour of this hypothesis (Fig. 7). In contrast, Chão island is composed dominantly of type 2 lava flows and Deserta Grande shows an alternation of lava flow sequences and pyroclastics proximal to eruptive centres. Considering the bathymetry to the west of Bugio, it appears that large parts of the southern Desertas edifice was removed by flank collapses or even giant landslides (Fig. 14). This would also explain the remarkably sickle-shaped form of the southernmost island. Likewise, the bathymetry to the west of the gap between Deserta Grande and Bugio may indicate thick deposits of marine erosion and collapses. Without detailed bathymetric data, however, these interpretations remain speculative.

As a third alternative, the evolving Desertas rift may have been characterised by two main volcanoes, one at Pedregal and one at southern Bugio. This scenario is a combination of the two hypotheses discussed above and cannot be distinguished from them by our data.

Inferences on the distribution of Madeira-Desertas volcanism

If the Desertas represented a discrete volcano rather than a rift arm as part of the Madeira system, the question arises why the Desertas volcanism occurs off the main hotspot axis and alternates with volcanic activity on Madeira. A conceivable model for the initiation of Desertas volcanism is lithospheric bending caused by the loads of Madeira and Porto Santo, combined with

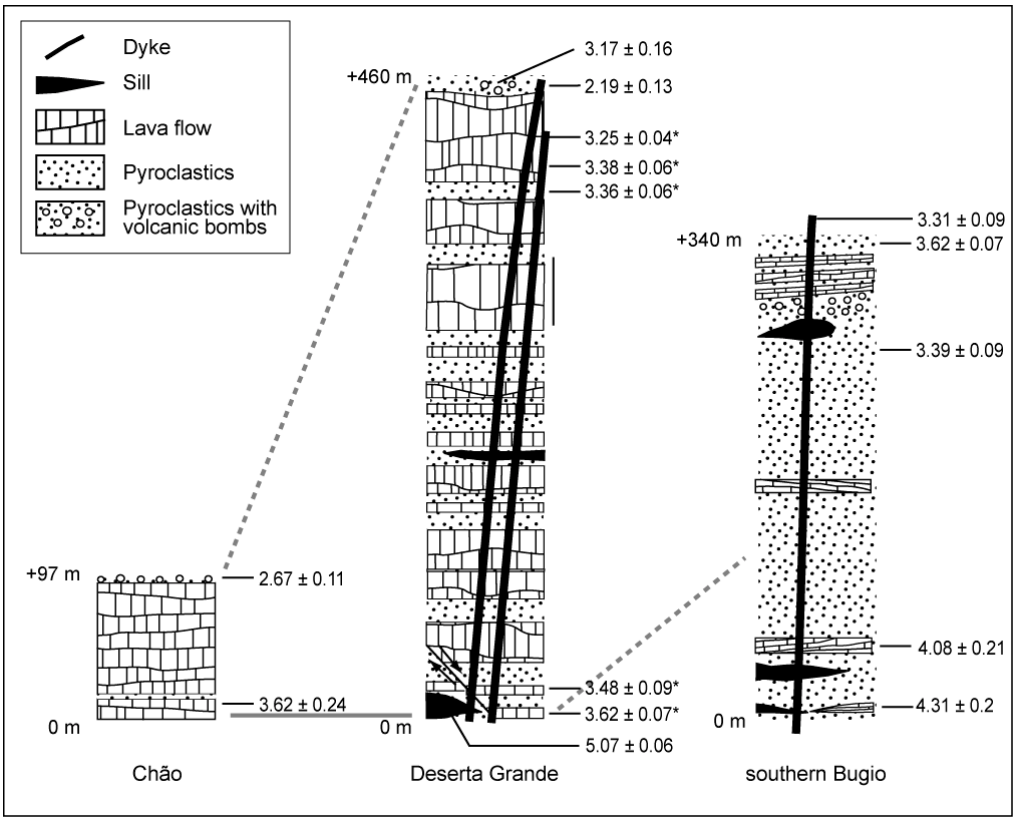

Fig. 15 Composite stratigraphic sections shown for Chão (left), Deserta Grande (centre) and the southern part of Bugio (right) summarising the subaerial units of the Desertas rift system. Elevations are given in m above sea level. Radiometric age data are given in Ma with 1σ errors. Numbers with one asterisk identify $^{40}Ar/^{39}Ar$ ages from Geldmacher et al. (2000), all other numbers are from this study.

distinct roots of the Desertas and Madeira volcanoes in the postulated mantle plume (Schwarz et al., 2004). This model implies that horizontal stresses are approximately zero at the transition between flexural depression and bulge of the bend (ten Brink, 1991; Hieronymus and Bercovici, 1999, 2001) which may have facilitated magma ascent through the lithosphere and thus the activation of Desertas volcanism.

Additional geodynamic factors to explain the distribution of volcanism include plume dynamics, plate velocity and possible changes in the direction of plate motion. First, the Madeira hotspot is ascribed to a weak, pulsating or blob-type plume (Geldmacher and Hoernle, 2000, 2001), the shape of which might be influenced by upper mantle convection. Thus, the axis of upwelling and the melting region within the plume head might shift laterally causing migration of surface volcanism with time (Schwarz et al., 2004). Second, the Madeira/Desertas complex is located on the slowly moving African plate whose dynamics have changed significantly around 6 Ma ago, i.e. near the beginning of the subaerial Madeira/Desertas shield stages. Prior to the onset of Madeira/Desertas volcanism, the pole of the counter-clockwise rotating African plate was located to the north-east of the archipelago (Purdy, 1975; Duncan, 1981; Morgan, 1983; Pollitz, 1991; Geldmacher et al., 2000) resulting in a NE-directed plate motion in the Madeira region. During the

build-up of the islands (< 6 Ma), the pole shifted to a position at about 19°N, 16°W (Pollitz, 1991) which should result in a SE-directed plate motion for the Madeira region as also indicated by the model of HS2-NUVEL-1 present-day global absolute plate motion (Gripp and Gordon, 1990). Since the postulated pole shift was most likely a gradual change over a few million years rather than an abrupt transition, and because the islands are close to the new rotation pole, we assume a nearly steady position for the Madeira and Desertas islands above the mantle plume during their subaerial shield stage (< 5 Ma). It is thus conceivable that the proposed blob of upwelling plume material beneath Madeira (Geldmacher and Hoernle, 2000) released its mantle melts into an almost fixed lithosphere area over the last 5 Ma. As a consequence, any plume-related lateral shift of the melting zone beneath Madeira, or changing lithospheric stress, may have affected the distribution of volcanism more than slow plate motion itself.

In summary, the load of the volcanic edifices of Madeira and Porto Santo might have caused a lithospheric flexure resulting in extensional stress and the initiation of Desertas volcanism. Combined with lateral variations of the melting region or two adjacent melting regions within the plume, this scenario could explain the simultaneous formation of the two neighbouring volcanic systems on an extremely slow moving plate. This leads to a more complex volcano pattern rather than a linear chain of volcanoes as is the case for the Hawaiian hotspot.

Conclusions

The results of detailed field study and $^{40}Ar/^{39}Ar$ age determinations reveal a significant insight in the evolution of the Desertas rift zone (Madeira archipelago) in the eastern North Atlantic. Our data presented in this study allow inferences on the interior structure of such rifts, their volcanotectonic origin and evolution.

1. Volcanic activity on the Desertas Islands lasted from at least 5.1 Ma to about 1.9 Ma and thus clearly overlaps with the Early Madeira rift phase (>4.6-3.9 Ma) and Late Madeira rift phase (3.0-0.7 Ma). Most rock ages fall within a range between 4 and 3 Ma indicating the main phase of subaerial volcanism.
2. Detailed mapping indicates that explosive volcanism due to magma-sea water interaction was dominant during the early subaerial stage of the Desertas resulting in the deposition of a basal tuff sequence. With increasing height of the islands, effusive processes became more important indicated by lava flows overlying the basal tuff.
3. It was shown that volcanic deposits which indicate proximity to eruptive centres increase along the rift towards south. Volcanic structures as well as the morphology of the Desertas ridge suggest that the former rift axis was oriented subparallel to the Desertas ridge and has been located to the west of Deserta Grande and along Bugio.

4. Major and trace elements show no temporal variation until the late subaerial shield stage when strongly REE- and Y-enriched lavas were erupted. Along the rift we did not observe any systematic variation in chemistry.
5. The conspicuous morphology of the Madeira/Desertas complex, the distribution of volcanics and rock ages suggest that the Desertas ridge represents a discrete volcanic system. This is supported by barometric data and by the exclusive occurrence of strongly REE-enriched lavas on the Desertas. We propose that the Desertas system became interconnected with Madeira by growth towards north-northeast starting from a centre either west of Deserta Grande or at the southern tip of Bugio. A conceivable explanation for the formation of the elongated Desertas rift are local gravitative stresses caused by the two overlapping Madeira and Desertas edifices resulting in preferred extension in-between. A significant difference to caldera-centred two-armed rift systems on Hawaii, which often serve as a rift prototype, is the lack of a central volcano underlain by a shallow magma chamber from where rift zones emanate.
6. General geodynamic conditions in the eastern North Atlantic may influence the distribution of volcanism of the Madeira hotspot. Changing motion dynamics of the African plate resulted in a nearly steady position of the Madeira/Desertas complex over the mantle plume during the last million years. Extensional stresses due to lithosphere flexure caused by the loads of the Porto Santo and Madeira shields may have led to the initiation of Desertas volcanism. Flexural stresses combined with plume irregularities, low or even pausing plate motion and a weak mantle plume possibly resulted in the simultaneous formation of two closely neighboured volcanic systems, namely Madeira and the Desertas, rather than a discrete chain of volcanoes as is the case in the Hawaiian Islands.

Acknowledgement We are grateful to Directors Costa Neves and Susana Fontinha and the staff from the Parque Natural da Madeira (in particular Gil Pereira) for their logistical support during our field trips on Madeira and the Desertas Islands. Field work on the islands would not have been possible without their help and generous support. We also thank Karsten Galipp for his excellent assistance during one of the field trips. The paper benefited from discussions with, and critical comments of, Kaj Hoernle, Colin Devey, Tom Walter and Bärbel Kleinefeld. The research was supported by the Deutsche Forschungsgemeinschaft (DFG grant KL1313/2-1).

Appendix

For detailed XRF- and ICP-MS analyses see the Appendix 5 and 6 of the *Electronic Appendix*.

For electronic suplement material (volcanological map and location map of measured dykes of the Desertas Islands) see *Electronic Appendix* , EMap1 and EMap2.

References

Anderson, E.M., 1951. The dynamics of faulting, 2nd edn. Oliver and Boyd, Edinburgh:

Carracedo, J.C., 1994. The Canary Islands: an example of structural control on the growth of large ocean-island volcanoes. J. Volcanol. Geotherm. Res. 60: 225-241.

Carracedo, J.C., 1999. Growth, structure, instability and collapse of Canarian volcanoes and comparisons with Hawaiian volcanoes. J. Volcanol. Geotherm. Res. 94: 1-19.

Chaffey, D.J., Cliff, R.A., Wilson, B.M., Characterization of the St Helena magma source. In: A.D. Saunders, M.J. Norry (Editors), Magmatism in the Ocean Basins. Geological Society Special Publication No. 42, pp. 257-276.

Clague, D.A., Dalrymple, G.B., 1987. The Hawaiian-Emperor volcanic chain, Part I: Geologic evolution. In: Volcanism on Hawaii, U.S. Geol. Surv. Prof. Pap. 1350: 5-54.

Delaney, R.I., Dvorak, J.J., 1993. Anatomy of a basaltic volcano. Nature 363, 125-133.

Dietrich, J.H., 1988. Growth and persistence of Hawaiian volcanic rift zones. J. Geophys. Res. 93 B5: 4258-4270.

Duffield, W.A., Christiansen, R.L., Koyanagi, R.Y., Peterson, D.W., 1982. Storage, migration and eruption of magma at Kilauea Volcano, Hawaii, 1971-1972. J. Volcanol. Geophys. Res. 13: 273-307.

Duffield, W.A., Dalrymple, G.B., 1990. The Taylor Creek Rhyolite of New Mexico: a rapidly emplaced field of domes and lava Flows. Bull. Volcanol. 52: 475-478.

Duncan, R.A., 1981. Hotspots in the southern oceans-An absolute frame of the reference for motion of the Gondwana continents. Tectonophysics 74: 29-42.

Gautneb, H., Gudmundson, A., 1992. Effect of local and regional stress fields on sheet emplacement in West Iceland. J. Volcanol. Geotherm. Res. 51: 339-356.

Geldmacher, J.,Hoernle, K.A., 2000. The 72 Ma geochemical evolution of the Madeira hotspot (eastern North Atlantic): recycling of Paleozoic (500 Ma) oceanic lithosphere. Earth Planet. Sci. Lett. 183: 73-92.

Geldmacher, J.,Hoernle, K.A., 2001. Corrigendum to: The 72 Ma geochemical evolution of the Madeira hotspot (eastern North Atlantic): recycling of Paleozoic (500 Ma) oceanic lithosphere. Earth Planet. Sci. Lett. 186: 133.

Geldmacher, J., Bogaard, P.v.d., Hoernle, K.A., Schmincke, H.-U., 2000. The $^{40}Ar/^{39}Ar$ age dating of the Madeira Archipelago and hotspot track (eastern North Atlantic). G3 Geochem. Geophys. Geosys. 1, 1999GC000018.

Gripp, A.E., Gordon, R.G., 1990. Current plate velocities relative to the hotspots incorporating the NUVEL-1 global plate motion model, Geophys. Res. Lett., 17, 1109-1112.

Halliday, A.N., Lee, D.-C., Tommasini, S., Davies, G.R., Paslick, C.R., Fitton, J.G., James, D.E., 1995. Incompatible trace elements in OIB and MORB and source enrichment in sub-oceanic mantle. Earth. Planet. Sci. Lett. 133: 379-395.

Hieronymus, C.F., Bercovici, D., 1999. Discrete alternating hotspot islands formed by interaction of magma transport and lithospheric flexure. Nature 397: 604-607.

Hieronymus, C.F., Bercovici, D. 2001. A theoretical model of hotspot volcanism: Control on volcanic spacing and patterns via magma dynamics and lithospheric stresses. J. Geophys. Res. 106 (B1): 683-702.

Hill, D.P., Zuca, J.J., 1987. Geophysical constraints on the structure of Kilauea and Mauna Loa volcanoes and some implications for seismomagmatic processes. In: Decker, R.W., Wright, T.W., Stauffer, P.H. (eds.), Volcanism in Hawaii. US Geol Surv Prof Paper 1350: 903-917.

Klügel, A., Walter, T.R., 2003. A new model for the formation of rift zones on oceanic island volcanoes. Geophys. Res. Abstr. 5: 03913.

Klügel, A., Walter, T.R., Schwarz, S., 2002. Gravitative spreading causes en-echelon diking along a volcanic rift zoen: observations from Madeira and an experimantal approach. Eos Trans. AGU, 83(47), Fall Meet. Suppl., Abstract T22A-1129.

Koppers, A., Staudigel, H., Wijbrans, J.R., 2000. Dating crystalline groundmass separates of altered Cretaceous seamount basalts by the $^{40}Ar/^{39}Ar$ incremental heating technique. Chem. Geol. 166: 139-158.

Lanphere, M.A., Dalrymple, G.B., 2000. First-Principles Calibration of ^{38}Ar Tracers: Implications for Ages of $^{40}Ar/^{39}Ar$ Fluence Monitors: US Geol. Surv. Prof. Pap. 1621, 10 pp.

Le Maitre, R.W., Bateman, P., Dudek, A., Keller, J., Lameyre, J., Le Bas, M.J., Sabine, P.A., Schmid, R., Sorensen, H.,Streckeisen, A., Wooley, A.R., Zanettin, B., 1989. A Classification of Igneous Rocks and Glossary of Terms -Recommendations of the International Union of Geological Sciences Subcommission on the Systematics of Igneous Rocks. Blackwell Scientific Publications (Oxford): pp. 193.

MacDonald, G.A., 1968. Composition and origin of Hawaiian lavas. In: Coats, R.R., Hay, R.L., Andersen, C.A. (eds.) Studies in volcanology: a memoir in honour of Howel Williams. Geol. Soc. Amer. Mem. 116: 477-522.

Morgan, W.J., 1983. Hotspot tracks and the early rifting of the Atlantic. Tectonophysics 94: 123-139.

Nakamura, K. 1980. Why do long rift zones develop in Hawaiian volcanoes; a possible role of thick oceanic sediments. Bull. Geol. Soc. Jpn. 25: 255-269.

Pollitz, F.F., 1991. Two-stage model of African absolute motion during the last 30 million years. Tectonophysics 194: 91-106.

Purdy, G.M., 1975. The eastern end of the Azores-Gibraltar Plate Boundary. Geophys. J. R. Astron. Soc. 43:973-1000.

Roest, W.R., Dañobeitia, J.J., Verhoef, J., Collete, B.J., 1992. Magnetic Anomalies in the Canary Basin and the Mesozoic evolution of the Central North Atlantic. Marine Geophys. Res. 14: 1-24.

Ryan, M.P., 1988. The mechanics and three-dimensional internal structure of active magmatic systems: Kilauea volcano, Hawaii. J. Geophys. Res. 93 B5: 4213-4248.

Schwarz, S., Klügel, A., Wohlgemuth-Ueberwasser, C., 2004. Melt extraction pathways and stagnation depths beneath the Madeira and Desertas rift zones (NE Atlantic) inferred from barometric studies. Contr. Mineral. Petrol. 147: 228-240.

Sleep, N.H., 1990. Hotspots and mantle plumes: some phenomenology. J. Geophy. Res. 95: 6715-6736.

Steiger, R.H., Jäger, E., 1977. Subcommission on geochronology: Convention on the use of decay constants in geo- and cosmochronology. Earth Planet. Sci. Lett. 36: 359-362.

Sun, S.S., McDonough, W.F., 1989. Chemical and isotopic systematics of oceanic basalts: implications for mantle composition and processes. In: A.D. Saunders, M.J. Norry (Editors), Magmatism in the Ocean Basins. Geological Society Special Publication No. 42, pp. 313-345.

Taylor, J.R., 1982. An Introduction to Error Analysis. University Science Books, Mill Valley, CA, 270 pp.

ten Brink, U., 1991. Volcano spacing and plate rigidity. Geology 19: 397-400.

van Westrenen, W., Blundy, J.D. and Wood, B.J., 2001. High field strength element/ rare earth element fractionation during partial melting in the presence of garnet; implications for identification of mantle heterogeneities. Geochem., Geophys., Geosys. 2, 2000GC000133.

Walker, G.P.L., 1987. The dike complex of Koolau volcano, Oahu: Internal strucutre of a Hawaiian rift zone. In: Volcanism in Hawaii. U.S. Geol. Surv. Prof. Pap. 1350: 961-993.

Walker, G.P.L., 1992. "Coherent intrusion complexes" in large basaltic volcanoes - a new structural model. J Volcanol. Geotherm. Res. 50: 41-54.

Walker, G.P.L., 1999. Valcanic rift zones and their intrusion swarms. J Volcanol Geotherm Res 94: 21-34 DOI 10.1016/S0377-0273(99)00096-7.

Walter, T.R., 2003 Buttressing and fractional spreading of Tenerife, an experimental approach on the formation of rift zones. Geophys. Res. Lett. 30 (6): 1296.

Weaver, B.L., 1991. The origin of ocean island basalt end-member compositions: trace element and isotopic constraints. Earth Planet. Sci. Lett. 104: 381-397.

Wright, T.L., Fiske R.S., 1971 Origin of the differentiated and hybrid lavas of Kilauea volcano, Hawaii. J. Petrol. 12: 1-65.

York, D., 1969. Least squares fitting of a straight line with correlated errors. Earth Planet. Sci. Lett. 5: 320–324.

Zbyszewski, G., Cândido de Medeiros, A., da Veiga Ferreira, O., Torrede Assunção, C., 1973. Carta geológica de Portugal 1/50,000, Noticia explicativa da Folha Ilhas Desertas, Serv. Geol. de Portugal, Lisbon.

Zbyszewski, G., de Veiga Ferreira, O., Cândido de Medeiros, A., Aires-Barros, L., Silva, L.C., Munha, J.M., Barriga, F., 1975. Carta geológica de Portugal 1/50,000, Noticia explicativa das Folhas A e B da Ilha Madeira, Serv. Geol. de Portugal, Lisbon.

IV Geochemical evolution of volcanic rift systems in the Madeira Archipelago (NE Atlantic)

Stefanie Schwarz[1)], Andreas Klügel[1)], Paul van den Bogaard[2)], Folkmar Hauff[2)], Kaj Hoernle[2)]

[1)] Departement of Geosciences, University of Bremen, Germany
[2)] IFM-GEOMAR, Kiel, Germany

To be submitted to Chemical Geology

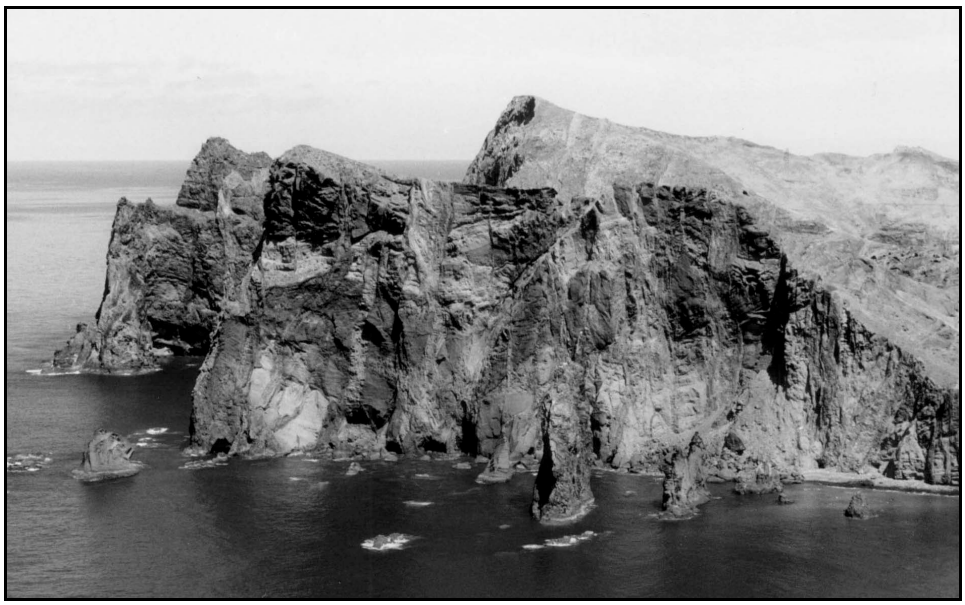

View into the Madeira rift zone at São Lourenço

Geochemical evolution of volcanic rift systems in the Madeira Archipelago (NE Atlantic)

Stefanie Schwarz[1)], Andreas Klügel[1)], Paul van den Bogaard[2)], Folkmar Hauff[2)], Kaj Hoernle[2)]

[1)] *Department of Geosciences, University of Bremen, Germany*
[2)] *IFM-GEOMAR, Kiel, Germany*

To be submitted to Geochemical Geology

Abstract

Madeira and the adjacent Desertas Islands (eastern North Atlantic) show two well-developed rift zones with temporally linked volcanic activity. Their axes intersect near São Lourenço peninsula, the easternmost tip of Madeira. We carried out a detailed field study at São Lourenço combined with age determinations and geochemical analyses to find out whether the magmatic systems of the Madeira and Desertas rifts were interconnected near the peninsula. $^{40}Ar/^{39}Ar$ age determinations revealed that the rift at São Lourenço was active from >5.3 to 0.9 Ma, i.e. during the entire subaerial shield stage of Madeira, with a period of eruptive quiescence between 4 and 2.5 Ma. Major element, trace element and Sr-Nd-Pb isotope data combined with ages of volcanic rocks from São Lourenço show a characteristic geochemical evolution over time with decreasing FeO_{tot}, SiO_2 and Mg# and a tendency to more radiogenic Sr and Pb isotope ratios and to less radiogenic $^{143}Nd/^{144}Nd$ ratios with decreasing age. Incompatible element signatures as well as Pb and Nd, isotope ratios from the peninsula are consistent with the presence of recycled oceanic crust in the Madeira source and progressive exhaustion of its eclogitic component during shield stage volcanism (Geldmacher and Hoernle, 2000, 2001). Among all Madeira and Desertas shield stage samples of similar age, the São Lourenço rocks include the most depleted isotope compositions (least radiogenic Pb ratios and most radiogenic $^{143}Nd/^{144}Nd$). In contrast, rocks from the neighbouring Desertas rift zone show the most enriched Pb and Nd isotope ratios and do not follow the overall Madeira trend, i.e. the tendency to more depleted Pb, Sr and Nd isotope ratios with decreasing age. The depleted isotope composition of São Lourenço lavas is not compatible with mixing of Desertas and Madeira melts at crustal or mantle depths or with magma transport from Madeira to the Desertas along the rift at São Lourenço. We propose that there is no volcanological interconnection of the Madeira and Desertas rift systems near the São Lourenço peninsula. Our model rather comprises a discrete Desertas volcano which roots in a particular sector of the melting region within the Madeira plume. A shift of volcanic activity between the two neighbouring Madeira and Desertas rifts, as indicated by rock ages, can be explained by an irregularly shaped plume causing lateral variations in melt production.

Keywords: Madeira; volcanic rift zone; $^{40}Ar/^{39}Ar$ geochronology; Sr-Nd-Pb isotopes; mantle plume

Introduction

Volcanic rift zones are primary structures of oceanic islands and have been described in settings such as Hawaii and the Canary Islands (e.g. Walker, 1999; Carracedo, 1994, 1999). They are narrow zones where volcanic activity concentrates by intrusion and extrusion resulting in elongated volcano piles. Characteristic features are dyke swarms, scoria and cinder cones stacked one onto another, lava flows extending from the rift zone and parallel graben structures. Rift zones are known to have a strong control on magma evolution and transport during ascent through the crust (e.g. Garcia et al., 1989; Delaney et al., 1990; Tilling and Dvorak, 1993; Klügel et al., 2000). Although a lot has been published about Hawaiian rifts such as Kilauea's East Rift Zone (Wright and Fiske, 1971; Duffield et al., 1982; Ryan, 1988; Yang et al., 1999; Quane et al., 2000; Johnson et al., 2002), little is known about the petrologic and geochemical evolution of a rift zone over time.

There are few examples where the interior of rift zones is well exposed, except on deeply eroded ocean islands such as Oahu (Hawaii). The Madeira Archipelago, located in the eastern North Atlantic, is an ideal place to undertake a detailed rift study since it has two well-developed and deeply eroded rift zones: (1) the E-W trending Madeira rift, and (2) the NNW-SSE oriented Desertas rift. Both may belong to the same volcanic system and form a two-armed rift analogous to those in Hawaii (Geldmacher et al. 2000; Geldmacher and Hoernle, 2000, 2001). Alternatively, barometric and volcanological studies combined with $^{40}Ar/^{39}Ar$ age determinations and major and trace element data suggest that the Desertas Islands are part of a discrete volcano (Schwarz et al., 2004a, 2004b). We address the following questions: (1) what is the temporal geological and geochemical evolution of a rift zone and two neighbouring rift systems as is the case for Madeira, and (2) was there an interconnection and possibly an interaction between both the Madeira and Desertas rift systems?

For this purpose, we investigate the São Lourenço peninsula, an extremely well-exposed part of the Madeira rift located at the easternmost tip of Madeira and near the projected junction of the two Madeira and Desertas rift axes. Due to its geographic position, São Lourenço may provide geochemical information about its possible role as a connector between the two neighbouring Madeira and Desertas rift systems. Additionally, the peninsula offers a good opportunity to study the temporal geochemical evolution of a rift zone, since its stratigraphic sequence covers the complete subaerial shield stage and thus resembles a section through the subaerial volcanic history of Madeira. Due to the limited dimension of the area studied, variations of e.g. magma chemistry can be ascribed to temporal changes rather than to spatial variations within the rift itself. Although geochemical studies of rock composition and age determinations have been carried out on Madeira (e.g. Hoernle et al., 1991; Mata et al., 1998; Geldmacher and Hoernle, 2000), no data has been

published from São Lourenço. Therefore, an additional aim of this study is to complete the data set for Madeira.

To elucidate the stratigraphic succession of São Lourenço, we have undertaken $^{40}Ar/^{39}Ar$ age dating combined with a detailed field study of volcanic structures. By means of these data combined with main element, trace element and Sr-Nd-Pb isotope data, we deduce the geochemical evolution of Madeira and its prominent rift zone during the subaerial shield stage. We compare the geochemical evolution of São Lourenço with that of the Desertas Islands and investigate if both the Madeira and Desertas rifts were interconnected. Finally, we discuss if plume irregularities might have influenced the evolution and distribution of hotspot-related volcanism in Madeira archipelago.

Geology and previous studies

The Madeira Archipelago is situated in the eastern North Atlantic 700 km from the north-western coast of Africa and comprises the islands Madeira, Porto Santo and the three Desertas Islands (from N to S: Chão, Deserta Grande, Bugio; Fig. 1). The islands are located on Cretaceous oceanic crust between magnetic anomalies M4 and M16 (ages between 126 and 142 Ma; Klitgord and Schouten, 1986; Roest et al., 1992) and Madeira represents the present locus of the Madeira hotspot that can be traced back to 70 Ma (Geldmacher et al. 2000). The main island rises from about 4000 m water depth to an elevation of 1896 m a.s.l., and the Desertas up to 480 m.

Madeira is a typical shield volcano with a pronounced E-W oriented volcanic rift zone and the Desertas Islands are interpreted to represent a NNW-SSE oriented rift (Fig. 1a, Geldmacher et al. 2000). The axes of these two rift zones intersect at an angle ~110° near São Lorenço peninsula, the easternmost tip of Madeira (Fig. 1). Madeira-Desertas volcanism is characterised by (1) a shield stage subdivided into the Early Madeira Rift Phase (EMRP, >4.6-3.9 Ma), the Desertas Rift Phase (DRP, 3.6-3.2 Ma), and the Late Madeira Rift Phase (LMRP, 3.0-0.7 Ma), and (2) a post-erosional stage (PE, <0.7 Ma; Geldmacher et al. 2000). It thus appears that Desertas volcanism coincided with a period of volcanic quiescence and erosion on Madeira. New $^{40}Ar/^{39}Ar$ age determinations, however, show that subaerial Desertas volcanism lasted from at least 1.9 to 5.3 Ma and that Madeira and the Desertas were simultaneously active (Schwarz et al., 2004b).

The islands of Madeira and the Desertas were interpreted to represent a single volcanic complex with two rift arms (Geldmacher et al. 2000) analogous to two-armed rift systems on Hawaii. Alternatively, thermobarometric data indicate that Madeira and the Desertas represent two discrete volcanic centres (Schwarz et al., 2004a) rather than a two-armed rift. Detailed field studies combined with $^{40}Ar/^{39}Ar$ age determinations suggest that the Desertas rift developed from a volcanic centre at the southern tip of the Desertas ridge to the north-northeast and thus became interconnected with Madeira (Schwarz et al., 2004b).

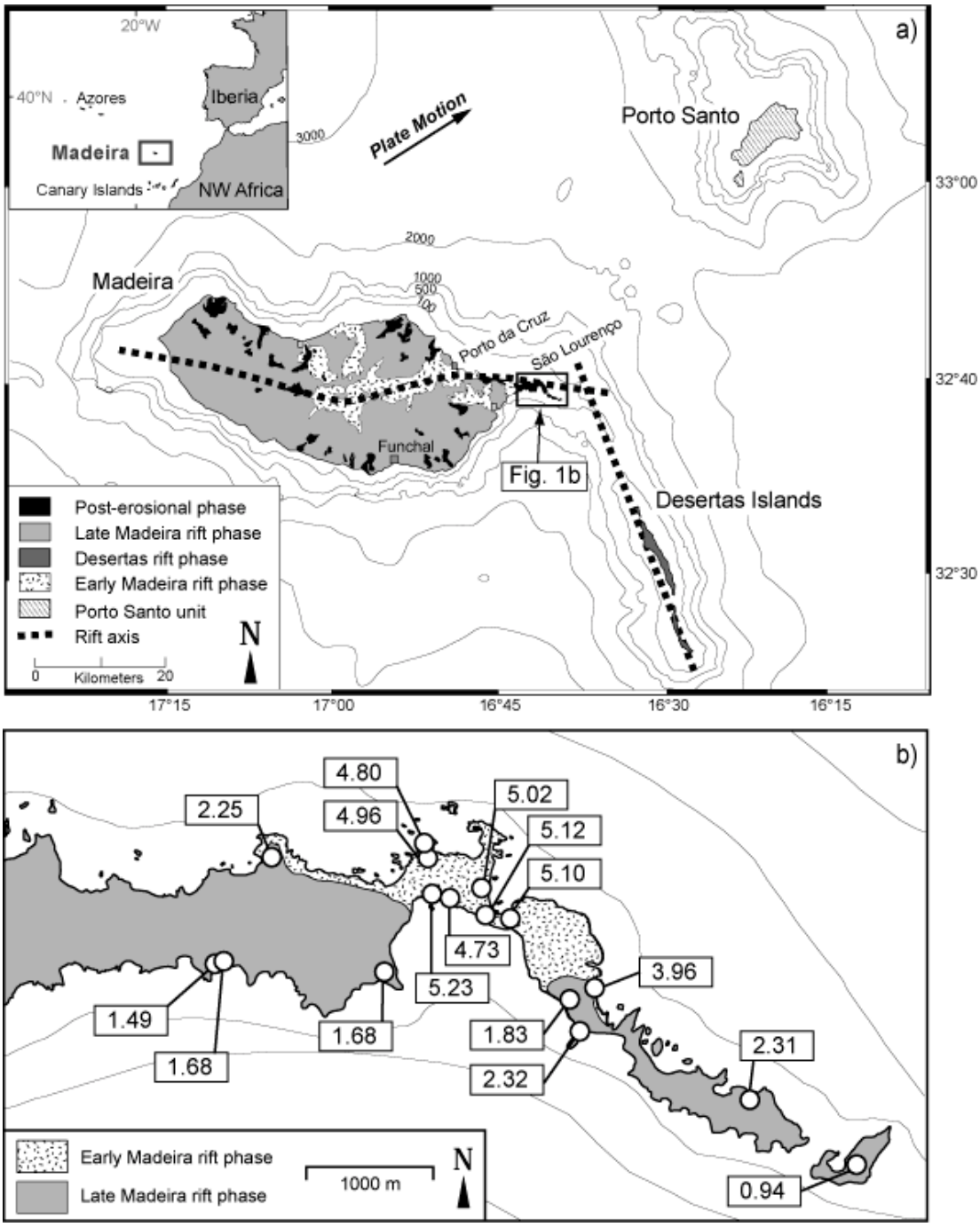

Fig. 1 a) Geological map of Madeira archipelago after Geldmacher et al. (2000) and Zbyszewski et al. (1975), bathymetry based on nautical maps. São Lourenço peninsula represents the easternmost tip of the Madeira rift zone. b) Enlargement of the São Lourenço peninsula showing sampling sites for age determination (white circles). Numbers are in million years. The São Lourenço peninsula can be divided into a lower and an upper unit overlapping in age with the Early Madeira and the Late Madeira rift phases (EMRP and LMRP).

Major element data from Madeira already have been published by several authors (Schmincke and Weibel, 1972; Hughes and Brown, 1972; Mata et al., 1998; Geldmacher and Hoernle, 2000). Alkali basaltic to mugearitc rock samples from Madeira were found to have a very low alkali content with high Na_2O/K_2O ratios (>2). Olivine and clinopyroxene are the most abundant phenocryst phases, whereas feldspar phenocrysts are rare.

To explain MORB-like Sr-and Nd-isotope compositions and as possible components of the Madeira source, Hoernle et al. (1991, 1995) suggested an interaction of a HIMU-type plume with a normal mid ocean ridge basalt (N-MORB)-like asthenosphere and lithosphere. In contrast, Mata et al. (1998) proposed that radiogenic isotope systematics result from a multicomponent source where HIMU and enriched mantle (EM1) interacted with depleted MORB source mantle (DMM) from the asthenosphere. Thirlwall (1997) and Widom et al. (1999) rather suppose that the Madeira source originated from a HIMU-type plume component mixed with shallow depleted asthenosphere containing a component of Palaeozoic oceanic crust.

Geldmacher and Hoernle (2000, 2001) confirm the presence of oceanic crust as a component of the Madeira source. Trace elements normalised to primitive mantle show characteristic HIMU signature with relative enrichment of Nb and Ta and depletion of K and Pb. Sr and Nd isotopic data overlap with the N-MORB field reflecting recycled oceanic crust present as garnet pyroxenite or eclogite in the source. Geldmacher and Hoernle (2000) observed a progressive evolution of Madeira volcanics with time: Major element data showed that SiO_2- and FeO_{tot}- contents and Mg# decrease with decreasing age reflecting decreasing fertility of the source over the last ~5 Ma. In addition, ratios of highly to less incompatible elements crudely increase with time which points to decreasing degrees of partial melting. Sr-Nd-Pb- isotope ratios show a tendency to less radiogenic ratios with decreasing age. The authors suggested the following two endmembers as possible source components of the Madeira/Desertas complex: (1) recycled upper (hydrothermally altered) basaltic oceanic crust reflected by high FeO_{tot}, SiO2 and Mg# contents, radiogenic Pb, Sr and Nd isotope ratios and relatively low $^{207}Pb/^{204}Pb$ ratios (strongly negative $\Delta 7/4$) mainly present during the early shield stage; and (2) recycled lower (gabbroic or ultramafic) oceanic crust plus lithospheric mantle characterised by lower FeO_{tot}, SiO_2 and Mg#, and more depleted isotope ratios dominant during the post-erosional phase. The observed decrease of isotopically enriched components over time was explained with progressive melting and exhaustion of recycled, hydrothermally altered, basaltic ocean crust in a discrete pulse of plume material (Geldmacher and Hoernle, 2000).

Methods used

Field work and sampling

In order to better reconstruct the evolution of the São Lourenço peninsula, stratigraphic successions and volcanic structures were studied and mapped in detail. Compass measurements of dyke azimuths were corrected to the IQRF magnetic declination. A detailed volcanological map and a location map of measured dykes is available as electronic supplementary material.

Based on results from detailed mapping, a suite of stratigraphically controlled samples has been collected from São Lourenço for $^{40}Ar/^{39}Ar$ age determinations, major and trace element as well as isotope analyses. The sample sites cover the entire stratigraphic as well as spatial succession of the peninsula. For isotope analyses, additional samples from the Desertas Islands have been collected. Major and trace element data and a detailed volcanological map of the islands previously have been published (Schwarz et al., 2004b). The sample suite for isotope analyses from the Desertas covers the islands' subaerial stratigraphy and their spatial succession from N to S.

Sample preparation and analytical methods

After removing weathered surfaces, the freshest parts from each sample were crushed and powdered with an agate mill. Samples with altered rims or vesicles filled with secondary mineral phases were hand-picked under a binocular microscope. Picked sample separates were washed in distilled water in an ultrasonic bath and subsequently powdered. Whole rock major element data and the trace elements Cr, V and Zn were determined by X-ray fluorescence spectrometry (XRF) on fused glass beads (dilution factor = 1:6) using a Philips X'Unique PW1480 X-ray fluorescence spectrometer at IFM-GEOMAR (Kiel, Germany) and calibrated with international standards. H2O and CO2 were analysed with an infrared photometer (Rosemount CSA 5003).

The trace elements Sc, Co, Ni, Cu, Ga, Rb, Sr, Y, Zr, Nb, Cs, Ba, Hf, Ta, Pb, Th, U and all REE were determined from pressure digests prepared by dissolving about 50 mg of sample material in an acid mixture (HF-aqua regia) in Teflon beakers with an EMS microwave operated at 210 °C. Analyte solutions were spiked with 1 ng/ml indium as internal standard and the final dilution factor was 1:5000 corresponding to 0.2 mg/ml of total dissolved solid (TDS). The analyses were carried out using a ThermoFinnigan Element2 inductively coupled plasma-mass spectrometer (ICP-MS) at the Institute of Geosciences, University of Bremen. In order to avoid mass interferences, the REE and Hf were measured at high resolution (10000), the transition metals at medium (4000) and all other elements at low (300) resolution. External precision as determined by repeated analyses of standard reference materials (SRM) is better than 5% for most elements. The accuracy of reference standards BHVO-2 and BCR-2, analysed along with the samples, is better than 10% except for Ta and Hf with up to 15 % and Cs (up to 20%) with respect to USGS reference values. Duplicate digests of samples yield a precision better than 10 % except for Tl and Cs (up to 20 %).

For Sr, Nd and Pb isotopic ratios were determined for selected São Lourenço samples and also for additional samples from the Desertas Islands. Samples of rock powder or rock chips (Ma234, SL13, SL117 and M51/1-447 DR-1) from São Lourenço were prepared and analysed at IFM-GEOMAR (Kiel, Germany). About 100 mg of rock material were dissolved in Teflon beakers

using a HF-HNO3 mixture. Sr, Nd and Pb ion chromatography followed closely the procedure outlined by Hoernle and Tilton (1991). The average Pb procedural blanks ranged between 20 and 60 pg Pb and thus are considered insignificant for the sample sizes. Samples were split after the final clean up in order to obtain a load of 50-100 ng Pb on the filament. Pb isotope ratios were measured in static mode on a Finnigan MAT262-RPQ2+ thermal ionisation mass spectrometer (TIMS) at IFM-GEOMAR. Measured values for NBS981 (N=49) and 2sigma external errors are $^{206}Pb/^{204}Pb$ = 16.900 ± 0.007, $^{207}Pb/^{204}Pb$ =15.437 ± 0.010, and $^{208}Pb/^{204}Pb$ = 36.528 ± 0.031 corresponding to an external reproducibility of 0.021%/amu. The measured Pb isotopic ratios were normalised to the NBS981 values given by Todt et al. (1996). Replicate analyses were carried out on 14 out of 28 samples and lie within 0.01 +/- 0.006 %/amu.

Sr and Nd isotope measurements were carried out on a ThermoFinnigan TRITON TIMS, operating in static mode and Sr and Nd isotope ratios being normalised within run to $^{86}Sr/^{88}Sr$ = 0.1194 and $^{146}Nd/^{144}Nd$ = 0.7219 respectively. Over two periods of analyses NBS987 along with external 2 sigma errors gave $^{87}Sr/^{86}Sr$ = 0.710258 ± 0.000005 (n = 13) and $^{87}Sr/^{86}Sr$ = 0.710275 ± 0.000007 (n = 9). Sr isotope data measured in the latter period are normalised to the NBS987 data of the first period. La Jolla gave $^{143}Nd/^{144}Nd$ = 0.511848 ± 0.000006 (n = 8) and our in-house Nd monitor SPEX gave $^{143}Nd/^{144}Nd$ = 0.511712 ± 0.000004 (n = 12).

$^{40}Ar/^{39}Ar$ age determination: Sample preparation and description

The ages of 19 samples were determined by incremental heating $^{40}Ar/^{39}Ar$ analyses using a 25 W Spectra Physics Ar-ion laser combined with a MAP-216 series mass spectrometer at the IFM-GEOMAR Geochronology Laboratory (Kiel, Germany). The mass spectrometer is equipped with a Baur-Signer-type source, a Johnston electron multiplier, and a gas extraction system connected to an ultra-clean gas cleanup line (~600 cc; Zr-Al getters; liquid nitrogen cold trap). For irradiation parameters and detailed description of laser incremental heating technique see Schwarz et al. (2004b).

4 aphyric and 15 porphyritic samples were selected for age determination based on their stratigraphic position, the abundance of plagioclase within the groundmass and a preferably low degree of alteration. After removing altered crusts, selected pieces of samples were crushed and sieved. Matrix grains were separated by hand-picking from the 0.25-0.5 mm fraction under a binocular microscope. Picked separates were washed in distilled water in an ultrasonic bath and subsequently dried at < 50 °C.

São Lourenço samples selected derive from lava flows, dykes, pyroclastic units and a sill. Their composition ranges from basanites and alkali basalt to hawaiite. Groundmass and aphyric samples

mainly consist of plagioclase laths and clinopyroxene associated with minor Ti-Fe-oxides and mostly iddingsitised olivine. Only in one sample (SL13), phlogopite was observed as a matrix component. Common phenocryst phases are Ti-rich augite and/or olivine, but some samples additionally contain plagioclase phenocrysts (SL103, SL 137). Sample SL116 contains minor biotite phenocrysts which were hand-picked for age determination. As an abundant weathering product, iddingsite occurs in most samples (except: SL 106, SL137) and replaces olivine partly to completely. Olivine crystals in samples SL106 and SL137 show serpentinisation along cracks as a result of hydrothermal alteration. Further secondary mineral phases were observed such as clay minerals, which replace plagioclase (SL103, SL123, SL137, SL155, SL158), and zeolithes as vesicle fillings (SL117, SL115). The amount of zeolithes within the groundmass separates could be minimised by careful hand-picking.

Age determinations

In order to better understand the evolution of São Lourenço and its geochronological setting within Madeira Archipelago, we dated rocks from various locations covering the entire stratigraphic succession (Fig. 1b). 18 samples ranging from basanitic to hawaiitic composition were analysed using $^{40}Ar/^{39}Ar$ incremental heating techniques, and one sample (Ma243) was analysed by single-particle total fusion. Results are compiled in Table 1 and displayed in age plateau diagrams in Fig. 2.

The subaerial rocks on São Lourenço fall within a range of 0.9 to 5.3 Ma which does not only cover the complete subaerial shield phase of Madeira island, but also comprises the oldest sample from this island dated so far. Similar to the Early and Late Madeira Rift Phases (Geldmacher et al., 2000), a pause in volcanic activity separates the São Lourenço volcanics in two units: (1) a lower unit exposed in the centre of São Lourenço, ranging from 4 to 5.3 Ma and overlapping with the EMRP, and (2) an upper unit in the western and eastern parts of the peninsula which ranges from 0.9 to 2.3 Ma and overlaps with the LMRP. Based on our field observations, there is no indication for a distinctive unconformity separating the two units. Remarkably, the ages found for the subaerial São Lourenço rocks show a clear overlap with those from the Desertas Islands ranging from 1.9 to 5.1 Ma (Fig. 3; Schwarz et al., 2004b) and the hiatus in volcanic activity on São Lourenço coincides well with the period of main subaerial Desertas volcanism which lasted from about 3 to 4 Ma.

Most rock samples from the EMRP unit occur in the central part of São Lourenço and gave ages between 4.7 and 5.3 Ma representing the highest subaerial ages for Madeira rocks. The oldest rock sample is a volcanic bomb occurring within a scoria cone at the base of the stratigraphic sequence

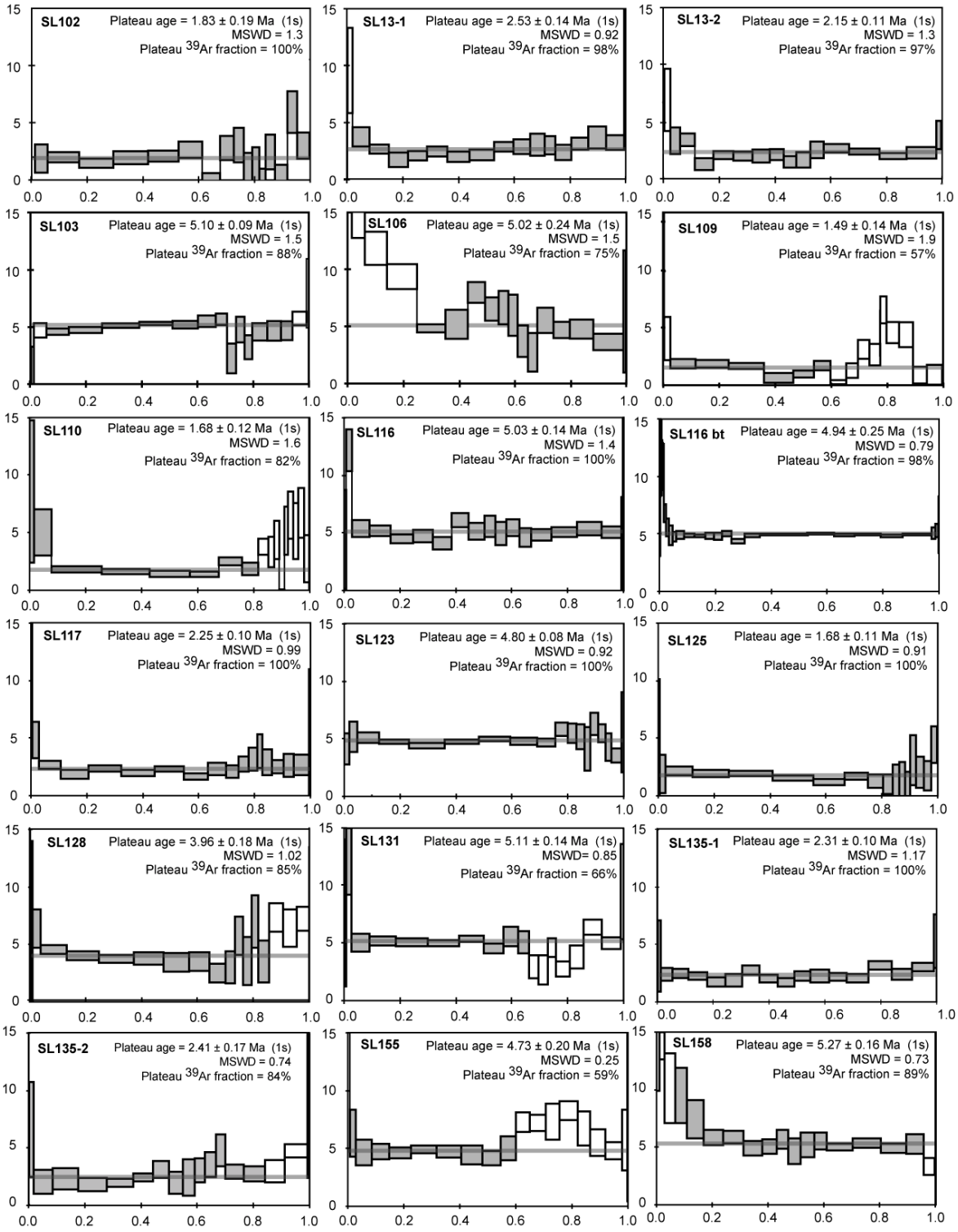

Fig. 2 Microcrystalline basalt groundmass $^{40}Ar/^{39}Ar$ incremental heating analyses. Reported $^{40}Ar/^{39}Ar$ dates are weighted age estimates and errors of the plateau fractions at the 1s confidence level including 0.08 % standard deviation in the J value. Plateau ranges and ^{39}Ar fractions as indicated. All samples were analysed using Taylor Creek Rhyolite TCR sanidine (27.92 Ma; Duffield and Dalrymple, 1990) as irradiation monitor standard.

Table 1. Incremental heating and single-particle total fusion 40Ar/39Ar analyses on groundmass separates from Sao Lourenco samples.

Sample	UTM Coordinates		Rock type	Analysis type	Age spectrum plateau age: Age ± 1σ Ma	^{39}Ar %	MSWD	n (N)	Total gas age: Age ± 1σ Ma	Inverse Isochron analysis: Age ± 1σ Ma	^{40}Ar/^{36}Ar intercept ± 1σ	MSWD
SL13	342700 / 3623125	Sill	B	HR-IHA	2,53 ± 0.14	98	0.92	16(20)	2.83 ± 0.18	2.51 ± 0.26	296.5 ± 3.6	1.54
				repeated	2.15 ± 0.11	97	1.30	16(20)	2.33 ± 0.14	1.40 ± 0.25	300 ± 1.2	0.84
				combined	**2,32 ± 0,09**							
SL102	342480 / 3623515	Flow	B	HR-IHA	**1.83 ± 0.19**	100	1.3	17(20)	1.99 ± 0.24	1.90 ± 0.30	294.9 ± 2.3	1.25
SL103	342200 / 3624075	Flow	AB	HR-IHA	**5.10 ± 0.09**	88	1.5	13(20)	4.84 ± 0.14	5.20 ± 0.10	290.8 ± 1.7	1.27
SL106	341920 / 3624220	Dyke	AB	HR-IHA	**5.02 ± 0.24**	75	1.5	13(20)	8.55 ± 0.48	3.62 ± 0.43	300.1 ± 0.7	1.84
SL109	339850 / 3623675	Dyke	B	HR-IHA	**1.49 ± 0.14**	57	1.9	6(20)	1.93 ± 0.17	1.19 ± 0.32	301.5 ± 3.2	3.32
SL110	339870 / 3623700	Flow	B	HR-IHA	**1.68 ± 0.12**	82	1.6	8(20)	2.44 ± 0.21	1.29 ± 0.21	307.4 ± 3.5	1.43
SL116	341570 / 3624525	Scoria	H	HR-IHA	5.03 ± 0.14	100	1.4	18(20)	5.17 ± 0.17	4.90 ± 0.18	298.9 ± 1.7	1.18
SL116 (bt)			H	HR-IHA	4.94 ± 0.03	98	0.8	21(37)	5.03 ± 0.05	4.92 ± 0.34	302.6 ± 1.7	1.15
				combined	**4,96 ± 0,07**							
SL117	340280 / 3624650	Flow	B	HR-IHA	**2.25 ± 0.10**	100	1.0	17(20)	2.57 ± 0.14	1.88 ± 0.17	307.3 ± 3.8	0.70
SL123	341500 / 3624610	Dyke	H	HR-IHA	**4.80 ± 0.08**	100	0.9	18(20)	4.83 ± 0.12	4.83 ± 0.09	295.3 ± 0.9	0.94
SL125	341100 / 3623760	Flow	B	HR-IHA	**1.68 ± 0.11**	100	0.9	16(20)	1.68 ± 0.15	1.67 ± 0.13	297.4 ± 3.4	0.90
SL128	342810 / 3623540	Flow	B	HR-IHA	**3.96 ± 0.18**	85	1.0	13(20)	4.46 ± 0.24	3.67 ± 0.25	301.4 ± 1.9	1.18
SL131	341970 / 3624110	Flow	AB	HR-IHA	**5.12 ± 0.14**	66	0.9	10(20)	5.03 ± 0.18	4.99 ± 0.18	297.1 ± 2.2	1.91
SL134	*343530 / 3622620*	*Dyke*	*AB*	*HR-IHA*	***2.63 ± 0.20***	*82*	*1.06*	*14(20)*	*3.73 ± 0.28*	*2.14 ± 0.29*	*301.0 ± 1.4*	*1.31*
				repeated	*3.86 ± 0.10*	*71*	*0.87*	10(20)	*4.02 ± 0.18*	*3.43 ± 0.20*	*302.5 ± 3.5*	*1.62*
				combined	*3,45 ± 0,12*							
SL135	344190 / 3622610	Flow	AB	HR-IHA	2.42 ± 0.17	84	1.2	14(20)	2.89 ± 0.23	1.90 ± 0.28	300.7 ± 1.5	0.86
				repeated	2.31 ± 0.10	100	1.2	20(20)	2.36 ± 0.12	2.03 ± 0.16	301.0 ± 2.2	0.85
				combined	**2,35 ± 0,10**							
SL136	*344170 / 3622375*	*Flow*	*AB*	*HR-IHA*	*5.20 ± 0.20*	*52*	*1.8*	*6(20)*	*4.82 ± 0.19*	*3.13 ± 0.38*	*302.2 ± 1.7*	*3.32*
SL137 (plag)	*341430 / 3624330*	*Dyke*	*B*	*HR-IHA*	***6.02 ± 0.61***	*95*	*0.84*	*15(20)*	*6.66 ± 0.84*	*5.63 ± 0.70*	*301.6 ± 3.9*	*0.74*
SL155	341700 / 3624185	Volcanic bomb	H	HR-IHA	**4.73 ± 0.20**	59	0.3	9(20)	5.81 ± 0.23	4.67 ± 0.32	301.2 ± 2.0	2.01
SL158	341520 / 3624235	Volcanic bomb	H	HR-IHA	**5.27 ± 0.16**	89	0.7	14(20)	5.96 ± 0.27	4.99 ± 0.20	299.6 ± 1.8	1.27
Ma243	345130 / 3622250	Flow	B	MSP-TF	**0.94 ± 0.06**	n.a.	0.91	10(10)	0.94 ± 0.06	0.79 ± 0.59	301 ± 21.3	1.02

HR-IHA = High-resolution incremental heating analyses; MSP-TF = multiple single-particle total fusions. Repeated = duplicate step-heating analyses on same sample. Combined = weighted average of duplicate runs. Reported ^{40}Ar/^{39}Ar dates are weighted age estimates and errors (1σ) including uncertainties in the J value (~0.08%). MSWD = Mean Square Weighted Deviates for plateau ages and inverse isochrons calculated for N-1 df. N = total number of heating steps. n = number of heating steps in plateau comprising percent fraction of cumulative ^{39}Ar release. Boldface: accepted ages based on single incremental heating analysis plateaus or weighted means from two duplicate runs. Oblique: results rejected because of plateau size deficiency, disturbed spectra or significant differences at 2sigma level (Combined data). bt/plag = analysis on biotite/plagioclase phenocrysts. Rock types: AB = alkali basalt, B = basalt, H = Hawaiite.

at the southern coast of central São Lourenço (SL158; 5.27±0.16 Ma; all indicated errors are 1σ). Lava flow samples SL103 and SL131 form the top of this sequence and yield identical ages of 5.10±0.09 and 5.12±0.014 Ma. Sample SL155 is a volcanic bomb from a scoria layer stratigraphically situated between SL158 and SL103, but yields a younger age than these (4.7±0.2 Ma). Although this seems contradictory, we accept these ages because, within the 2sigma error interval, they are consistent with the stratigraphy.

Groundmass age determination of sample SL116 gives an age of 5.03 ± 0.14 Ma and incremental heating of biotite crystals of the same sample yields an identical age within error (4.94 ± 0.03 Ma). This agreement demonstrates the reliability of matrix ages presented in this study. Both analyses combined give an age of 4.96 ± 0.07 Ma. Dykes, which cut the entire EMRP sequence, give ages of 5.02 ± 0.24 and 4.80 ± 0.08 Ma (SL106, SL123). Another dyke from the same swarm yielded an unreasonably higher age of 6.01 ± 0.61 Ma. Due to its large error (2sigma = 1.2 Ma) and hence low precision, however, this data was rejected. The youngest sample of the EMRP unit comes from a lava flow just below the stratigraphically young scoria cone of Pico do Furado Saco and was dated at 3.96 ± 0.18 Ma (SL128).

The following three samples of the LMRP unit show similar ages within error: an 2.32 ± 0.09 Ma old sill which intruded into the scoria cone Pico do Furado Saco (SL13), a 2.25 ± 0.1 Ma old lava flow on top of the Ponta do Rosto (SL117; Fig. 2) and a lava flow from Desembarcadouro island at the eastern tip of São Lourenço (Fig. 4) with an age of 2.31 ± 0.1 Ma (SL135). Two more samples (SL134, SL136) from Desembarcadouro, which are stratigraphically similar to SL135, yielded doubtful ages (Table 1). Duplicate incremental heating analyses of SL134 gave two differing ages of 2.63 ± 0.2 and 3.86 ± 0.1 Ma. These two age values do not overlap within 2σ error and the latter is inconsistent with the age of the stratigraphically similar lava flow SL135. The discrepancy between first and duplicate analysis was interpreted to result from groundmass heterogeneity with respect to irregular plagioclase distribution. Sample SL136 yielded an unlikely high age of 5.2 ± 0.2, which is inconsistent with its stratigraphic position, and the analysis produced a small plateau of only 52%. Due to these uncertainties, age data of these two samples have been rejected.

Two lava flows from beneath the morphologically preserved scoria cone of Pico Sra. da Piedade at the south coast of São Lourenço give similar ages of 1.68 ± 0.12 and 1.68 ± 0.11 Ma (SL110 and SL125). The feeder dyke within the cone stratigraphically above these 1.68 Ma old flows was dated at 1.49 ± 0.14 Ma (SL 109). The youngest sample dated in this study comes from a lava flow at the easternmost island belonging to São Lourenço (Ilhéu Farol, Fig. 4) giving an age of 0.94 ± 0.06 Ma; (Ma 243).

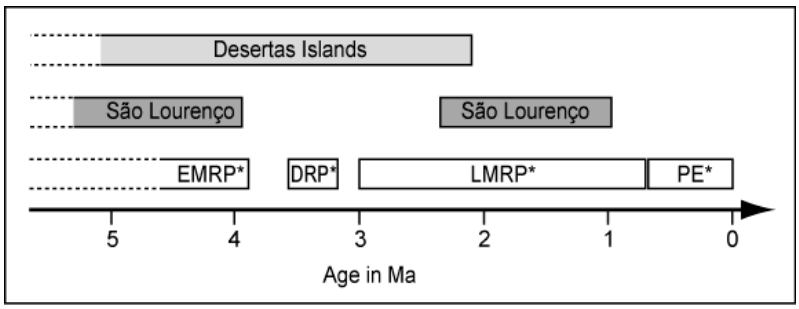

Fig. 3 Time scale illustrating subaerial volcanic activity on Madeira and the Desertas Islands. Boxes surrounded by solid lines represent ranges of rock ages of the respective areas. Ages of the Desertas Islands were taken from Geldmacher et al. (2000) and Schwarz et al. (2004b). Abbreviations with asterisks represent volcanic phases of the Madeira/Desertas complex after Geldmacher et al. (2000). Rock ages from São Lourenço from this study clearly overlap with the EMRP and LMRP, respectively, and with those from the Desertas Islands.

Field data

Volcanic structures of São Lourenço

Since the geological map of the São Lourenço peninsula by Zbyszewski et al (1975) is not adequate to ascertain the stratigraphy and to exactly classify dated and geochemically analysed samples, we have undertaken a detailed field study of volcanic and tectonic structures and the stratigraphic sequence.

The peninsula shows an E-W oriented elongation in accordance with the general trend of the Madeira rift zone. In the East, the two islands Desembarcadouro and Ilhéu Farol form the prolongation and the eastern tip of São Lourenço. The north coast is characterised by steep cliffs with an elevation up to 170 m as a result of intense marine erosion being more energetic in the north than in the south due to trade winds from the NE. The terrain is inclined towards south and steep cliffs along the south coast with elevations up to 100 m a.s.l. exclusively occur in eastern São Lourenço. The south coast of western São Lourenço is characterised by gentle slopes. Apart from three stratigraphically young and morphologically preserved scoria cones (from W to E: Cancela, Pico Sra da Piedade and Pico do Furado Saco, Fig. 4), the peninsula's paleo relief has been leveled by erosion.

We distinguished the following volcanic units: (1) proximal pyroclastic deposits such as thick tuff, scoria and/or cinder partly with volcanic bombs; (2) lava flows; and (3) dykes and sills. Moreover, aeolian sediments, reworked volcanic material and scree deposits were observed. For the sake of clarity, in Fig. 4 all sediment types were combined in a single unit. A detailed volcanological map of São Lourenço is available as electronic background data set.

Our age determinations indicate that deposits of São Lourenço can be divided into a lower unit, which corresponds to the EMRP, and an upper unit overlapping in age with the LMRP. A discordance between the lower and the upper units is expected from this data, but is not obviously visible in the field.

Units of the *Early Madeira Rift Phase* are exclusively exposed in the centre of the peninsula (Fig. 1b). At the base, they are built up by an up to 140 m thick sequence consisting of

predominantly lapilli tuff with intercalated cinder or spatter and locally spindle bombs (Fig. 3a). This basal tuff sequence represents a facies proximal to eruptive centres, and, in the Estreito by area (Fig. 4), it is stratigraphically overlain by basanitic, aphyric lava flows which are slighlty inclined towards the south-west (max. 5-10°). Individual flows have a thickness of up to 30 m and are separated from each other by uniform layers of tuff or lapilli tuff interpreted as distal fallout (e.g. Estreito bay, Figs. 4, 5b). The stratigraphic succession is cut by a swarm of basanitic to basaltic dykes and partly capped by scree deposits. The groundmass of dykes and lavas consists of plagioclase, clinopyroxene, olivine and Fe-Ti-oxides. Porphyritic samples contain olivine, clinopyroxene (Ti-augite) and rare plagioclase phenocrysts, and locally occur ankaramitic lava flows or dykes with abundant olivine and clinopyroxene phenocrysts (>20 %) of 0.2 to 2 cm in size.

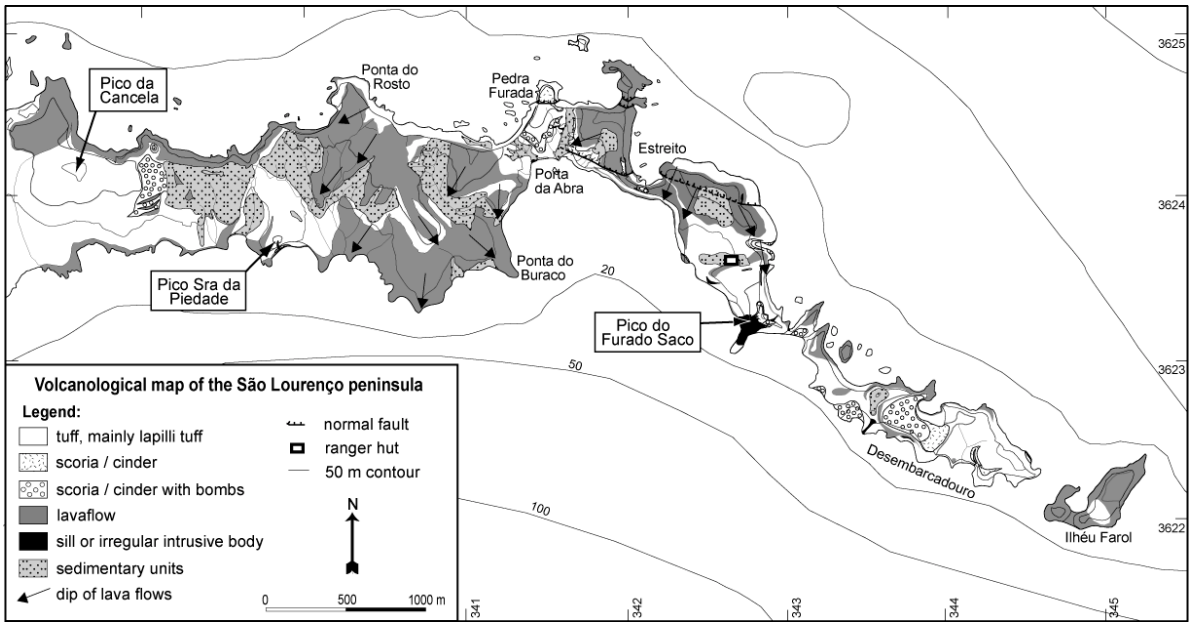

Fig. 4 Schematic volcanological map of the São Lourenço peninsula.

Volcanic units of the western as well as the easternmost parts of São Lourenço were deposited during the *Late Madeira Rift Phase*. The western part consists dominantly of a sequence of slightly south-dipping lava flows which are stratigraphically overlying the EMRP basal tuff sequence at the north coast. They are picritic to basanitic in composition and contain olivine phenocrysts. the lava flow sequence is capped by two stratigraphically young scoria cones (Pico Cancela and Pico Sra da Piedade, Fig. 4) where Pico Sra da Piedade shows a well-exposed feeder dyke. Between these cones, well-sorted sand caps the LMRP volcanic sequence. These sediments show cross-cutting and were interpreted to be of aeolian origin, deposited during the Würm glacial period when sea level was about 100 m lower and sand was transported from the beaches to where they are today

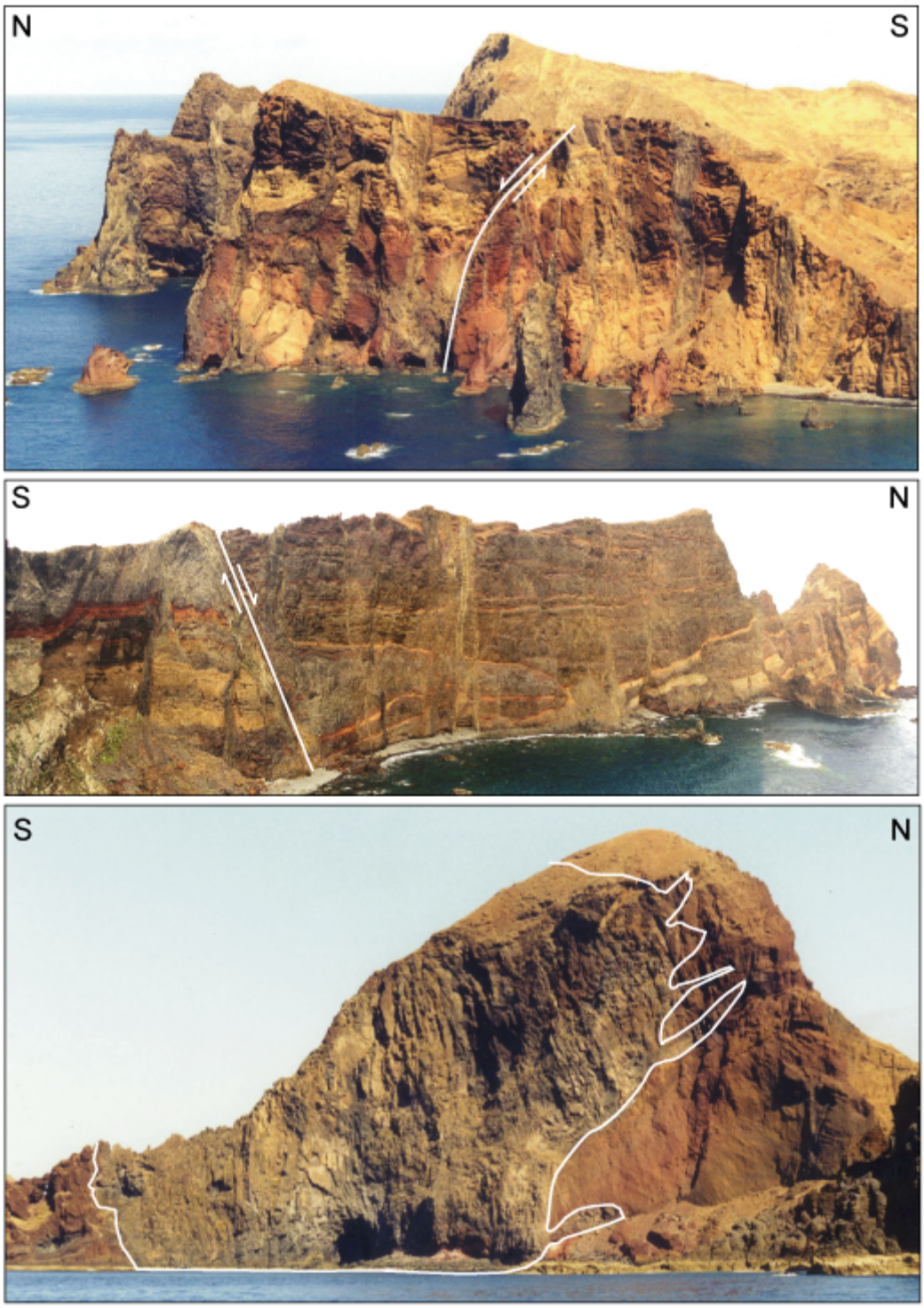

Fig. 5 Photographs illustrating volcanic features of São Lourenço (for localities, see Fig. 4). a) The steep cliff at Pedra Furada represents a section through the interior of the Madeira rift at São Lourenço exposing a 140 m thick sequence of tuff, cinder and spatter cut by a swarm of subvertical dykes. The solid line marks a N-dipping normal fault. b) The Estreito bay offers a spectacular view on the internal structure of the peninsula. A sequence of lava flows and fallout layers is cut by a dyke swarm and several N-dipping normal faults (e.g. solid white line). c) An irregularly shaped sill (outlined) intruded into, and interfingers with, the morphologically preserved volcano cone of Pico do Furado Saco.

(Zbyszewski et al., 1975). These dune sands contain volcanic particles and terrestrial gastropods (Mitchell-Thomé, 1976) and are unique on the entire island. Apart from aeolian sediments, reworked material was deposited near Pico Sra ad Pieced (Fig. 4).

In the eastern part of São Lourenço, a prominent volcanic cone (Pico do Furred Sao, Figs. 4, 5c), consisting of scoriaceous lapilli, cinder and spatter, caps the EMRP lava flows and consists of. Two basanitic sill-like bodies intruded into this cone and strongly interfingered with the pyroclastics (Fig. 5c). Desembarcadouro island in east São Lourenço is formed by a sequence of lapilli tuff, scoria and spindle bombs (Fig. 4). Only few dykes and subordinate lava flows occur within the tuff containing 10-15 % olivine and 3-5 % clinopyroxene phenocrysts in a groundmass composed of plagioclase, clinopyroxene (Ti-Augite), olivine and Fe-Ti-oxides. The easternmost island (Ilhéu Farol, Fig. 4) consists of basanitic lava flows and minor tuff deposits.

In summary, systematic petrographic differences between EMRP and LMRP lavas were observed: (1) phenocryst-rich samples such as ankaramites exclusively occur in EMRP units; (2) phenocrysts with >2 mm in size are far more abundant in EMRP lavas than in those erupted during the LMRP; (3) in EMRP lavas, olivine phenocrysts are commonly associated with clinopyroxene, whereas LMRP samples mostly contain olivine as the only phenocryst phase; and (4) plagioclase phenocrysts exclusively occur in EMRP lavas.

Structural geology

A distinctive dyke swarm, whose density (defined by the number of dykes per 50 m) increases towards north, occurs within the EMRP units with most dykes cutting the entire stratigraphic sequence exposed. The average strike of the dykes is 105° and coincides with the general E-W trend of the Madeira rift zone (Figs. 1a, 6). No change of strike direction from W to E along the rift axis at São Lourenço was observed (Fig. 6c). Dykes dip towards north and south with angles between 60 and 90°. Most dykes are <5 m wide (95 %), and only four dykes measured have widths between 5 and 10 m. Parallel to the dyke swarm within EMRP units, north-dipping normal faults can be observed. The main fault exposed in the Estreito

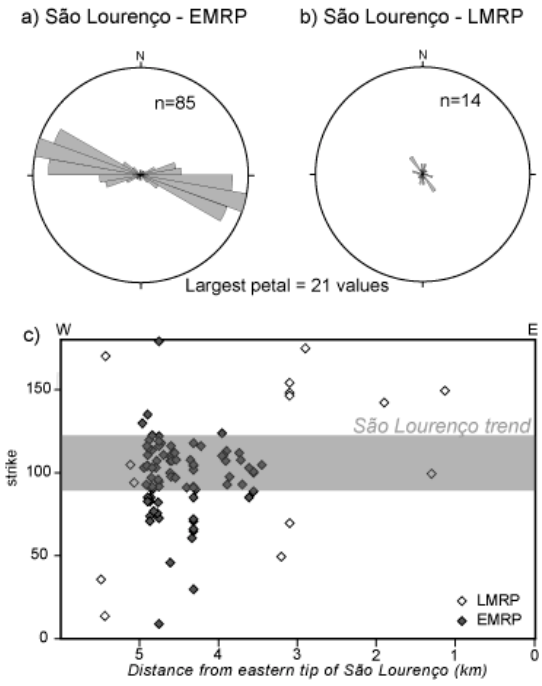

Fig. 6 Orientation of dykes on São Lourenço. a) Strike of dyke complex during the EMRP with a main strike between 100 and 105°. b) Orientation of dykes during the LMRP. c) Lateral distribution of dyke strike from W to E without systematic spatial variation in dyke orientation.

bay (Fig. 5b) dips to the north, has a downthrow of about 60 m and is associated with smaller normal faults (downthrow between 10 and 20 m). Within the LMRP unit, no faults were observed and only few single dykes occur. These show a strong variation of strike (10 to 180°, Fig. 6b), dips between 66° and 88° and widths of 0.3-3 m.

Geochemical results

Major and trace elements

Major and trace elements of whole rock analyses are given in the Appendix (Tables A1 and A2). Samples from São Lourenço completely overlap in major and trace element composition with those from the Early and Late Madeira Rift Phases of the island's mainland (Geldmacher and Hoernle, 2000). They range from basanites and alkali basalts to hawaiites (Fig. 7). CaO/Al_2O_3 decreases and Al_2O_3, alkalis and P_2O_5 increase with decreasing MgO consistent with olivine and clinopyroxene fractionation (Fig. 8). TiO_2 increases and FeO_{tot} and SiO_2 show little variation >5 wt.% MgO, then FeO and TiO_2 decrease and SiO_2 increases, indicating fractionation of Ti-Fe oxides and augmented Ti-augite crystallisation relative to olivine. Co, Ni and Cr correlate positively and most incompatible elements (e.g. Rb, Ba, Sr, Nb, La, Nd, P, Zr, Y) show moderate to good negative correlation with MgO.

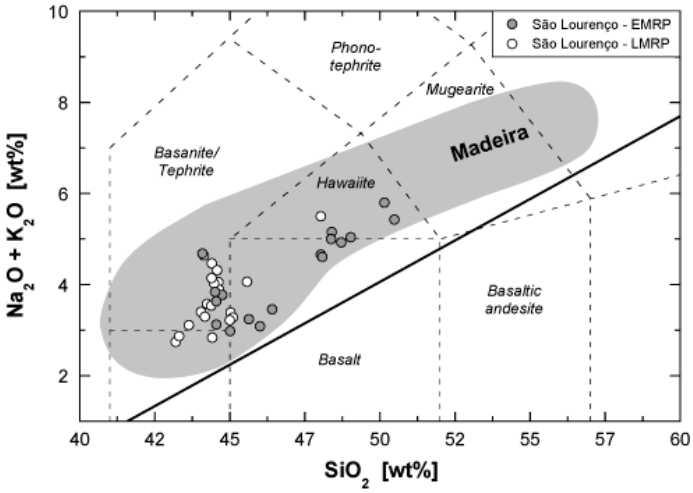

Fig.7 Total alkalis versus SiO_2 diagram including São Lourenço samples from this study using the field boundaries of Le Maitre et al. (1989). Volcanic rocks are subdivided into alkalic and subalkalic after McDonald (1968). Field for Madeira is based on data from Geldmacher and Hoernle (2000). Nearly 50 % of EMRP samples but only one out of 20 LMRP samples analysed in this study fall into the field for hawaiites.

On an incompatible element diagram (Fig. 9), primitive samples from São Lourenço show features characteristic of HIMU ocean island basalts, e.g. St. Helena, which include relative enrichment in Nb and Ta and negative anomalies of K and Pb. The HIMU character was interpreted to reflect recycled oceanic crust (Geldmacher and Hoernle, 2000). The rare earth elements (REE) decrease with increasing atomic numbers as typical for OIB (Fig. 9) with $(La/Yb)_N$ ~ 10-22 and $(Sm/Yb)_N$ ~ 3,4-5,6, indicating the presence of residual garnet in the source.

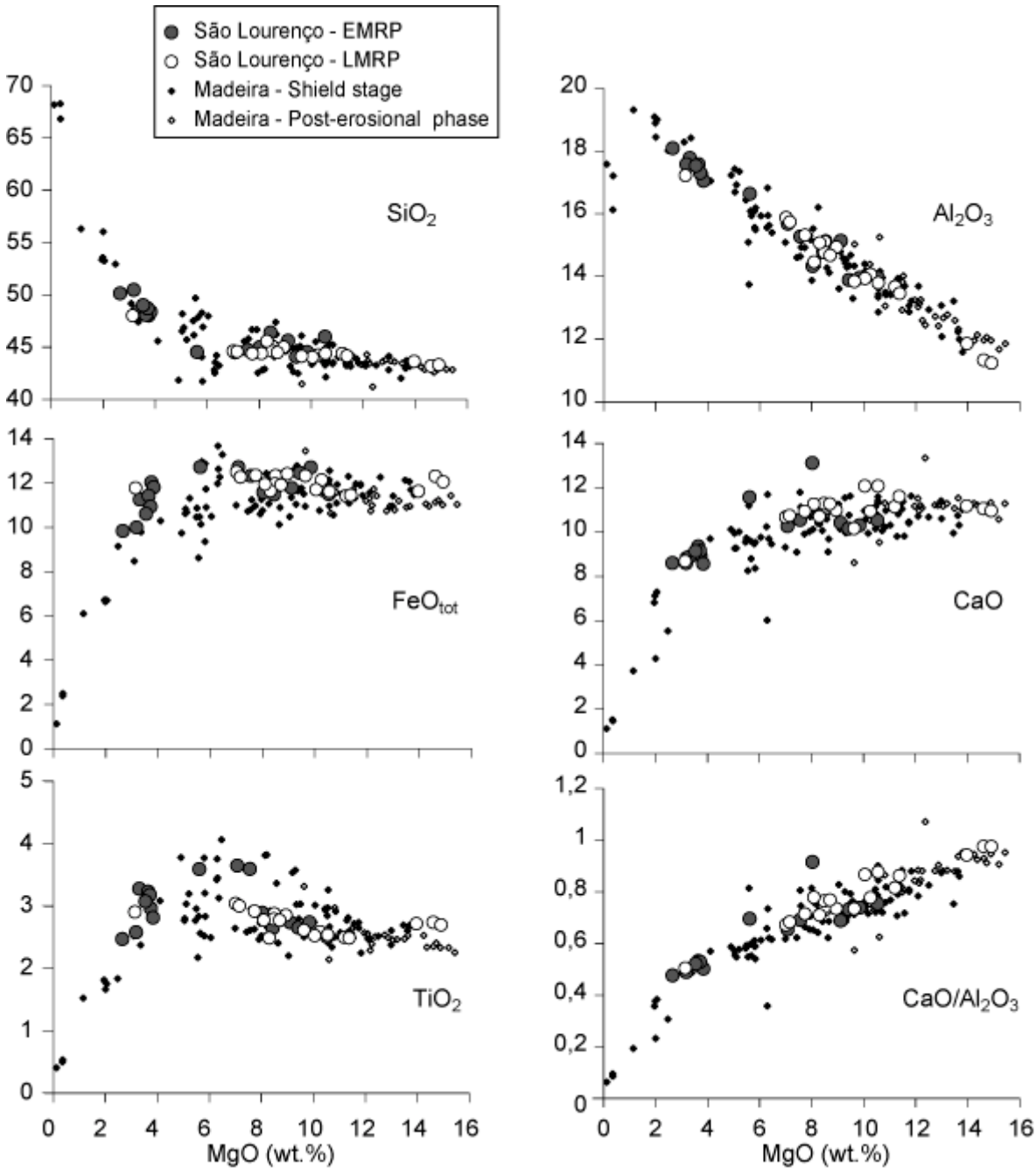

Fig. 8 Selected major element variations versus MgO for samples from São Lourenço. Data for the Madeira shield and post-erosional phases are from Geldmacher and Hoernle (2000).

Samples from São Lourenço show variations over time in their major element composition and trace element ratios: SiO_2, Al_2O_3 and alkali contents of LMRP rocks tend to be lower than those of EMRP rocks, and there is a tendency to higher MgO, Co, Ni, CaO and CaO/Al_2O_3 with decreasing age. These variations reflect that lavas erupted during the LMRP are less differentiated. The decreasing degree of differentiation is in accordance with petrographic observations showing that phenocryst-rich lavas such as ankaramites exclusively occur in EMRP units and lavas with >2 mm phenocrysts are more common in EMRP units than in those of the LMRP. Clinopyroxene and

plagioclase phenocrysts are abundant in EMRP lavas, whereas in many LMRP samples olivine is the only phenocryst phase.

Ratios of more to less incompatible elements (e.g. La/Yb, Sm/Yb, Nb/(Zr, Y)) crudely increase with decreasing age (Fig. 10) possibly reflecting a decrease of melting degrees with time. In contrast, ratios of highly incompatible elements to U and Th show large variations but no correlation with time, except for Nb/U which decreases crudely with decreasing age.

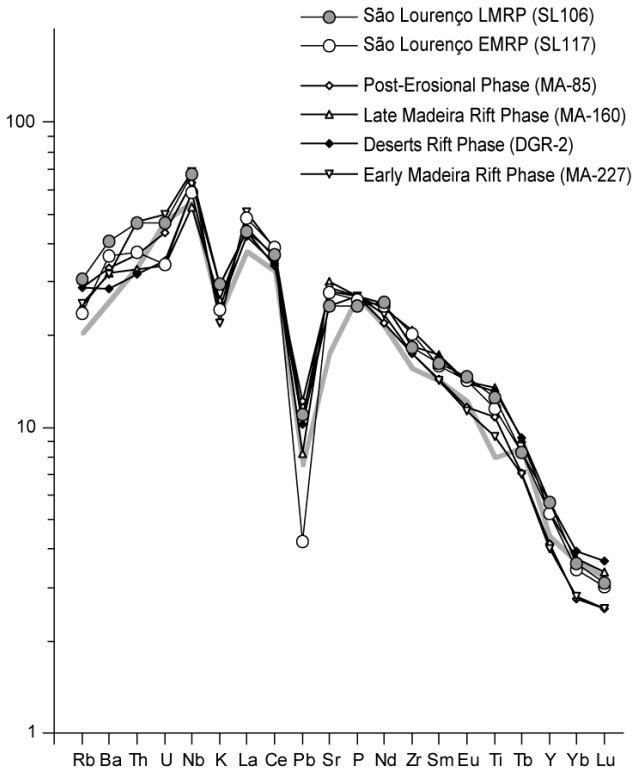

Fig. 9 Incompatible trace element concentrations normalised to primitive mantle after Sun and McDonough (1989) of representative primitive LMRP (SL106) and EMRP (SL117) samples from São Lourenço compared with HIMU basanite from St. Helena (sample 68 from Chaffey et al., 1989)). For comparison, primitive samples from each volcanic phase of Madeira after Geldmacher and Hoernle (2000) are given.

Sr-Nd-Pb isotopes

Representative samples from São Lourenço and the Desertas Islands and two submarine samples dredged during cruise M51/1 of RV METEOR were analysed for their Sr, Nd and Pb isotope ratios and results are presented in Table 2. São Lourenço samples overlap in their isotopic composition with samples from the Madeira shield phase (Fig. 10; Geldmacher and Hoernle, 2000) but show a distinctive separation between EMRP and LMRP samples. Isotope ratios of Desertas rocks also fall within in the field for the Madeira shield phase but show a well-confined range.

$^{206}Pb/^{204}Pb$ and $^{87}Sr/^{86}Sr$ ratios correlate negatively with $^{143}Nd/^{144}Nd$ and show considerable overlap with the field for Atlantic N-MORB (Fig. 10, 11). $^{208}Pb/^{204}Pb$ and $^{207}Pb/^{204}Pb$ ratios show positive correlation with the $^{206}Pb/^{204}Pb$ ratio for all samples (Fig. 11). All samples plot beneath the Northern Hemisphere reference line (NHRL) on the uranogenic Pb diagram with $\Delta 7/4$ as low as –4.4 in the most radiogenic EMRP samples and –6.2 in the most radiogenic samples from the Desertas (Fig. 11).

In samples from São Lourenço, Pb and Sr isotope ratios decrease and Nd isotope ratios increase with decreasing age (Fig. 12) which is consistent with Geldmacher and Hoernle (2000). Differences in isotope compositions between EMRP and LMRP samples, however, are far more pronounced at São Lourenço than at central Madeira, defining two distinct groups with the EMRP rocks having more radiogenic Sr and Pb isotope ratios and lower Δ7/4 and $^{143}Nd/^{144}Nd$ (Figs. 10, 11). Sr isotope ratios of EMRP samples from São Lourenço are the most radiogenic ratios found for Madeira island. Since the peninsula is located near sea level and samples of this study were not leached in an aqua regia solution for Sr analyses, in contrast to samples from mainland Madeira (Geldmacher and Hoernle, 2000), it is conceivable that this increase of $^{87}Sr/^{86}Sr$ results from seawater alteration (Hoernle, 1998).

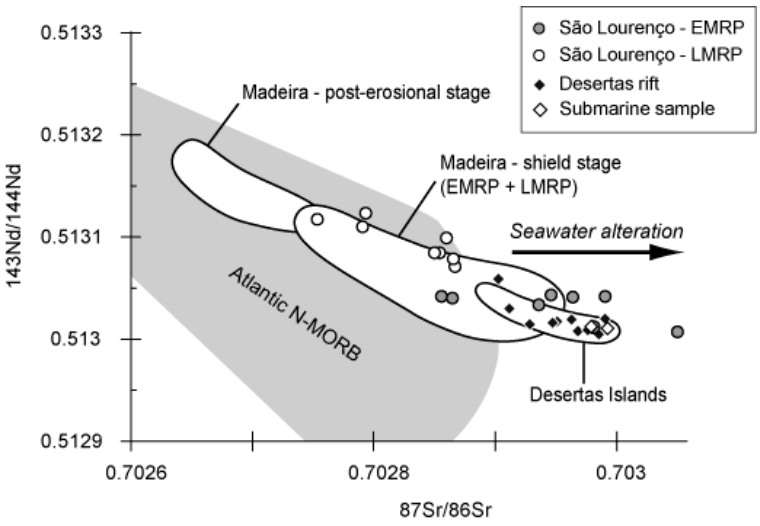

Fig. 10 $^{87}Sr/^{86}Sr$ versus $^{143}Nd/^{144}Nd$ isotope correlation diagram for volcanics from São Lourenço and the Desertas Islands. Samples show considerable overlap with the array of the Madeira shield phase comprising EMRP and LMRP samples. São Lourenço rocks form two clearly distinct groups for the Early and Late Madeira Rift Phases with the EMRP samples having more radiogenic Sr and less radiogenic Nd. EMRP samples from São Lourenço have the most radiogenic Sr isotope composition observed for Madeira island which may be related to seawater alteration. Errors are smaller than plot symbols. Arrays for Madeira island from Geldmacher and Hoernle (2000), and the field for Atlantic N-Morb between 10°N and 30°N from Dupré and Allègre (1980), Ito et al. (1987) and Cohen and O'Nions (1982).

Isotope ratios of Desertas samples fall within the Madeira array but scatter over a smaller range than shield stage volcanics from the archipelago's main island. Within the Madeira array, the Desertas rocks tend towards the most radiogenic compositions with high $^{87}Sr/^{86}Sr$, high Pb isotope ratios and low $^{143}Nd/^{144}Nd$ which do not correlate with rock ages. The submarine sample M51/1-447DR-1, dredged at the southernmost tip of the Desertas ridge, falls within the range defined by other Desertas samples. A submarine sample (M51/1-444DR-1) from a cone at the ridge flank between São Lourenço and the Desertas yielded Pb isotopes which fall into the range of EMRP samples from São Lourenço, and Nd-Sr isotope ratios of this sample overlap with EMRP as well as Desertas samples.

Due to rock ages ≤ 5.3 Ma, calculated values for initial Sr-Pb-Nd isotope ratios of all samples fall within the 2σ range of analysed isotope ratios (Table 1), except for sample SL13 from a sill-like intrusive body (Figs. 4, 5c). This sample has a high μ (=134) and is thus characterised by initial

Pb isotope ratios lower than the ratios observed. Because SL13 shows Nd/Pb ratios considerably higher than the average of São Lourenço samples but other mobile elements do not show any depletion relative to immobile elements, the low Pb contents and high μ are interpreted to result from post-eruptive hydrothermal alteration associated with preferred Pb removal. This interpretation is supported by the fact that sample SL13 is from the largest intrusive body exposed at São Lourenço, being located at sea level and prone to intense long-lived hydrothermalism.

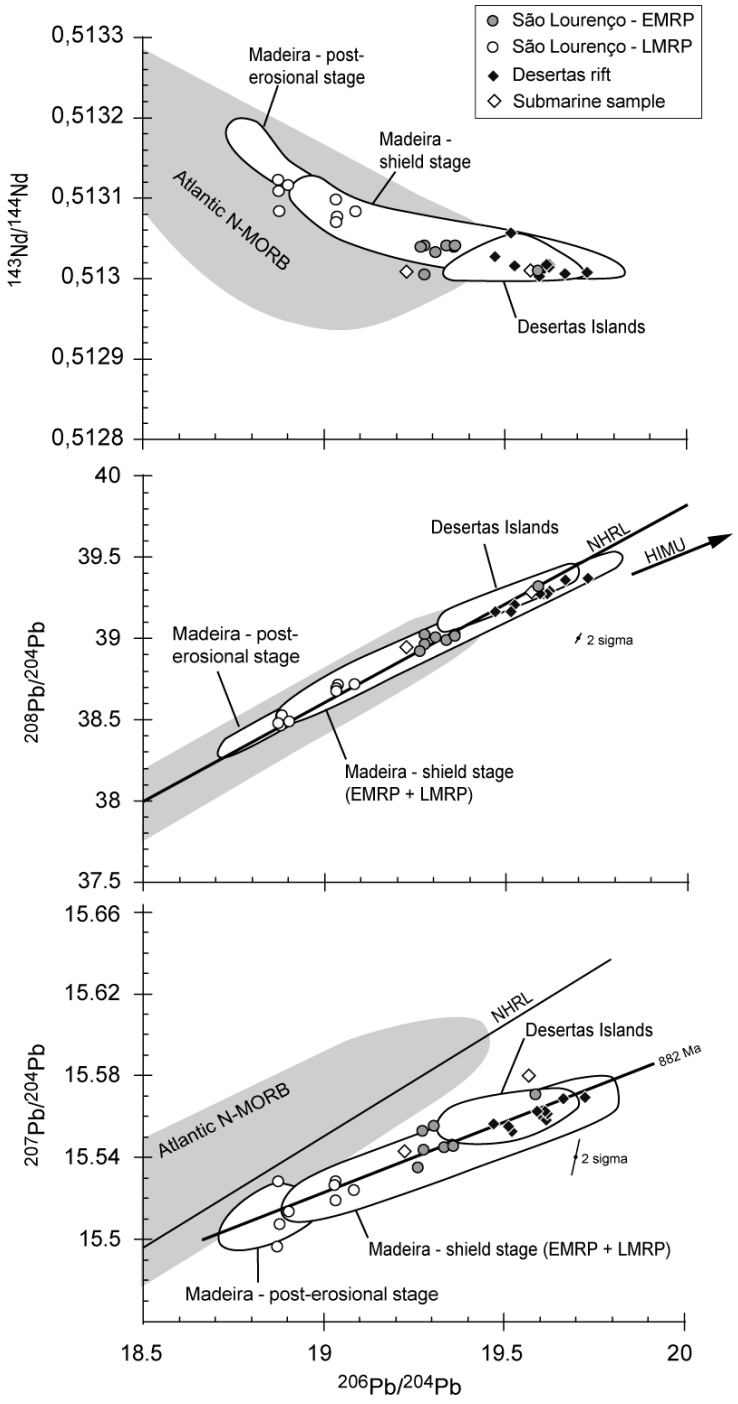

Fig. 11 $^{143}Nd/^{144}Nd$, $^{207}Pb/^{204}Pb$ and $^{208}Pb/^{204}Pb$ versus $^{206}Pb/^{204}Pb$ for São Lourenço and Desertas samples. In all diagrams, all samples show a considerable overlap with the array for the Madeira shield phase (EMRP and LMRP). EMRP and LMRP samples from São Lourenço define two distinct groups with the EMRP rocks having more enriched compositions. Except for one sample, the Pb isotope ratios of EMRP samples from São Lourenço show no overlap with the Desertas samples plotting at the radiogenic end of the Madeira array. Errors for the $^{143}Nd/^{144}Nd$ versus $^{206}Pb/^{204}Pb$ diagram are smaller than plot symbols.Data sources: fields for Madeira see Fig. 11, NHRL (Hart, 1984), field for Atlantic N-MORB (from the literature, e.g. Sun, 1980; Ito et al., 1987).

Table 2 Sr-Nd-Pb isotope data from Sao Lourenco and the Desertas Islands. Ages in parentheses are estimated from their stratigraphic position.

Sample	Rock type	Age	$^{87}Sr/^{86}Sr$	±2σ*	$^{143}Nd/^{144}Nd$	±2σ*	$^{206}Pb/^{204}Pb$	±2σ	$^{207}Pb/^{204}Pb$	±2σ	$^{208}Pb/^{204}Pb$	±2σ
Madeira												
Sao Lorenco												
SL 13	Basanitic sill	2.2	0.702865	2	0.513070	3	19.039	0.003	15.520	0.003	38.700	0.007
SL 103	Alkali basaltic lava flow	5.1	0.702961	3	0.513040	2	19.359	0.001	15.546	0.001	39.024	0.003
SL 106	Alkali basaltic dike	5.0	0.702978	3	0.513010	2	19.589	0.002	15.571	0.002	39.322	0.005
SL 109	Basanitic dike	1.5	0.702864	2	0.513077	3	19.034	0.001	15.528	0.001	38.687	0.003
SL 110	Basanitic lava flow	1.7	0.702793	2	0.513122	3	18.879	0.002	15.507	0.002	38.463	0.004
SL 116	Hawaiitic scoria	5.0	0.702987	2	0.513040	3	19.337	0.002	15.545	0.002	38.988	0.004
SL 117	Basanitic lava flow	2.3	0.702790	2	0.513108	2	18.880	0.002	15.497	0.002	38.456	0.004
SL 123	Hawaiitic dike	4.8	0.702933	2	0.513032	3	19.306	0.001	15.555	0.001	39.006	0.002
SL 125	Basanitic lava flow	1.7	0.702753	2	0.513116	2	18.905	0.002	15.513	0.002	38.485	0.005
SL 128	Basanitic lava flow	4.0	0.703046	3	0.513006	2	19.277	0.002	15.553	0.001	39.025	0.003
SL 136	Alkali basaltic lava flow	(2.3)	0.702858	2	0.513098	3	19.032	0.001	15.527	0.001	38.673	0.003
SL 148	Alkali basaltic lava flow	(1.5)	0.702853	2	0.513083	3	19.084	0.001	15.524	0.001	38.715	0.003
SL 155	Hawaiitic lava flow	4.7	0.702854	3	0.513041	3	19.361	0.001	15.546	0.001	39.016	0.002
SL 158	Hawaiitic bomb	5.3	0.702943	3	0.513042	3	19.277	0.001	15.544	0.001	38.959	0.003
Ma243	lava flow	1.0	0.702849	3	0.513083	4	18.884	0.001	15.529	0.001	38.517	0.003
Ma231	Hawaiitic bomb	(5.3)	0.702863	2	0.513039	5	19.264	0.002	15.535	0.002	38.922	0.004
Desertas Islands												
Chao												
K16	Hawaiitic lava flow	2.7	0.702973	3	0.513008	3	19.725	0.001	15.570	0.001	39.368	0.003
Deserta Grande												
DGR 26	Alkali basaltic lava flow	(3.5)	0.702900	3	0.513057	2	19.513	0.003	15.556	0.002	39.165	0.006
DGR 41	Alkali basaltic lava flow	(3.4)	0.702960	2	0.513018	3	19.618	0.005	15.559	0.004	39.278	0.009
DGR 46	Alkali basaltic lava flow	(3.4)	0.702945	2	0.513015	2	19.619	0.003	15.562	0.003	39.292	0.007
DGR 54	Alkali basaltic lava flow	(3.4)	0.702987	2	0.513019	3	19.612	0.005	15.562	0.004	39.279	0.010
DGR 106	Alkali basaltic dike	(3.2)	0.702909	2	0.513028	3	19.470	0.001	15.557	0.001	39.163	0.003
DGR 114	Hawaiitic scoria	(3.3)	0.702982	2	0.513003	2	19.593	0.002	15.563	0.002	39.278	0.005
Bugio												
DBU60		2.0	0.702926	2	0.513013	4	19.605	0.004	15.560	0.003	39.278	0.007
DBU 113	Alkali basaltic lava flow	4.1	0.702965	2	0.513007	3	19.665	0.003	15.569	0.002	39.363	0.006
K 6	Alkali basaltic dike	(3.4)	0.702948	2	0.513016	2	19.524	0.003	15.553	0.002	39.211	0.005
Submarine samples												
M51/1-444DR-1	Basanite		0.702990	2	0.513011	2	19.226	0.001	15.543	0.001	38.970	0.002
M51/1-447DR-1	Basanite		0.702976	3	0.513011	2	19.673	0.002	15.562	0.002	39.338	0.004

* 2σ errors have to be multiplied with 10^{-6}

Discussion

Our $^{40}Ar/^{39}Ar$ age determinations show that São Lourenço exposes the oldest rocks dated on Madeira and covers the complete shield stage of the island. Geochemical results combined with rock ages and the stratigraphy of the peninsula allow us to reconstruct in detail the temporal geochemical evolution of the Madeira rift and a comparison with the neighbouring Desertas rift. Based on the geochemical evolution of the rift zones and the distribution of volcanism within the archipelago, inferences on the nature of the Madeira plume can be made.

Rift structure of São Lourenço

The EMRP units of central São Lourenço were deposited between >5.3 and 3.9 Ma and expose mainly rocks that indicate proximity to the centre of a rift zone such as remnants of tuff and scoria cones, volcanic bombs, sills and a distinctive dyke swarm. Therefore, we interpret this part of the peninsula as the deeply eroded, easternmost interior of the early Madeira rift. This is in accordance with São Lourenço being the geographic prolongation of the EMRP dyke complex (Fig. 1a), which contains basaltic dykes with ages of 4.5 - 4.6 Ma (Geldmacher et al., 2000). Although the LMRP units of São Lourenço comprise only few dikes, the overall field relations indicate similar rift structures as during the EMRP implying that the late Madeira rift extended to São Lourenço as well. It is remarkable that some of our São Lourenço rocks dated show the highest ages found so far on Madeira (4.7-5.3 Ma). These ages are consistent with coralliferous limestones found in northern Madeira at an elevation of 360-400 m a.s.l. which contain a fossil fauna from the late Miocene and the incipient Pliocene, i.e. around 5.1 Ma (Zbyszewski et al., 1975; Mitchell-Thomé, 1976). Since at this time the sea level was 80-90 m higher than at present (Hardenbol et al., 1998), the location of these reef carbonates clearly indicates uplifting processes affecting the volcanic edifice of Madeira. Such uplift most plausibly occurred by intrusions concomitant to volcanic activity, but it is unknown to what extent São Lourenço had been affected. Our field work did not reveal any submarine sediments or any indication for submarine eruptions on São Lourenço. The EMRP is rather characterised by a basal tuff sequence up to 140 m a.s.l. (e.g. at Pedra Furada; Figs. 4, 5a), which we interpret as being erupted subaerially by explosive volcanism due to magma-seawater interaction during the early subaerial stage. These observations suggest minor subsidence rather than uplift at São Lourenço since 5 Ma and hence different vertical movement than at northern Madeira. This apparent contradiction indicates that uplift by volcanic intrusions varied on a km-scale and was most pronounced in the centre of the volcanic edifice.

The volcanic structures at São Lourenço allow to reconstruct the former rift geometry based on the following characteristics of rift zones: (1) dykes and normal faults are usually oriented rift-parallel and their strike is perpendicular to the direction of minimum principal compressive stress

σ3 at the time of intrusion and faulting (Anderson, 1951; Nakamura, 1980); (2) the density of dyke swarms typically increases with depth and towards the rift axis (Walker, 1987, 1992); (3) most lava flows originate near, and dip away from, the rift axis (Carracedo, 1994). Consequently, dyke azimuths and dip directions, dyke distribution as well as the dip of lava flow sequences can be used to infer the orientation and former location of the rift axis.

Based hereon, the following observations indicate that, during the EMRP as well as the LMRP, the rift axis was located to the north of São Lourenço peninsula: (1) the density of the EMRP dyke swarm increases towards north, (2) LMRP lava flows dip southward, and (3) the morphology of the peninsula shows increasing elevation towards N (Fig. 1a). Due to this inferred location of the rift axis, we conclude that large parts of Madeira's northwest coast were removed by erosion. Our interpretation is in accordance with the occurrence of steep cliffs up to 170 m a.s.l. preferably at the north coast of São Lourenço, and 3-4 km wide abrasion platforms north of São Lourenço (Fig. 1a) resulting from marine erosion possibly combined with flank collapses. The dominant strike of dykes and normal faults between 100° and 110° indicate that the former rift axis was oriented slightly oblique to the general E-W trend of the Madeira rift axis.

Persistence of the Madeira rift zone

Our new age data show that subaerial volcanic activity on São Lourenço lasted from about 5 to 1 Ma, implying that the easternmost part of the Madeira rift zone was active during the entire subaerial shield stage, i.e. over a period of more than 4 Ma with a 2.5 Ma break in activity (**Fig. 3**). To our knowledge, this life-span of a rift zone is the longest reported for hotspot-related oceanic island volcanoes except for tectonic-controlled rifts such as on Iceland (e.g. Gudmundsson, 2000) or the Azores (e.g. Walker, 1999). For comparison, the maximum subaerial activity of a single rift is ~3 Ma for the Desertas rift, Madeira (Fig. 3; Schwarz et al. 2004b), ~ 3.5 Ma for Tenerife, Canary Islands (Carracedo, 1998 and references therein), and less than 1 Ma for Hawaiian volcanoes (Clague and Dalrymple, 1987). We suggest that the different life-spans of rift zones depend on plate motion and magma production rates. At Hawaii, the Pacific plate moves at 9 cm/a over the hotspot which results in relatively rapid initiation of new, discrete volcanoes along the direction of plate motion (Clague and Dalrymple, 1987). In contrast, the slowly and irregularly moving African plate with an average Cenozoic plate velocity near Madeira of ~ 1.2 cm/a (Geldmacher et al., 2000) leads to a nearly fixed position of the lithosphere above the hotspot and thus results in long-standing volcanic activity with persistent rift systems.

The inferred period of volcanic quiescence at Madeira lasted from about 3.9 to 3 Ma in the central island (Geldmacher et al., 2000) and about 4 to 2.5 Ma at São Lourenço. As discussed above, the field relations show that at both São Lourenço and central Madeira volcanism during the

LMRP was organised along the same rift as during the EMRP. This indicates that old rift structures can be reactivated after a >1 Ma long pause of activity, possibly because passive gravitative spreading of the volcanic edifice caused relaxation of the local stress field and favoured the anewed injection of rift-parallel dykes. We suppose that the quasi-fixed position of the African plate at Madeira is not only responsible for the rift persistence over several million years but also resulted in this rift reactivation.

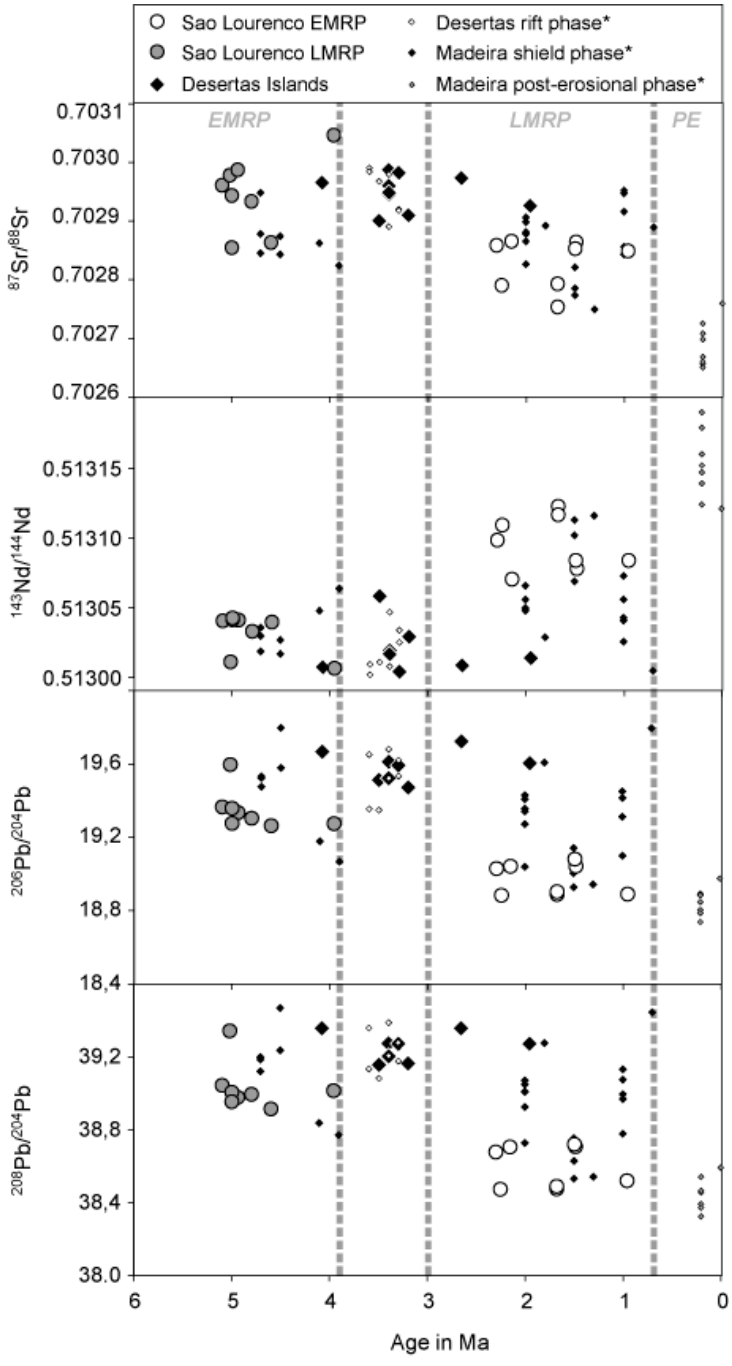

Fig. 12 Sr-Nd-Pb isotope ratios versus rock ages from central Madeira, São Lourenço and the Desertas Islands. Isotope compositions reflect a progressive evolution of the mantle source over time, i.e. from the Early Madeira Rift Phase (EMRP) to the post-erosional phase (PE), from more to less enriched isotope ratios. This trend is distinctively pronounced by São Lourenço samples. The isotope compositions of Desertas samples overlap with the isotopically enriched end of the isotope arrays formed by shield stage rocks from Madeira but show no distinct temporal trend. Data for the Madeira and Desertas shield phase and the Madeira post-erosional phase (in the legend marked with asterisks) from Geldmacher and Hoernle (2000).

Geochemical evolution of São Lourenço compared with central Madeira

An advantage of our geochemical investigations focussing on São Lourenço is the limited area of the peninsula, which inevitably relates any variations in geochemistry to temporal changes in magma composition but not to spatial variations along the rift. Because rock ages from São Lourenço cover the entire subaerial shield stage of Madeira, our data reflect the chemical evolution at a fixed locality of the Madeira rift during the last 5 Ma. As has to be expected, major and trace element compositions and isotopic data from the peninsula overlap with samples from main Madeira (Figs. 8, 9). A closer look on the data, however, reveals that the temporal evolution at São Lourenço is shown much clearer especially with respect to isotope ratios. São Lourenço samples show a distinctive tendency to more radiogenic Sr and Pb isotope ratios and to less radiogenic Nd isotope ratios with decreasing age. This distribution confirms the model of Geldmacher and Hoernle (2000) explaining the geochemical evolution of the Madeira/Desertas complex implying the presence of recycled oceanic crust within the plume source and progressive exhaustion of its eclogitic component during shield stage volcanism. In agreement with new rock ages, Sr-Pb-Nd isotope data of samples from São Lourenço form two clearly distinct groups for the EMRP and the LMRP. These groups show a far more restricted compositional range for each rift phase than the respective samples from main Madeira with a complete overlap of EMRP and LMRP data (Figs. 10, 11; Geldmacher and Hoernle, 2000). The comparatively large spread of the Madeira data may partly reflect spatial variations since these samples represent a far larger part of the Madeira rift than São Lourenço. The central part of a large volcano is known to be underlain by intrusive complexes, partly of highly evolved compositions (e.g. Staudigel et al., 1986), implying that crustal contamination processes during magma ascent are likely to be more intense and more variable beneath central Madeira than beneath São Lourenço. In addition, the complex stratigraphy of central Madeira complicates unequivocal assignment of samples to the EMRP and LMRP, respectively, thus obscuring the field boundaries of isotope compositional ranges.

Among the Madeira and Desertas samples of similar age, the São Lourenço rocks include the most depleted isotope compositions with the least radiogenic Pb ratios and the most radiogenic $^{143}Nd/^{144}Nd$ ratios (Fig. 12). The occurrence of the most depleted compositions at São Lourenço is surprising since samples from the peninsula would be expected to show more compositional overlap with shield stage samples from main Madeira with which they are associated. We suppose that these “extreme” compositions are related to the marginal geographic position of the peninsula, possibly associated with specific contamination or magma-wall rock interaction within the crust beneath São Lourenço, although this hypothesis cannot be tested with our data.

The role of São Lourenço in the evolution of the Madeira-Desertas rift complex

Based on age determinations and alternating volcanic activity, Madeira and the Desertas ridge were interpreted to form a single volcanic complex with two rift arms (Geldmacher et al., 2000). This concept ultimately considers São Lourenço as some sort of physical connector between both rifts as it is located near their geometric intersection (Fig. 1a). This connection would involve either a central volcano near São Lourenço feeding both rifts or lateral magma transport from Madeira to the Desertas along São Lourenço. If this were the case, we would expect respective field indications and/or geochemical data supporting, or at least not ruling out, this hypothesis.

Recent data and our field studies, however, argue against such an interconnection and give evidence for Madeira and the Desertas rifts representing two distinct volcanic systems (Schwarz et al., 2004a, 2004b): (1) There is no morphological or volcanological indication for a central volcano from where the two rift arms could have emanated. (2) Barometric data of lavas and xenoliths from the Desertas Islands differ from those from São Lourenço implying distinct magma pathways at depth and separated volcanic systems (no lateral transport). (3) Detailed field studies on the Desertas Islands combined with age determinations suggest the former presence of two neighbouring Madeira and Desertas volcanoes that coalesced during growth. Yet the alternating volcanic activity at Madeira and the Desertas, confirmed by our new data (Fig. 3), leave no doubt that some sort of coupling exists between both. This coupling may occur either in the upper mantle (related to melting processes) or at crustal levels (related to rift processes) or both. In either case, some mixing of melts would result.

Our new data from São Lourenço allow to address the nature of this coupling from the geochemical perspective. The data published so far indicate that samples from the Desertas almost completely overlap in major and trace elements and Sr-Nd-Pb isotope compositions with those from the Madeira shield stage (EMRP and LMRP) (Geldmacher and Hoernle, 2000; Schwarz et al., 2004b). This indicates that, by means of geochemical parameters, Madeira and the Desertas cannot be unequivocally distinguished from each other and are related to the same mantle source.

Likewise, with respect to their major and trace element compositions, São Lourenço samples completely overlap with those from central Madeira and the Desertas (Figs. 8, 9). In contrast, Sr-Nd-Pb isotope ratios of São Lourenço samples fall within the array of the Madeira shield stage but show only minor overlap with Desertas rocks (Figs. 10, 11). If São Lourenço were a physical connector between the two rift systems, we would expect, for samples of similar age, the isotope compositions of São Lourenço samples lying somewhere between the Madeira and Desertas fields. This is not shown by our data as is apparent from Figs. 10, 11 and 12. Especially, Nd and Pb isotope ratios of the LMRP samples from São Lourenço plot at the extreme edge of the array for the Madeira shield stage with a tendency to low $^{208}Pb/^{204}Pb$, $^{207}Pb/^{204}Pb$ and $^{206}Pb/^{204}Pb$ and high

$^{143}Nd/^{144}Nd$, which is contrary to the Desertas isotope ratios showing well-confined ranges at the isotopically enriched end of the array formed by samples of the Madeira shield stage. This extreme isotope composition of São Lourenço lavas is thus not compatible with mixing of Desertas and Madeira melts at crustal or mantle depths or with magma transport from Madeira to the Desertas along the rift at São Lourenço. In addition, the isotope data for the Desertas do not follow the overall "Madeira trend", i.e. the tendency to more depleted Pb, Sr and Nd isotope ratios with decreasing age, which is especially pronounced on São Lourenço (Fig. 12). We suggest, therefore, that São Lourenço is merely the easternmost part of the Madeira volcanic system but no connector between the Madeira and the Desertas rifts. This in turn confirms the interpretation of the Desertas rift as a discrete volcanic system thus making the geochemical data consistent with petrologic and field data (Schwarz et al., 2004a, 2004b).

An extended model for the Madeira plume

Although our data suggest that little or no mixing of Madeira and Desertas magmas took place, they must have had a common magma source as is indicated by the considerable overlap in ages, major and minor element as well as isotope compositions of Desertas and Madeira rocks (Geldmacher and Hoernle, 2000; Schwarz et al., 2004b). Both requirements can qualitatively be reconciled with the model of Schwarz et al. (2004a) proposing that the Desertas system roots in a particular sector of the melting region within the Madeira mantle plume (Fig. 13). The confined isotope range of Desertas rocks, plotting at the isotopically enriched end of the arrays for Madeira shield stage rocks as shown on Sr-Nd-Pb isotope correlation diagrams (Figs. 10, 11), may be explained by predominant melting and exhaustion of recycled upper (basaltic) oceanic crust within the Desertas melting region, whereas Madeira magmatism involved progressive melting of a more heterogeneous section of recycled upper and lower crust and lithospheric mantle (Geldmacher and Hoernle, 2000).

The question arises how the apparent coupling of Madeira and Desertas volcanism (Fig. 3) can be reconciled with the concept of different melting regions within a rising mantle plume. Since the Madeira hotspot track is ascribed to a weak, pulsating plume (Geldmacher et al., 2000), it is conceivable that the plume shape and flow are influenced by mantle convection, similar to what has been found by numerical simulations (Christensen and Hofmann, 1994). Instead of appearing as a simply cylindrical conduit or a spherical blob, the plume would be irregularly shaped and the plume shape at solidus depth would change with time thus causing lateral variations of the melting region (Fig. 13). We thus propose the following scenario: During the Early Madeira Rift Phase, the Madeira and Desertas systems were supplied with magmas from a common melting region within an irregularly shaped plume (Fig. 13a). Because of the irregular shape, further ascent of plume

material resulted in a gradual shift of the melting columns to the south-east. During the Desertas Rift Phase, eruption rates on Madeira decreased and between 3 and 4 Ma the main volcanic activity shifted to the Desertas Islands reflecting the location of maximum melt production (Fig. 13b). At this time, Madeira was characterised by erosion and probably by low-volume eruptions of low-degree partial melts. Near the beginning of the Late Madeira Rift Phase, north-westward movement of the melting region caused the maximum melt production to be located beneath Madeira (Fig. 13c). Volcanic activity on the Desertas Islands ceased while high eruption rates on Madeira created thick lava sequences covering any low-volume volcanics that may have been erupted during the Desertas rift phase. As the plate continued to move north-eastward, volcanism on Madeira graded into the low-volume post-erosional volcanism explained by minor melting of more depleted material above the downstream portion of the plume. Our model is thus consistent with the concept of progressive depletion of a heterogeneous plume source containing recycled oceanic lithosphere (Geldmacher and Hoernle, 2000) but additionally explains the occurrence of distinct volcanoes with coupled volcanic activity on a plausible yet speculative basis.

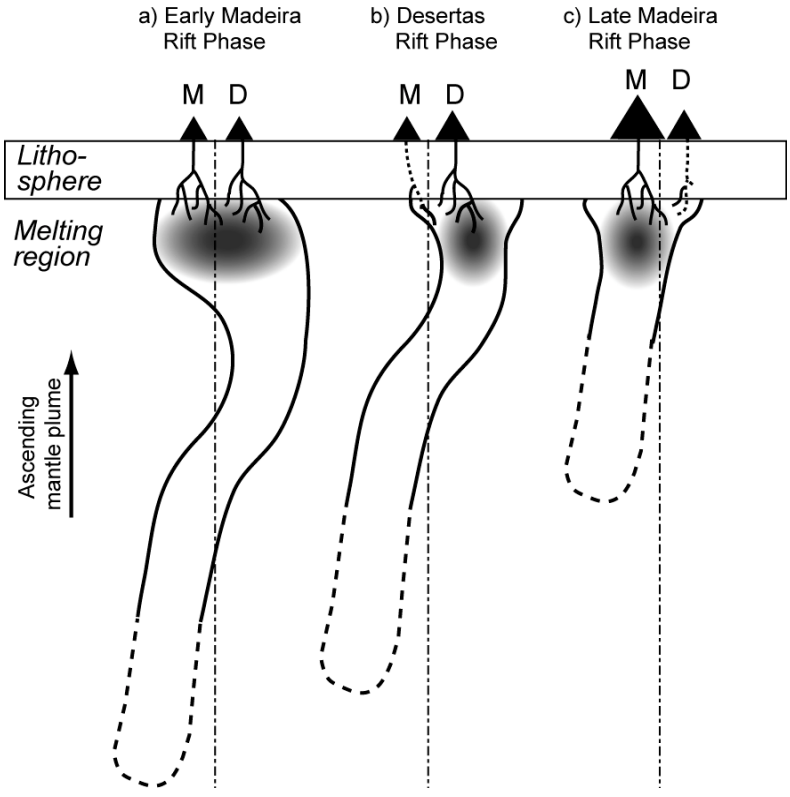

Fig. 13 Simplified cartoon of a model for an irregular plume; vertical dashed line for orientation. Mantle convection may influence the shape and flow of the slowly upwelling plume beneath the Madeira hotspot. Instead of appearing as a simply cylindric conduit, it can be irregularly shaped causing lateral variations of the melting region. The locus of the plume centre controls. The position of the melting region controls whether magma focus in the volcanic system or not. t_1: During their submarine stages and the Early Madeira Rift Phase, both Madeira and the Desertas have been located above the melting region. $t_2 > t_1$: Due to the plume's irregular shape, Madeira was located above the rim of the plume head during the Desertas Rift Phase. Volcanic activity decreased on Madeira, since magmas focussed mainly in the Desertas system. $t_3 > t_2$: At the beginning of the Late Madeira Rift Phase, presumably only Madeira was located above the plume centre, so that magmas focussed preferably in the Madeira system and activity ceased on the Desertas Islands.

Conclusion

This study shows that São Lourenço peninsula represents the eastern prolongation of the Madeira rift zone where volcanic activity lasted from at least 5 to 1 Ma, i.e. during the entire subaerial shield stage of Madeira. A period of eruptive quiescence between 4 and 2.5 Ma divides the São Lourenço stratigraphy in a lower and an upper unit corresponding to the Early and Late Madeira Rift Phases, respectively. These results show that volcanic rift zones can be persistent during a period of several million years and reactivated after a >1 Ma lasting period of inactivity.

The São Lourenço stratigraphy combined with rock compositions reveal a geochemical evolution with decreasing FeOtot, SiO2 and Mg# and depletion of Sr-Pb-Nd isotope ratios with decreasing age. This is consistent with published data and confirms the model that the mantle source beneath Madeira contains recycled oceanic crust that was progressively exhausted by its basaltic component over time. São Lourenço lavas, however, show much clearer the variations of isotope ratios as typical for Madeira with a distinctive tendency to higher $^{87}Sr/^{86}Sr$ and Pb ratios and lower $^{143}Nd/^{144}Nd$ with decreasing age. Contrary to rocks from central Madeira with isotope ratios of all shield stage samples scattering over a wide range, EMRP and LMRP samples from São Lourenço form two distinct and well-confined groups with respect to their isotope compositions. This difference between the peninsula and main Madeira can be explained by contamination processes being more intense and more variable beneath central Madeira than beneath São Lourenço.

Samples from São Lourenço include the most depleted isotope compositions among Madeira and Desertas shield stage samples of similar ages, and they show only minor overlap with Desertas at the opposite, enriched end of the isotope array of Madeira shield stage (most radiogenic Pb and Sr ratios, lower $\Delta 7/4$ and $^{143}Nd/^{144}Nd$). These results cannot be reconciled with magma mixing of Madeira and Desertas melts or lateral magma transport from Madeira to the Desertas and suggests that São Lourenço is only a part of the Madeira rift zone rather than a connector between Madeira and the Desertas. The considerable overlap in rock ages and rock compositions, however, indicates a common magma source for the Madeira and Desertas volcanoes. We thus propose that the Desertas ridge represents a discrete volcano which roots in a particular sector of the melting region within the Madeira plume. The coupling and shift of volcanic activity between Madeira and the Desertas, as indicated by rock ages, may result from lateral variations of the melting region in an irregularly shaped plume. This model might explain the shift of volcanic activity between Madeira and the Desertas Islands and of other hotspot volcanoes as well.

Acknowledgements The directors Costa Neves and Susana Fontinha and the staff from the Parque Natural da Madeira are gratefully acknowledged for their logistical support during our field trips on Madeira and the Desertas Islands. We are grateful to Heike Anders and Imme Martelock (ICP-MS laboratory, Institute of

Geosciences at the University of Bremen), Dagmar Rau (XRF laboratory, IFM-GEOMAR) and Silke Vetter (TIMS laboratory, IFM-GEOMAR) for their help during sample preparation and the analytical work. Cora Wohlgemuth-Ueberwasser and Jana J. Köster are gratefully acknowledged for providing the results from their field work on São Lourenço as parts of their master theses. Many thanks goes to Jörg Geldmacher for providing samples and for fruitful discussion. Further versions of the manuscript benefited from discussions with Colin Devey and Thor Hansteen. This work is part of the project funded by Deutsche Forschungsgemeinschaft (DFG grant KL1313/2-1).

Appendix

For detailed XRF- and ICP-MS analyses see the Appendix 5 and 6 of the *Electronic Appendix*.

For electronic suplement material (volcanological map and location map of measured dykes of the São Lourenço peninsula) see *Electronic Appendix*, EMap3 and EMap4.

References

Anderson, E.M., 1951. The dynamics of faulting, 2nd edn. Oliver and Boyd, Edinburgh:

Carracedo, J.C., 1994. The Canary Islands: an example of structural control on the growth of large ocean-island volcanoes. J. Volcanol. Geotherm. Res. 60: 225-241.

Carracedo, J.C., Day, S., Guillou, H., Rodriguez Badiola, E., Canas, J.A., Pérez Torrado, F.J., 1998. Hotspot volcanism close to a passive continental margin: the Canary Islands. Geol. Mag. 135: 591-604.

Carracedo, J.C., 1999. Growth, structure, instability and collapse of Canarian volcanoes and comparisons with Hawaiian volcanoes. J. Volcanol. Geotherm. Res. 94: 1-19.

Chaffey, D.J., Cliff, R.A., Wilson, B.M., Characterization of the St Helena magma source. In: A.D. Saunders, M.J. Norry (Editors), Magmatism in the Ocean Basins. Geological Society Special Publication No. 42, pp. 257-276.

Christensen, U.R. and Hofmann, A.W., 1994. Segregation of subducted oceanic crust in the convecting mantle. Journal of Geophysical Research, 99(B10): 19867-19884.

Clague, D.A., Dalrymple, G.B., 1987. The Hawaiian-Emperor volcanic chain, Part I: Geologic evolution. In: Volcanism on Hawaii, U.S. Geol. Surv. Prof. Pap. 1350: 5-54.

Cohen, R.S., O'Nions, R.K., 1982. The lead, neodymium and strontium isotopic structure of oceanic ridge basalts. J.Petrol. 23: 299-324.

Delaney, P.T., Fiske, R.S., Miklius, A., Okamura, A.T., Sako, M.K., 1990. Deep magma body beneath the summit and rift zones of Kilauea Volcano, Hawaii. Science 247: 1311-1316.

Duffield, W.A., Christiansen, R.L., Koyanagi, R.Y., Peterson, D.W., 1982. Storage, migration and eruption of magma at Kilauea Volcano, Hawaii, 1971-1972. J. Volcanol. Geotherm. Res. 13: 273-307.

Duffield, W.A., Dalrymple, G.B., 1990. The Taylor Creek Rhyolite of New Mexico: a rapidly emplaced field of domes and lava Flows. Bull. Volcanol. 52: 475-478.

Dupré, B., Allègre, C.J., 1980. Pb-Sr-Nd isotopic correlation and the geochemistry of the North Atlantic mantle. Nature 286: 17-21.

Garcia, M.O., Ho, R.A., Rhodes, J.M., Wolfe, E.W., 1989. Petrologic constraints on rift-zone processes; results from episode 1 of the Puu Oo eruption of Kilauea Volcano, Hawaii. Bull. Volcanol. 52: 81-96.

Geldmacher, J., Hoernle, K.A., 2000. The 72 Ma geochemical evolution of the Madeira hotspot (eastern North Atlantic): recycling of Paleozoic (≤500 Ma) oceanic lithosphere. Earth Planet. Sci. Lett. 183: 73-92.

Geldmacher, J.,Hoernle, K.A., 2001. Corrigendum to: The 72 Ma geochemical evolution of the Madeira hotspot (eastern North Atlantic): recycling of Paleozoic (≤500 Ma) oceanic lithosphere. Earth Planet. Sci. Lett. 186: 133.

Geldmacher, J., Bogaard, P.v.d., Hoernle, K.A., Schmincke, H.-U., 2000. The $^{40}Ar/^{39}Ar$ age dating of the Madeira Archipelago and hotspot track (eastern North Atlantic). G3 Geochem. Geophys. Geosys. 1, 1999GC000018.

Gudmundsson, A., 2000. Dynamics of volcanic systems in Iceland: Example of tectonism and volcanism at juxtaposed hot spot and mid-ocean ridge systems. Ann. Rev. Earth Planet. Sci., 28: 107-140.

Hardenbol, J., Thierry, J., Farley, M.B., Jaquin, T., de Graciansky, P.C., Vail, P.R., 1998. Mesozoic and cenozoic sequence chronostratigraphic framework of European basins. In: P.C. de Graciansky, J. Hardenbol, T. Jaquin, P.R. Vail (Editors). Mesozoic and Cenozoic Sequence Stratigraphy of European Basins. SEPM Special Publications 60: p. 60.

Hart, S.R., 1984. A largescale anomaly in the Southern Hemisphere mantle. Nature 309: 753-757.

Hoernle and Tilton (1991) Sr-Nd-Pb isotope data for FUerteventura (Canary Islands) basal complex and subaerial volcanics: application to maga genesis and evolution, Schweiz. Min. Petrol. Mitt. 71: 5-21.

Hoernle, K.A, Schmincke, H-J., Tilton, G. (1991) Sr, Nd and Pb isotope Geochemistry of volcanics from Madeira and Porto Santo Islands, North Atlantic Ocean EOS Trans. Am. Geophys. Union 72 (44): 528.

Hoernle, K.A., Zhang, Y.S., Graham, D., 1995. Seismic and geochemical evidence for large-scale mantle upwelling beneath the eastern Atlantic and western and central Europe. Nature 374: 34-39.

Hoernle, K.A., 1998. Geochemistry of Jurassic Oceanic Crsut beneath Gran Canaria (Canary Islands): Implications for Crustal Recycling and Assimilation. J. Petrol. 39: 859-880.

Hughes, D.J., Brown, G.C., 1972. Basalts from Madeira: a petrological contribution to the genesis of oceanic alkali rock series. Contrib. Mineral. Petrol. 37: 91-109.

Ito, E., White, W.M., Göpel, C. 1987. The O, Sr, Nd and Pb isotope geochemistry of MORB. Chem. Geol. 62: 157-176.

Johnson, K.T.M., Reynolds, J.R., Vonderhaar, D., Smith, D.K., Kong, L.S.L., 2002. Petrological Systematics of Submarine Glasses From the Puna Ridge, Hawai'i: Implications for Rift Zone Plumbing and Magmatic Processes. In: E. Takahashi, P.W. Lipman, M.O. Garcia, J. Naka, S. Aramaki (Editors). Hawaiian Volcanoes: Deep Underwater Perspectives. Am. Geophys. Union, Geophys. Monogr. 128: 143-159.

Klitgord, K.D., Schouten, H., 1986. Plate kinematics of the central Atlantic. In: P.R. Vogt, B.E. Tucholke (Editors): The Geology of the North America: The Western North Atlantic Region. Geol. Soc. Am. M: 351-378.

Klügel, A., Hoernle, K.A., Schmincke, H.U., White, J.D.L., 2000. The chemically zoned 1949 eruption on La Palma (Canary Islands): Petrologic evolution and magma supply dynamics of a rift-zone eruption. J. Geophys. Res. 105 (B3): 5997-6016.

Le Maitre, R.W., Bateman, P., Dudek, A., Keller, J., Lameyre, J., Le Bas, M.J., Sabine, P.A., Schmid, R., Sorensen, H.,Streckeisen, A., Wooley, A.R., Zanettin, B., 1989. A Classification of Igneous Rocks and Glossary of Terms -Recommendations of the International Union of Geological Sciences Subcommission on the Systematics of Igneous Rocks. Blackwell Scientific Publications (Oxford): pp. 193.

MacDonald, G.A., 1968. Composition and origin of Hawaiian lavas. In: Coats, R.R., Hay, R.L., Andersen, C.A. (Editors.). Studies in volcanology: a memoir in honour of Howel Williams. Geol. Soc. Amer. Mem. 116: 477-522.

Mata, J., Kerrich, R., MacRae, N.D., Wu, T.-W., 1998. Elemental and isotopic (Sr, Nd and Pb) characteristics of Madeira Island basalts: evidence for a composite HIMU-EM1 plume fertilizing lithosphere. Can. J. Earth Sci. 35: 980-997.

Nakamura, K. 1980. Why do long rift zones develop in Hawaiian volcanoes; a possible role of thick oceanic sediments. Bull. Geol. Soc. Jpn. 25: 255-269.

Mitchell-Thomé, R.C., 1975. Geology of the Middle Atlantic. Beiträge zur Regionalen Geologie der Erde, Band 12, Bornträger, Berlin.

Quane , S.L., Garcia, M.O., Guillou, H., Hulsebosch, T.P., 2000. Magmatic history of the East Rift Zone of Kilauea Volcano, Hawaii based on drill core from SOH 1. J. Volcanol. Geotherm. Res. 102: 319-338.

Roest, W.R., Dañobeitia, J.J., Verhoef, J., Collete, B.J., 1992. Magnetic Anomalies in the Canary Basin and the Mesozoic evolution of the Central North Atlantic. Marine Geophys. Res. 14: 1-24.

Ryan, M.P., 1988. The mechanics and three-dimensional internal structure of active magmatic systems: Kilauea volcano, Hawaii. J. Geophys. Res. 93 B5: 4213-4248.

Schmincke, H.-U, Weibel, M., 1972. Chemical study of rocks from Madeira, Porto Santo and São Miguel, Terceira (Azores). N. Jb. Miner. Abh. 117: 253-281.

Schwarz, S., Klügel, A., Wohlgemuth-Ueberwasser, C., 2004a. Melt extraction pathways and stagnation depths beneath the Madeira and Desertas rift zones (NE Atlantic) inferred from barometric studies. Contr. Mineral. Petrol. 147: 228-240.

Schwarz, S., Klügel, A., van den Bogaard, P., Geldmacher, J., 2004b. Internal structure and evolution of a volcanic rift system in the eastern North Atlantic: The Desertas rift zone, Madeira archipelago. J. Volcanol Geotherm. Res., in review.

Staudigel, H., Feraud, G., Giannerini, G., 1986. The history of intrusive activity on the Island of La Palma (Canary Islands). J. Volcanol. Geotherm. Res. 27: 299-322.

Sun, S.S., 1980. Lead isotopic study of young volcanic rocks from mid-ocean ridges, ocean islands and island arcs. Philosoph. Trans. Royal Soc. London, Series A 297: 409–445.

Sun, S.S., McDonough, W.F., 1989. Chemical and isotopic systematics of oceanic basalts: implications for mantle composition and processes. In: A.D. Saunders, M.J. Norry (Editors), Magmatism in the Ocean Basins. Geological Society Special Publication No. 42, pp. 313-345.

ten Brink, U., 1991. Volcano spacing and plate rigidity. Geology 19: 397-400.

Tilling, R.I., Dvorak, J.J., 1993. Anatomy of a basaltic volcano. Nature 363: 125-133.

Thirlwall, M.F., 1997. Pb isotopic and elemental evidence for OIB derivation from young HIMU mantle. Earth Planet. Sci. Lett. 139: 51-74.

Todt, W., Cliff, R.A., Hanser, A., Hofmann, A.W. (1996). Evaluation of a Pb-Pb double spike for high precision lead isotope analyses. In: A. Basu and S. Hart (Editors), Earth Processes: Reading the isotopic code. Geophys. Monograph. 95, AGU, Washington, pp. 429-437

Walker, G.P.L., 1987. The dike complex of Koolau volcano, Oahu: Internal strucutre of a Hawaiian rift zone. In: Volcanism in Hawaii. U.S. Geol. Surv. Prof. Pap. 1350: 961-993.

Walker, G.P.L., 1992. "Coherent intrusion complexes" in large basaltic volcanoes - a new structural model. J Volcanol. Geotherm. Res. 50: 41-54.

Walker, G.P.L., 1999. Volcanic rift zones and their intrusion swarms. J Volcanol Geotherm Res 94: 21-34 DOI 10.1016/S0377-0273(99)00096-7.

Widom, E., Hoernle, K.A., Shirey, S.B., Schmincke, H.-U., 1999. Os isotope systematics in the Canary Islands and Madeira: Lithospheric contamination and mantle plume signatures. J. Petrol. 40: 279-296.

Wright, T.L., Fiske, R S., 1971. Origin of the differentiated and hybrid lavas of Kilauea volcano, Hawaii. J. Petrol. 12: 1-65.

Yang, H.-J., Frey, F.A., Clague, D,A.,Garcia, M.O., 1999; Mineral chemistry of submarine lavas from Hila Ridge, Hawaii: implications for magmatic processes within Hawaiian rift zones. Contrib. Mineral. Petrol. 135: 355-372.

Zbyszewski, G., de Veiga Ferreira, O., Cândido de Medeiros, A., Aires-Barros, L., Silva, L.C., Munha, J.M., Barriga, F., 1975. Carta geológica de Portugal 1/50,000, Noticia explicativa das Folhas A e B da Ilha Madeira, Serv. Geol. de Portugal, Lisbon.

V Conclusions and perspectives

The volcanic rift zones of easternmost Madeira (São Lourenço peninsula) and the neighbouring Desertas Islands have been investigated in detail using data from field studies, $^{40}Ar/^{39}Ar$ geochronology, fluid inclusion barometry, clinopyroxene-melt thermobarometry, major and trace element as well as Sr-Nd-Pb isotope analyses. The research mainly focussed on the genesis and evolution of volcanic rift zones in the North Atlantic. Of special interest was the question if and how models for Hawaiian rift zones are transferable to rift zones of other oceanic island volcanoes such as Madeira or the Canary Islands.

The main results of this study are:

- Barometric analyses indicate significant differences between the magma fractionation and stagnation levels beneath the rift zones of Madeira and the adjacent Desertas Islands inferring two separated magma supply systems. In accordance with the barometric data, the conspicuous morphology of the Madeira/Desertas complex, the volcanic structures and new rock ages suggest that Madeira and the Desertas ridge represent two discrete volcanic systems.

- The considerable overlap in rock ages and rock compositions of samples from the Desertas with those from Madeira indicates a similar magma source for both volcanoes and implies some kind of coupling of the two rift zones. The new data from São Lourenço suggest that this coupling is not related to mixing of melts or lateral magma transport along this peninsula within the lithosphere but must have deeper roots. Since the Desertas represent a separate volcanic system, it is suggested that they root in a particular sector of the melting region within the Madeira plume.

- Lithosphere bending due to the loads of Madeira and Porto Santo, combined with an irregularly shaped plume, slow or even pausing motion of the African plate and a weak mantle plume, possibly resulted in the simultaneous formation of the two closely neighbouring volcanic systems of Madeira and the Desertas rather than a discrete chain of volcanoes as is the case for Hawaiian Islands.

- A model was developed that relates the coupling and shift of volcanic activity between Madeira and the Desertas to an irregularly shaped plume causing lateral and temporal variations of the melting region. This model is also qualitatively able to explain the shift of volcanic activity between other adjacent hotspot-related volcanoes lacking a regular hotspot track with clear age progression, e.g. the Canary Islands.

- The morphological interconnection between the Madeira and Desertas rift zones is related to growth of a proto-Desertas volcano towards north-northeast starting from a volcanic centre either in central part or at the southern tip of the Desertas ridge. A conceivable explanation for the formation of the elongated Desertas rift is a local gravitative stress field caused by the two overlapping Madeira and Desertas edifices resulting in preferred extension in-between. Such a rift evolution differs significantly from caldera-centred two-armed rift systems on Hawaii, which often serve as a rift prototype.

- These results show that models for Hawaiian rift zones are not directly transferable to North Atlantic rift systems due to differing geodynamic conditions such as plate motion and magma supply rates. The new model for rift zone formation as presented in this study might serve as a type example being transferable to rift zones of other ocean island volcanoes located on slowly moving plates and related to weak mantle plumes such as the Canary Islands.

Outlook:

Although this study extends the knowledge of the structure and evolution of volcanic rift zones, some questions still remain and can be the subject of further studies:

- *What is the nature of the temporal evolution of magma plumbing systems during shield stage volcanism on North Atlantic ocean islands?* A detailed thermobarometric study of samples from the deeply eroded central Madeira rift, from where neither fluid inclusion data nor other barometric data have been published, may improve the understanding of temporal variations of magma plumbing systems. Since shield stage volcanism lasted for at least 4 million years, Madeira Island would be particularly suitable to examine magma stagnation levels and their variations in depths over time.

- *How do compositional heterogeneities within the volcanic edifice influence variations in magma geochemistry along a rift zone?* Due to excellent and structurally deep exposures, the Madeira rift zone would be an ideal place to carry out a detailed geochemical study in order to investigate variations in magma compositions along a rift zone and the possible influence of lithological heterogeneities within the volcanic edifice. Such an intrusive complex may include an intrusive complex within the volcano centre, possibly comprising evolved rocks that can become assimilated and thus modify magma compositions.

- *Do local gravitative stresses, caused by two overlapping volcanic edifices, play an important role during rift zone evolution?* Experiments by mounting analogue sand piles onto a sand and viscous PDMS (polydimethylsiloxane) substratum show that gravitative spreading of two volcanoes may provoke an extensional stress field in-between facilitating the genesis of prominent rift zones, as shown for some of the Canary islands (Tenerife; Walter, 2003; La Palma; Klügel and Walter, 2003). In order to test if the conspicuously elongated Desertas rift was influenced by such processes, similar experiments should be carried by simulating the volcano constellation of Madeira Archipelago. These results could confirm the model for rift zone evolution of the present study and would improve our understanding of rift zone evolution.

References

Ancochea, A., Hernán, F., Cendrero, A., Cantagrel, J.M., Fúster, J.M.,Ibarrola, E., Coello, J., 1994. Constructive and destructive episodes in the building of a young oceanic island, La Palma, Canary Islands, and genesis of the Caldere de Taburiente. J.Volcanol. Geotherm. Res. 60: 243-262.

Anderson, E.M., 1951. The dynamics of faulting, 2nd edn. Oliver and Boyd, Edinburgh:

Carracedo, J.C., 1994. The Canary Islands: an example of structural control on the growth of large ocean-island volcanoes. J. Volcanol. Geotherm. Res. 60: 225-241.

Carracedo, J.C., 1999. Growth, structure, instability and collapse of Canarian volcanoes and comparisons with Hawaiian volcanoes. J. Volcanol. Geotherm. Res. 94: 1-19.

Clague, D.A., Dalrymple, G.B., 1987. The Hawaiian-Emperor volcanic chain, Part I: Geologic evolution. In: Volcanism on Hawaii, U.S. Geol. Surv. Prof. Pap. 1350: 5-54.

Delaney, P.T., Fiske, R.S., Miklius, A., Okamura, A.T., Sako, K., 1990. Deep magma body beneath the summit and rift zones of Kilauea Volcano, Hawaii. Science 247: 1311-1316.

Dieterich, J.H., 1988. Growth and persistence of Hawaiian volcanic rift zones. J. Geophys. Res. 93 B5: 4258-4270.

Duffield, W.A., Stieltjes, L., Varet, J., 1982. Huge landslide blocks in the growth of piton de la fournaise, La Reunion, and Kilauea volcano, Hawaii. J.Volcanol. Geotherm. Res. 12: 147-160.

Fiske, R.S., Jackson, E.D., 1972. Orientation and growth of Hawaiian volcanic rifts: the effect of regional structure and gravitational stresses. Proc. R. Soc. London A 329: 299-326.

Garcia, M.O., Ho, R.A., Rhodes, J.M., Wolfe, E.W., 1989. Petrologic constraints on rift-zone processes; results from episode 1 of the Puu Oo eruption of Kilauea Volcano, Hawaii. Bull. Volcanol. 52: 81-96.

Garcia, M.O., Rhodes, J.M., Trusdell, F.A., Pietruszka, A.J., 1996. Petrology of lavas from the Puu Oo eruption of Kilauea Volcano: III. The Kupaianaha episode (1986-1992). Bull. Volcanol. 58: 359-379.

Garcia, M.O., Ito, E., Eiler, J.M., Pietruszka, A.J., 1998. Crustal contamination of Kilauea Volcano magmas revealed by oxygen isotope analyses of glass and olivine from Puu Oo eruption lavas. J. Petrol. 39: 803-817.

Gautneb, H., Gudmundson, A., 1992. Effect of local and regional stress fields on sheet emplacement in West Iceland. J. Volcanol. Geotherm. Res. 51: 339-356.

Gee, M.J.R., Masson, D.G., Watts, A.B., Mitchell, N.C., 2001. Offshore continuation of volcanic rift zones, El Hierro, Canary Islands. J.Volcanol. Geotherm. Res. 105: 107-119.

Geldmacher, J., Bogaard, P.v.d., Hoernle, K.A., Schmincke, H.-U., 2000. The $^{40}Ar/^{39}Ar$ age dating of the Madeira Archipelago and hotspot track (eastern North Atlantic). G3 Geochem. Geophys. Geosys. 1, 1999GC000018.

Gudmundsson, A., 2000. Dynamics of volcanic systems in Iceland: Example of tectonism and volcanism at juxtaposed hot spot and mid-ocean ridge systems. Ann. Rev. Earth Planet. Sci., 28: 107-140.

Hill, D.P., Zuca, J.J., 1987. Geophysical constraints on the structure of Kilauea and Mauna Loa volcanoes and some implications for seismomagmatic processes. In: Decker, R.W., Wright, T.W., Stauffer, P.H. (eds.), Volcanism in Hawaii. US Geol Surv Prof Paper 1350: 903-917.

Holcomb and Searle (1991). Large landslides from oceanic volcanoes. Mar. Geotech. 10: 19-32.

Klitgord, K.D., Schouten, H., 1986. Plate kinematics of the central Atlantic. In: P.R. Vogt, B.E. Tucholke (Editors): The Geology of the North America: The Western North Atlantic Region. Geol. Soc. Am. M: 351-378.

Klügel, A., Hoernle, K.A., Schmincke, H.U., White, J.D.L., 2000. The chemically zoned 1949 eruption on La Palma (Canary Islands): Petrologic evolution and magma supply dynamics of a rift-zone eruption. J. Geophys. Res. 105 (B3): 5997-6016.

Klügel, A., Walter, T.R., 2003. A new model for the formation of rift zones on oceanic island volcanoes. Geophys. Res. Abstr. 5: 03913.

Morgan, W.J., 1981. Hotspot tracks and the opening of the Atlantic and Indian Oceans. In: C Emiliani (Editors): The Sea: Oceanic Lithosphere, vol. 7. John Wiley, New York, pp. 443-487.

Moore, J.G., Normark, W.R., Holcomb, R.T., 1994. Giant Hawaiian landslides. Ann. Rev. Earth Planet. Sci. 122: 119-144.

Nakamura, K. 1980. Why do long rift zones develop in Hawaiian volcanoes; a possible role of thick oceanic sediments. Bull. Geol. Soc. Jpn. 25: 255-269.

Roest, W.R., Dañobeitia, J.J., Verhoef, J., Collete, B.J., 1992. Magnetic Anomalies in the Canary Basin and the Mesozoic evolution of the Central North Atlantic. Marine Geophys. Res. 14: 1-24.

Ryan, M.P., 1988. The mechanics and three-dimensional internal structure of active magmatic systems: Kilauea volcano, Hawaii. J. Geophys. Res. 93 B5: 4213-4248.

Sleep, N.H., 1990. Hotspots and mantle plumes: some phenomenology. J. Geophy. Res. 95: 6715-6736.

Smith, W.H.F., Sandwell, D.T., 1997. Global seafloor topography from satellite altimetry and ship depth soundings. Science 277: 1956-1962.
Swanson, D.A., Duffield, W.A., Fiske, R.S., 1976. Displacement of the south flank of Kilauea Volcano: The result of forceful intrusion of magma into the rift zones U.S. Geol. Surv. Prof. Paper 963: pp. 39.
Tilling, R.I., Dvorak, J.J., 1993. Anatomy of a basaltic volcano. Nature 363: 125-133.
Walker, G.P.L., 1987. The dike complex of Koolau volcano, Oahu: Internal strucutre of a Hawaiian rift zone. In: Volcanism in Hawaii. U.S. Geol. Surv. Prof. Pap. 1350: 961-993.
Walker, G.P.L., 1992. "Coherent intrusion complexes" in large basaltic volcanoes - a new structural model. J Volcanol. Geotherm. Res. 50: 41-54.
Walker, G.P.L., 1999. Valcanic rift zones and their intrusion swarms. J Volcanol Geotherm Res 94: 21-34.
Walter, T.R., 2003 Buttressing and fractional spreading of Tenerife, an experimental approach on the formation of rift zones. Geophys. Res. Lett. 30 (6): 1296.
Wright, T.L., Fiske, R.S., 1971. Origin of the differentiated and hybrid lavas of Kilauea volcano, Hawaii. J. Petrol. 1: 21-65.

Electronic Appendix

Data files are available as download from the data base PANGAEA (http://www.pangaea.de).

Contents

Electronic maps (pdf-files):

EMap 1: Volcanological map of the Desertas Islands (Madeira Archipelago)

EMap 2: Location map of measured dykes on the Desertas Islands (Madeira Archipelago)

EMap 3: Volcanological map of São Lourenço (Madeira Archipelago)

EMap 4: Location map of measured dykes on São Lourenço (Madeira Archipelago)

eTables
(electronic supplement material to Schwarz et al. (2004) – Melt extraction pathways and stagnation depths beneath the Madeira and Desertas rift zones (NE Atlantic) inferred from barometric studies)

eTable 1: Compositions of glass and fused groundmass (wt.%);

eTable 2: Compositions of clinopyroxene rims (wt.%)